University of Cyprus

Master Thesis

Fabrication and characterization of electrospun polymeric phase change fibers for potential use in thermal energy storage

Kyriakos Avraam

Department of Mechanical and Manufacturing Engineering

May 2022

UNIVERSITY OF CYPRUS
DEPARTMENT OF MECHANICAL AND MANUFACTURING ENGINEERING

Fabrication and characterization of electrospun polymeric phase change fibers for potential use in thermal energy storage

Kyriakos Avraam

Supervisor
Dr. Theodora Krasia-Christoforou

A dissertation submitted in partial fulfilment of the requirements for the degree of Master of Science in Advanced Materials and Nanotechnology

2022

Acknowledgments

First and foremost, I thank God for the good health and well-being that helped me to implement this Master Thesis. Reaching the end of my thesis, I would like to express my gratitude to everyone who has assisted me in achieving my aim. I would first like to thank my thesis supervisor Dr Theodora Krasia, Associate Professor and the Head of the Polymers/ Polymer processing Laboratories at the Department of Mechanical and Manufacturing Engineering, University of Cyprus. Her vast expertise and wealth of experience have aided me throughout my academic career and daily life. She always let me do my own research, but she always steered me in the correct direction when she thought I needed it.

I would also like to thank Dr Claus Rebholz and Dr. Dimokratis Grigoriadis Associate Professors at the Department of Mechanical and Manufacturing Engineering, University of Cyprus, for participating in my M.Sc. Thesis examination committee and I am grateful for his valuable comments.

I would also like to acknowledge the experts who contributed in this research project: Dr Chryssafis Konstantinos, Professor at the Physics Department, Aristotle University of Thessaloniki and Mrs Iouliana Chryssafi, PhD Student at the Physics Department, Aristotle University of Thesaloniki. This project would not have been completed without their enthusiastic participation and the performing of Differential Scanning Calorimetry experiments in their Laboratory of Advanced Materials & Devices at Physics Department at the Aristotle University of Thessaloniki.

More than academic help was required to complete my dissertation, and I owe a debt of gratitude to many people for listening to and, at times, tolerating me over the past two years. I must express my very profound gratitude to my parents, Marios and Andri, to my brother, Tasos and to my friends, Antonis, Angelina, Panagiotis, Antri and Thekla for providing me with unfailing support and continuous encouragement throughout my years of study and through the process of researching and writing this Master thesis. This accomplishment would not have been possible without them. Thank you.

Author,

Kyriakos Avraam

Abstract

The need for energy is constantly growing, making it necessary to effectively implement systems to meet the needs of the world's growing population while avoiding energy crises. As the levels of greenhouse gases in the environment continue to rise at an alarming rate, it is critical to develop non-fossil fuelbased energy sources. Renewable Energy, provides clean energy alternatives, however the intermittency of renewable energy sources, is a key barrier in terms of round-the-clock energy production from them. This can be managed by incorporating thermal energy storage (TES) into more efficient and cleaner energy systems, so improving the reliability of thermal energy from renewable sources. TES employing heat transfer medium such as phase change materials (PCMs), has steadily become an important study subject in recent decades.

Form stable Phase Change Fibers (PCFs) have been introduced for their unique advantages such as direct use without encapsulation, cost-effective and flexible dimensions and excellent thermal performances. They are used for thermal energy storage because they can store energy at different levels of temperature by latent heat storage.

In the present study, ultrafine PEO/ PMMA/ n-eicosane composite nano/microfibers as form-stable phase change materials were successfully developed by the uniaxial electrospinning technique. N-eicosane, a hydrocarbon with melting point near the human body temperature and high latent heat was chosen as the PCM. Systematic parametric studies were carried out in order to determine the optimum experimental conditions for obtaining fibrous membranes. Electrospun PEO/ PMMA (80/ 20) and PEO/ PMMA (50/ 50) beaded and bead-free fibers were employed as matrices for the incorporation of n-eicosane.

The effect of n-eicosane content on the morphology and thermal properties of the form-stable PEO/ PMMA/ n-eicosane phase change fibers was scientifically investigated by using scanning electron microscopy (SEM) and differential scanning calorimeter (DSC). The membrane seems to be very stable, and the fibers remain intact in the form of PCFs without observing any n-eicosane leaching phenomena or material alteration. In general, the enthalpies of the systems were high and comparable to the ones reported for other phase change materials based on n-eicosane or other paraffins.

Contents

List of Figures

List of Tables

Appendices

Chapter 1

1 INTRODUCTION

1.1 Energy – Theoretical Background

The need for energy is continually increasing, making it critical to implement systems to fulfill the needs of the world's growing population and avoid energy crises. Using 2004 as a base year, demand for energy is predicted to rise by 65% by 2030 at the current pace of use [1]. The globe consumes a lot of fossil fuels, which causes climate change and depletes fossil fuel reserves more quickly [2]. Currently, nonrenewable energy sources such as coal-fired power plants provide the majority of the world's energy. Estimates for global annual TFEC (total final energy consumption) of 2021 range from 18.53 TWyr (Terawatt-years) to 20.13 TWyr (Terawatt-years) depending on the source (Knoema Corporation, International Energy Agency (IEA) intergovernmental organization, British Petroleum Company). A graph showing the evolution of global primary energy demand is shown in Fig. 1.1 [3].

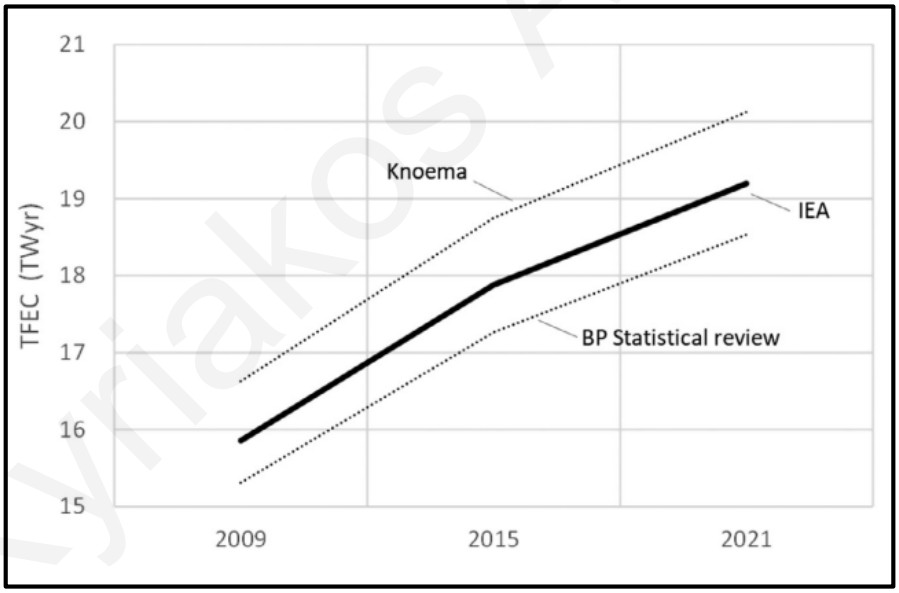

Figure 1.1: The evolution of global primary energy demand according to Knoema, International Energy Agency and British Petroleum sources. [3].

Figures 1.2 and 1.3 show the World electricity generation by share in 2020 [4]. According to the first chart, fossil fuels are the greatest contributors to electricity generation worldwide. In 2020, coal and oil accounted for roughly 37.9% of the global power mix, while natural gas followed with a 23.4% share. Fossil fuel use notwithstanding, the share of renewable energy

sources in global electricity has seen a more pronounced year-on-year growth in recent years, following increased efforts by governments to combat global warming and a decrease in levelized costs [4]. By 2040, projections show renewable sources to have surpassed fossil fuels as the main power source. [4]

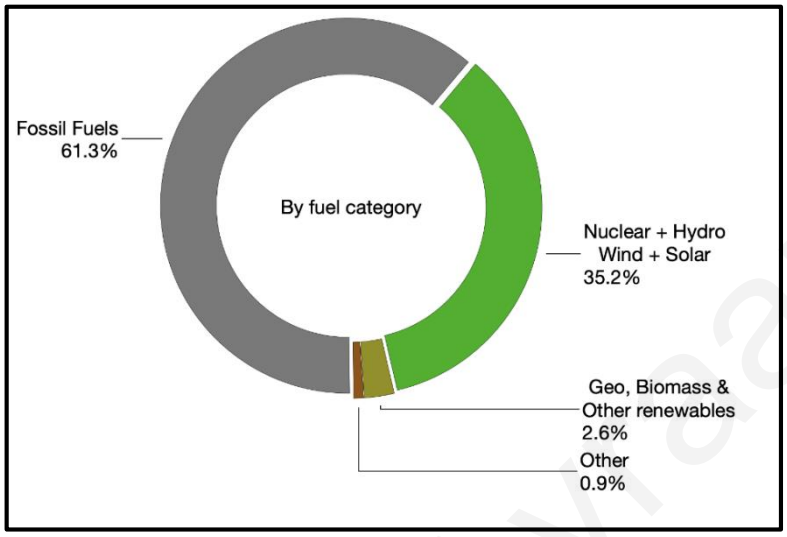

Figure 1.2: The World electricity generation by fuel category in 2020. [3].

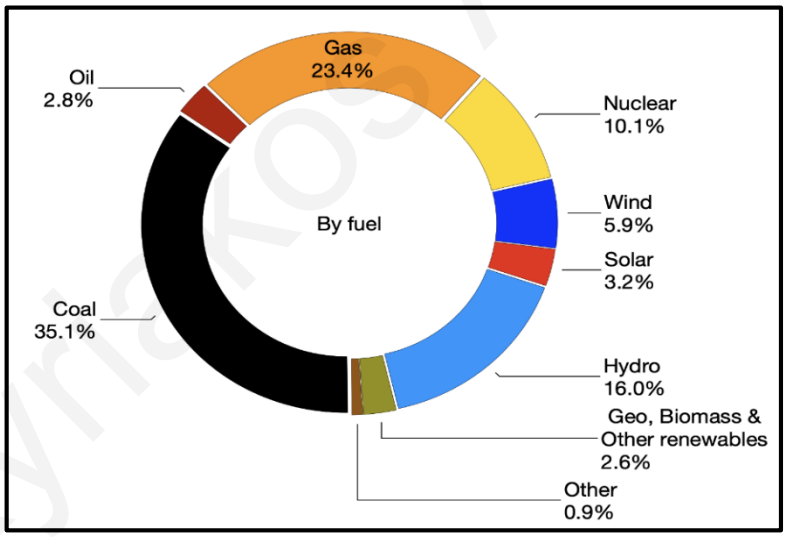

Figure 1.3: The World electricity generation by fuel in 2020. [3].

A continuous increase in greenhouse gas emissions into the environment, as well as the high cost of fossil fuels, are the primary motivators for more efficient energy use in all aspects of human activity [5]. It is critical to create non-fossil fuel based energy sources as the levels of greenhouse gases in the atmosphere continue to rise at an alarming rate. The three main sources of energy are fossil fuels, nuclear resources, and renewable energy. Renewable Energy, in contrast to fossil fuels, provides clean energy alternatives [6]. Because of their long-term

availability, accessibility, and environmental friendliness, renewable energy sources are definitely preferred over the exploitation of nonrenewable resources [7]. Solar and wind energy are the most promising renewable energy sources, with increased interest in their use around the world [6]. Solar energy, which reaches the earth's surface every year in the amount of 79,000 TWyr (Terawatt-years) is the world's most readily available energetic resource. [3]

Starting with demand-side consumption and progressing through all supply-side finite and renewable sources, Fig. 1.4 compares the RARs (Reasonably Assured Recoverable Reserves) of each element. The RARs show the quantity of energy that can be extracted in a reasonable amount of time under current technical and economic conditions. In the case of renewable resources, it refers to the quantity that might be generated with reasonable land use and conversion efficiency restrictions. For conventional finite resources, it is a function of the overall resource of a specific energy source and the proportion of this resource that has been found and can be economically harvested today - which is strongly reliant on the available technology.

Terawatt-years (TWyr) (1 TWyr = 8.76 × 1012 kWh) are used to measure all energy reserves and consumption. The area between the circles reflects practically ensured recoverable energy reserves from both finite and renewable resources for the next 30 years. These areas can be compared to total demand (earth picture) [3]. The 30-year reasonably exploitable solar reserves are 8,300 TWyr30, and the 30-year reasonably exploitable wind RARs are roughly 1,500 TWyr30, based on current estimates. Over that time span, solar energy accounts for around 12 times and the wind energy accounts for about 2.5 times the world primary demand. [3]

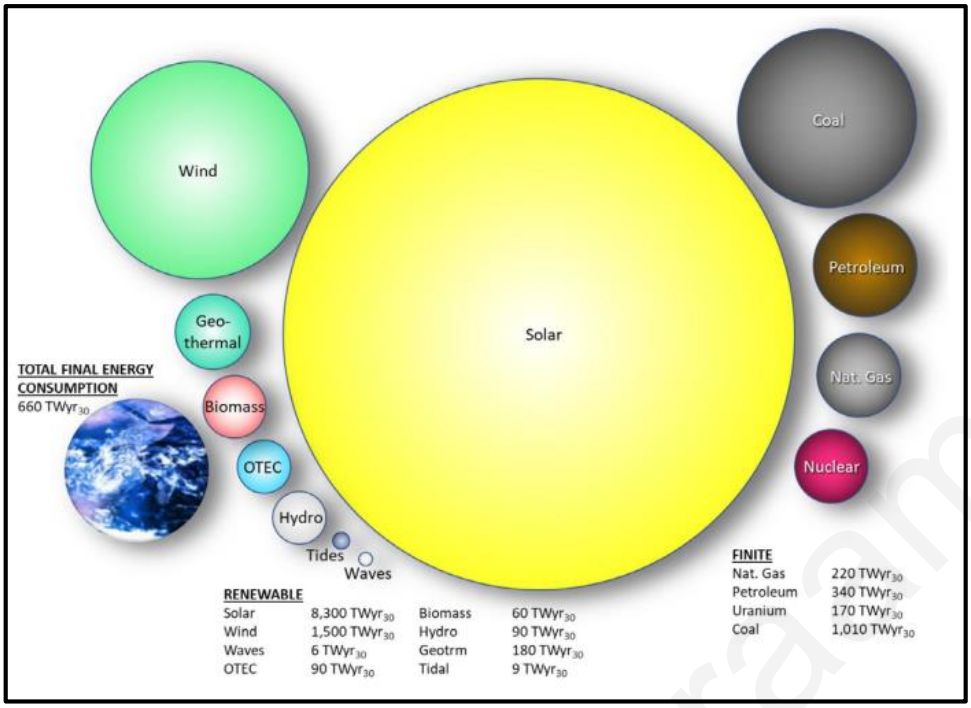

Figure 1.4: Reasonably Assured Recoverable Reserves (RARs) of each element. [3].

However, the intermittency of renewable energy sources, notably solar and wind energies, is a key barrier in terms of round-the-clock energy production from them, and special measures must be developed to accommodate their adaptability [7]. This can be managed by incorporating thermal energy storage (TES) into more efficient and cleaner energy systems, so improving the reliability of thermal energy from renewable sources and, as a result, reducing global warming. Furthermore, TES systems can be used to store surplus energy and bridge the demand–supply gap by providing during peak power demand if energy output exceeds energy demand. [7]

1.1.1 Thermal Energy Storage

Thermal energy storage (TES) employing heat transfer medium such as phase change materials (PCMs), has steadily become an important study subject in recent decades after the two oil crises in the 1970s [8]. Thermal Energy Storage (TES) is a technique for storing excess thermal energy in a suitable medium so that it can be accessed later and productively re-applied in a particular operation. Because it is freely available from solar radiation, thermal energy is one of the most promising clean and renewable energy source [9]. Solar energy is a great renewable energy source, but it is also an intermittent one. At night or on cloudy days, solar energy is unavailable. Latent heat thermal energy storage technologies can help to solve this problem. [10]

Thermal energy can be stored in three different ways at different temperatures. First, by heating a liquid or solid storage medium, Sensible Heat Storage (SHS) is achieved (e.g., water, mineral oil, molten salts, sand, rocks and concrete). SHS is popular because it is both inexpensive and safe, as it is made from non-toxic components. The thermochemical heat storage, which is achieved by endothermic and exothermic reactions, is the second method (e.g. potassium oxide and lead oxide). The last one is the Latent Heat Storage (LHS) by using Phase Change Materials (PCMs). [10]

The Latent Heat Storage technique is the most competitive of the three TES methods due to its advantages, such as significant energy storage density, small temperature variation during the heat storage process, chemical stability, low cost and non-corrosiveness. [9] However, due to the limited thermal conductivity, changes in thermo-physical characteristics over long cycles, high flammability, incongruent melting, phase segregation, supercooling, leakage of molten PCMs and volume change, there are various practical challenges with latent heat storage [11]. The mass and latent heat of fusion of the PCMs determine the amount of heat stored in LHS [7]. For latent heat storage, many solid–liquid phase change materials (PCM) have been studied, and they are currently commercially produced for a variety of purposes [12].

1.2 Phase Change Materials

The liquid–gas, solid–gas, solid–solid, and solid–liquid phase transformations, as well as vice versa, are used to classify Latent Heat TES systems. TES systems based on liquid-gas or solid-gas phase transformation are impractical due to the huge volume needs, volumetric changes associated with the phase transition, and high pressure of the system, such as the water-steam system, which is not financially viable for large-scale TES. Additionally, when comparing solid-solid PCMs to solid-liquid PCMs, the heat of phase transition in solid-solid PCMs is considerably lower. [7]

Solid-liquid phase transition materials make up the majority of PCMs evaluated for TES. Solid-liquid PCMs store energy when they change from solid to liquid phase (endothermic process) and retrieve it when they change back to solid phase (exothermic process) [13]. When a material's temperature increases over a certain point, chemical bonds in the material begin to break down, and the material absorbs the heat, changing state from solid to liquid in an endothermic process [14]. When the phase transition temperature is reached, the material starts to melt. Then, the temperature remains constant until the melting process is completed. The

heat absorbed during the material's phase shift (melting process) is referred to as latent heat [11]. Finally, the material will give off energy and return to a solid form as the temperature drops in an exothermic process [14].

The temperature range varies based on the phase change materials utilized [14]. The melting temperature of PCMs can be classified as low, middle, or high. Low melting temperature is considered when the melting point is below 120℃, high melting temperature when the melting point is above 300℃, and when it is in the range in between, it is referred as middle melting temperature [15].

1.2.1 Classification of Phase Change Materials into organic, inorganic and euthetic materials

The advantages of organic PCMs include no supercooling and a high latent heat of fusion. Organic PCMs can be further divided into paraffin and non-paraffin materials. Non-toxic, chemically stable, compatible with metal containers, and cheap are all advantages of paraffins. They do, however, have low thermal conductivity and density, a high volume change, a poorly defined melting point, and can be flammable [10]. *Paraffins* are most typically commercially used, which are composed of linear n-alkanes chains [10]. The liquid paraffins have carbons between C5 to C15, whereas the waxy solids have C16 and higher. It is primarily composed of linear chain hydrocarbons with melting temperatures ranging from 23 to 67 ℃. The melting temperature and heat of fusion are generally higher, the longer the average length of the hydrocarbon chain is. When exposed to oxygen, they exhibit chemical stability and slow oxidation. The heat of fusion of paraffin waxes is high, and they are non-reactive and safe [11]. *Non-paraffin* materials are the most diverse in terms of materials and properties. Unlike paraffins, which have essentially similar properties, each of these materials will have its own set of characteristics. Because these materials are combustible, they should not be exposed to extreme heat, flames, or oxidizing chemicals [11]. The phase transition of fatty acids which are *non-paraffin* materials is well-defined and can be easily replicated. They also have low thermal conductivity, as well as toxicity, corrosivity, instability, and flammability, in addition to being significantly more expensive than paraffins [10].

Inorganic PCMs are divided into two subcategories: metallics and salt hydrate. Metallics are made up of metals with low melting points compared to most metals, and salt hydrates are made up of inorganic salts and water ($AB{\bullet}nH_2O$). Thermal conductivity and latent heat of fusion per volume are higher in both types of inorganic PCMs than in organic PCMs. Salt

hydrates have a low volume change, a high density, and are both cheap and widely available. However, they can cause supercooling, phase segregation, and corrosion on metal containers. They also have low thermal stability and can be toxic. Metallics have several drawbacks, including a high cost, a low specific heat, and a low latent heat of fusion per weight unit. [10]

Eutectic PCMs are made up of two or more PCMs that have been blended in certain ratios to achieve the lowest melting point feasible. The amount of each material can be changed to adjust the melting point of the material. Eutectic materials have advantages such as high thermal conductivity and latent heat of fusion, but they can have a drawback in terms of cost. [10]

1.2.2 Desired properties of Phase Change Materials

Phase change materials must have different properties depending on their intended use. First, in order to take full advantage of the PCM, the *phase transition temperature* must be suitable for the environment, the location in the building, and the type of system in which the PCM is installed. The PCM must then have a *high latent heat of fusion* per unit volume and weight and a high specific heat. It is preferable to get more out of latent heat storage when using a small amount of PCM. *Chemically stable materials* allow the PCM to operate for a long time at a given temperature and effect, and reduce the likelihood of the PCM reacting with materials it comes into contact with, extending the life of the PCM. For PCMs to have longer lifetimes, they must be able to reproduce crystals that are phase-shifted thousands of times without degradation. After that, because there must be *no harmful emissions* during a fire or if the encapsulation ruptures during normal operation, PCMs that are neither hazardous nor poisonous can be allowed for use in a variety of applications. The fabrication of the material should also produce no harmful emissions into the environment. Additionally, the encapsulating material must allow for PCM expansion since the PCM expands during solidification. As a result, *structural stability* of the PCM is crucial for allowing for small volume changes during solidification. Another key fact is that if a material has a *high thermal conductivity*, heat will diffuse through or leave it more quickly, allowing the PCM to charge or discharge energy at a faster rate. Furthermore, to make the technology more appealing and possible to deploy on a large scale, it is important that the materials used are *abundant and cost effective.* Finally, an acceptable PCM should have a specific phase change temperature so that the phase change can be predicted, allowing for proper material selection for optimal design. Because supercooling affects the temperature of the phase change, only *a small degree of supercooling is preferred*. [14]

1.2.3 Micro/Nanoencapsulated Phase Change Materials

Encapsulation methods are significant for enhancing the stability and heat transfer yield of PCMs, as well as making scaling up processing easier. Advanced PCMs with lower reactivity with the outside environment, and controlled volume changes during the phase transition can be made using microencapsulation processes. Microencapsulated phase change materials (MEPCMs) have attracted high attention for over 20 years for these reasons. [16]

Microcapsules are particles with a core material covered by a coating or shell with dimensions ranging from 1 to 1000 micrometers [16]. PCMs make up the core of encapsulated PCMs, whereas polymers or inorganics make up the shell. Polymerization, sol-gel, and electrohydrodynamic processes are the most important methods for producing micro- as well as nanoencapsulated PCMs, and they will be explored in the following sections [17].

Emulsion polymerization (chemical technique): The insoluble monomer is first disseminated in the reaction media using surfactants and emulsifiers while being stirred. The polymer membrane is created on the surface of the core in the next phase by adding the initiator, and the nanocapsules are then fabricated (Fig.1.5) [17]. Table 1.1 shows the melting temperature and enthalpy of nanocapsules that were fabricated for thermal energy applications using emulsion polymerization. [18] [19]

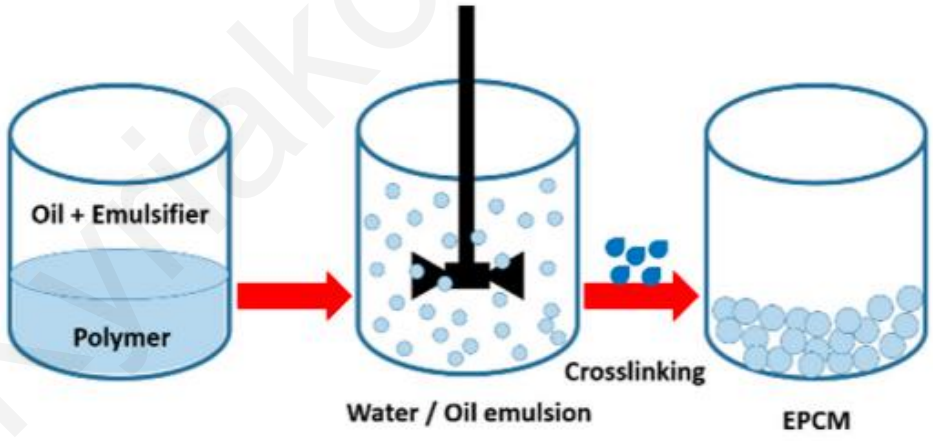

Figure 1.5: Schematic representation of the emulsion polymerization [17]

Mini-emulsion polymerization (chemical technique): The polymerization reaction in this technique occurs within small decentralized droplets as long as their size remains at the nanoscale due to the strong shear force effect, which includes the monomers, water, emulsifier, and initiator (Fig.1.6). At the moment, this process is the most common way to make nano

PCMs [17]. Table 1.1 presents the melting temperature and enthalpy of nanocapsules fabricated for thermal energy applications using mini-emulsion polymerization. [20]

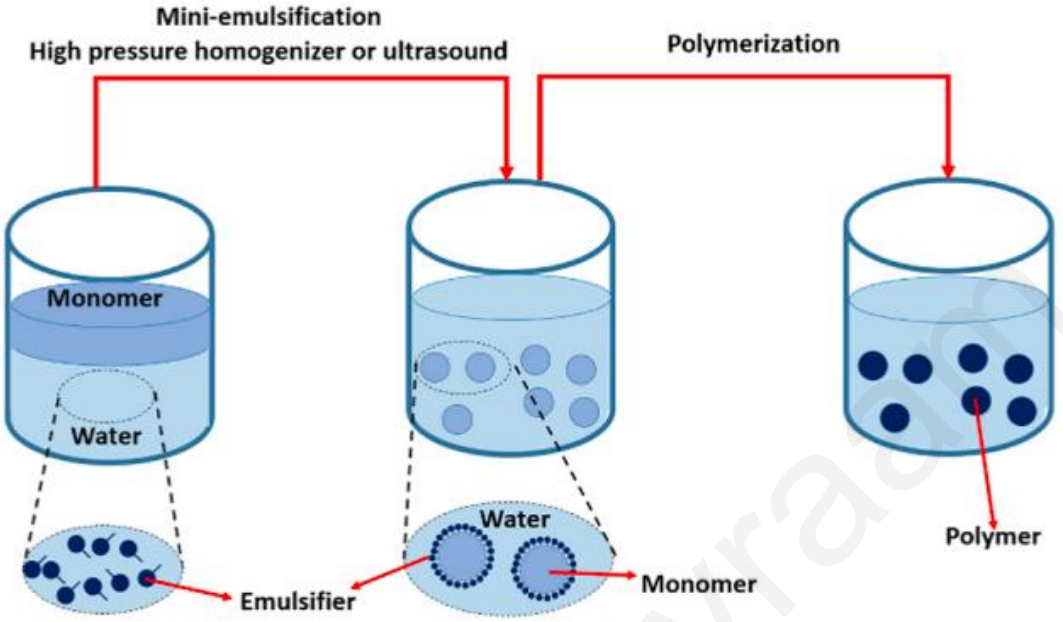

Figure 1.6: Schematic representation of the mini-emulsion polymerization [17]

Interfacial polymerization (chemical technique): To synthesize nano PCMs using this method, the core material is emulsified by making Oil/ Water or Water/ Oil emulsions with the use of a suitable emulsifier. The produced capsules are removed from the oil or water phase after the wall polymer is formed onto the surface of the core through polymerization of the monomers. Interfacial polycondensation of ethylene diamine and tolylene diisocyanate with Fe_3O_4 nanoparticles, followed by interfacial polymerization, resulted in nanocapsules (Figure 1.7) [17]. Table 1.1 presents the melting temperature and enthalpy of nanocapsules that were fabricated for thermal energy applications using interfacial polymerization. [21] [22]

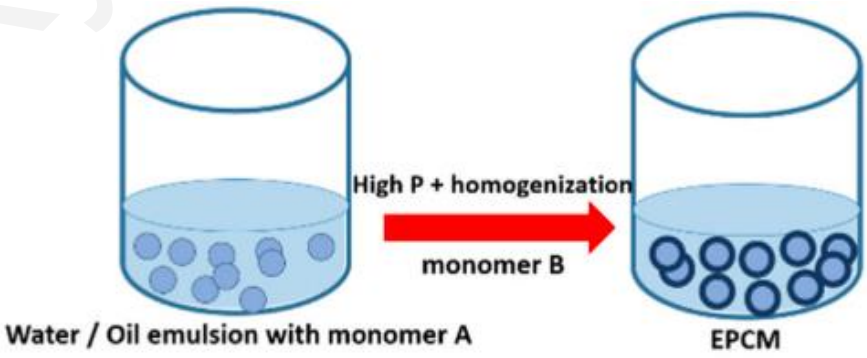

Figure 1.7: Schematic representation of the interfacial polymerization [22]

Table 1.1: The melting temperature and enthalpy of nano/microcapsules fabricated for thermal energy applications using different encapsulation methods.

No	Shell Material	Core Material	Encapsulation technique	Application	Melting Temperature	Melting enthalpy
1	PMMA	Heneicosane (C21) and octacosane (C28)	Emulsion polymerization	Thermal energy storage	39–60 °C	138 – 152 J/g
2	PMMA	Octacosane	Emulsion polymerization	Thermal energy storage	21℃	98 J/g
3	PMMA	n-eicosane	Mini-Emulsion polymerization	Thermal energy storage	34.66 ℃	124.7 J/g
4	Polyurethane	Paraffin	Interfacial polymerization	Energy storage and release performance of the system	69.3 ℃	153.9 J/g
5	PMMA	Paraffin	Interfacial polymerization	Thermal energy storage	21.42 ℃	64.93 J/g

Physicochemical techniques (sol–gel encapsulation): The sol-gel process is schematically illustrated in Fig. 1.8. The solvent is first mixed with a metal alkoxide, a complexing agent, and a catalyst. The next stage is to develop a stable and transparent colloidal formulation for hydrolysis and condensation chemical reactions. Following that, the aging of the sol, curing, sintering, and drying processes are carried out. [17]

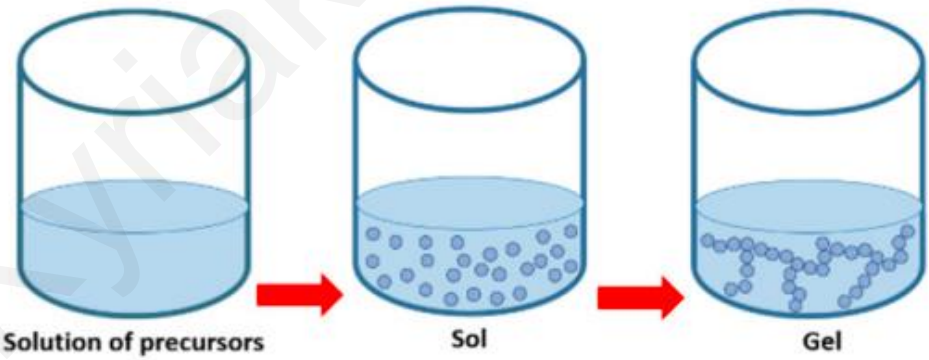

Figure 1.8: Schematic representation of the sol–gel encapsulation [17]

1.2.4 Form-stable Phase Change Fibers (PCFs)

Form stable PCFs have been introduced for their unique advantages such as direct use without encapsulation, cost-effective and flexible dimensions [9]. Also, other PCFs' benefits are huge surface-to-volume ratio, and excellent thermal performances. Phase change fibers (PCFs) have

attracted the interest of academic and industrial researchers over the last three decades as fibrous form-stable PCMs with intriguing applications in smart fabrics and clothing. [9] Also, they are used for thermal energy storage because they can store energy at different levels of temperature by latent heat storage. [23] [9]

Form stable PCFs are composed by PCMs and the Supporting Materials. Supporting materials are used to avoid the flow and leakage of PCMs when these change into the liquid phase. The most important characteristic of the supporting material is the higher melting temperature in comparison with PCM. Filling, coating, and wet/melt spinning were all used to fabricate traditional PCFs of several micrometers in diameter. [9]

Electrospinning is one of the most extensively used processes for producing fibers with cross-sectional dimensions ranging from tens to hundreds of nanometers. It is a very simple, scalable, and cost-effective technique, particularly suitable for the manufacturing of fibrous nanomaterials on an industrial scale [24]. Electrospinning is currently the only industrial technology for fabricating micro/nanofibers [17]. Ultrafine PCFs have been utilized and researched in the recent decade due to the advancement of electrospinning [9].

Nevertheless, there are different electrospinning approaches for the fabrication of electrospun ultrafine PCFs which have both advantages and disadvantages. The first approach is the uniaxial electrospinning, the second one is the co-axial electrospinning and the third one is the multifluidic electrospinning. We can achieve the desired properties and characteristics of fibers using these three techniques, by altering the experimental parameters or modifying the electrospinning set-up.

Uniaxial electrospinning uses only one channel for the solution because the phase change material and the supporting material are used in a same homogeneous solution. The advantages of this technique are the simple setup, the convenience in the fabrication of ultrafine electrospun phase change fibers and the ability to use polymers with high molecular weight to fabricate ultrafine phase change fibers. By using this technique, the encapsulation of PCM in the supporting matrix is only partial because the PCM may also distribute on the surface of the fiber. [9]

Coaxial electrospinning uses two separate channels, one for each solution. The first one is used for the PCM solution and the second one for the supporting material solution. This technique is beneficial because it can be used to fabricate bicomponent nanofibers, which are core/shell

nanofibers. Furthermore, the complete encapsulation of PCM in the supporting matrix can be achieved. However, the disadvantage of this technique is the unstable electrospinning process. [25]

Multifluidic electrospinning with several spinnerets is commonly seen as a step forward from coaxial electrospinning. This approach is distinguished by the use of two or more solid-liquid PCM solutions as the core solution. The PCFs have a special multichannel tubular microstructure that allows them to controllably encapsulate different PCMs into the channels separately, resulting in a multiresponsive effect. Coaxial electrospinning and multifluidic electrospinning both have two major drawbacks: (a) Compared to uniaxial electrospinning, their setup and technological process are too difficult, resulting in PCFs with unstable morphology and thermal characteristics; (b) the content of solid-liquid PCMs encapsulated in PCFs is too low, resulting in PCFs with low phase transition enthalpies. [9].

The electrospinning technique depends on different working parameters. Those parameters may be categorized in **process parameters, solution parameters and ambient parameters**.

Process parameters are the applied voltage, flow rate, the type of the collector and the distance between the collector and the metallic needle. The distance between the tip at the edge of the syringe and the collector is an important influencing factor since upon increasing this distance it gives time for the solvent to evaporate. By decreasing the distance, fibers that are not completely dried are produced due to incomplete solvent evaporation [26].

Solution parameters include the polymer solution viscosity, the surface tension and solution concentration. Collapsed particles are formed at low polymer solution concentrations. Spherical particles can be produced by raising the concentration. The electrospun fibers are generating micro-sized beads on the fibers as the concentration rises approaching the lower critical concentration (bead-on-string morphology). Smooth nanofibers can be produced after the critical concentration is attained. The diameters of the fibers normally decrease as the surface tension is increased. Conversely, as the polymer solution concentration and solution viscosity increase, the diameters of the fibers often increase [26].

Ambient parameters include temperature and humidity. By increasing temperature, the fibers diameters typically decrease and if the humidity increases, the fibers diameters typically increase [26].

1.2.5 Thermal energy storage applications of Phase Change Materials

Telkes and Raymond pioneered the study of phase change materials in the 1940s [27]. However, this field did not attract much attention until the late 1970s and early 1980s energy crisis, when it was actively explored for usage in various applications. A great deal of effort has gone into investigating the use of PCMs in applications, such as building air conditioning, underfloor heating, building envelope refrigeration, electronics cooling and textiles [27]. Solar energy storage systems for water heating, green houses, space heating and cooling, cooking and waste heat recovery systems are just a few of the areas that have been researched to date. [11]. PCMs can also be directly incorporated into building materials like concrete and wallboards, allowing them to be used in projects with few changes to the original design. [14]. A discussion on a few of these applications is presented in the following.

Thermal storage in buildings:

Due to the rising expense of fossil fuels and environmental concerns, TES employing PCMs for space heating and cooling is becoming more popular. Electrical energy consumption varies substantially during the day and night particularly in cold or hot places, mainly due to shifting demand for household heating or cooling. PCMs in passive and active storage systems can reduce these variances and have been extensively explored. [28]

It was around 2004 when Phase Change Materials first began to make advances into architecture. During this time period, BASF, the world's largest chemical company, developed the Micronal product. They used a microscopically small acrylic plastic sphere to encapsulate a paraffin wax storage medium. BASF claims that 5mm of its product, branded as SmartBoard by Knauf (Fig. 1.9), has the thermal mass properties of "a 140mm thick concrete wall or a 3650 mm thick brick wall" when combined in a plasterboard. They also point out that 1g of the material has a surface area of $3m^2$. The device has been tested for 10,000 phase changes without losing effectiveness, which corresponds to a 30-year life cycle, according to the manufacturer. Based on these tests, BASF is certain that their Micronal PCM will last the life of the building. [29]

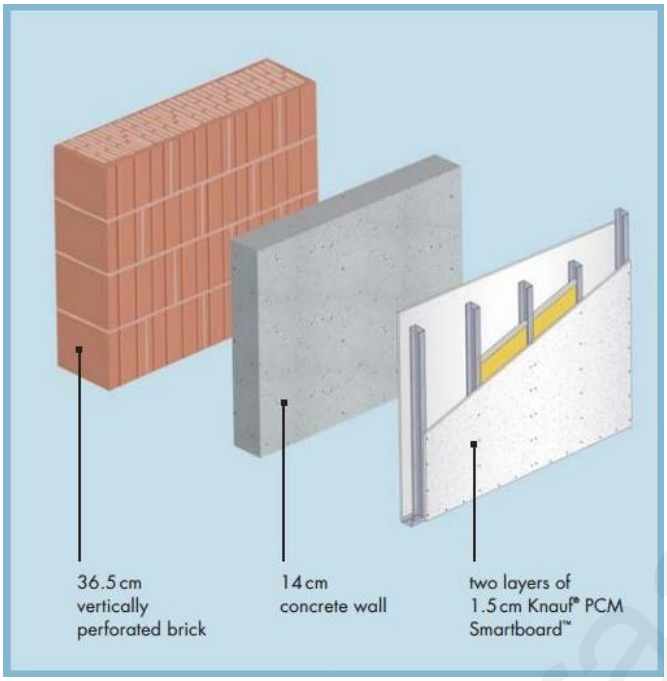

Figure 1.9: Micronal product which developed by BASF, the world's largest chemical company [29]

Tate Access Floors uses PCMs in their flooring as well. They recommend that the panels be placed around the perimeter of the structure on the sunward side. The phase change materials blended with structural cement and contained within steel welded shells absorb the increased temperature when it enters the office. When compared to a standard concrete slab floor, Tate's technology reduces air conditioning demand by 17.7%, according to their tests. [29]

Figure 1.10: Panels which were placed around the perimeter of the structure on the sunward side. [29]

Solar water heating: Solar water heaters are becoming increasingly popular as a replacement for gas or electric hot water systems. They are also cost effective and quite affordable to

manufacture and maintain [11]. TES systems, are critical for storing solar thermal energy for water heating. Using an appropriate PCM, solar-thermal energy can be stored in the form of latent heat. Integrating solar thermal heating systems with TES technology based on solid-liquid PCMs might improve the efficiency of existing solar-thermal water heating systems. The amount of heat that a PCM-equipped water tank can absorb is significantly more than that of a standard water tank filled solely with water. For solar water heating, paraffin wax (melting point: 54 °C) is a widely utilized latent heat storage PCM. [7]

Photovoltaic-Thermal: The use of PCMs to improve the overall efficiency of a Photovoltaic (PV) cell is beneficial. PV/ PCM is a new technology that combines a PV module and a PCM into a single module for thermal management of silicon-based PV cells, resulting in increased system reliability. [7]

Thermal energy storage for textile applications:
Space: Space suits and gloves using phase change materials were designed to protect astronauts from the extreme temperatures in space while also keeping them comfortable. PCM absorbs, stores, and discharges heat in response to temperature fluctuations. [30]

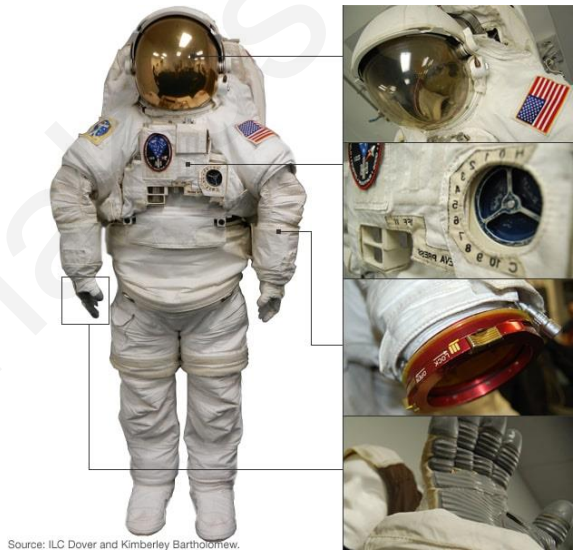

Figure 1.11 Space suits and gloves using phase change materials [31]

Sportswear: In order to improve the thermal performance of active-wear garments, clothing textiles with thermo-regulating properties are widely used [32]. PCMs with a melting point of 28–35 °C are used to make thermal-regulating fibers. When the temperature of the environment or the body rises, the PCMs in the textile fiber absorb the heat and undergo phase

transformation, storing the latent heat. The heat stored in the PCM incorporated fiber is released as soon as the ambient or body temperature start to drop, keeping the covered body in a comfortable temperature range. [28] PCMs can be found in snowboard gloves, activity wear, ice climbing, and underwear for cycling.

Microelectronics: Non-volatile memory devices frequently use PCMs based on chalcogenide glasses. Non-volatile memory (NVM) refers to memory devices that can store data even when power is turned off. It is commonly found in computers, cell phones, digital music players, and digital cameras as a supplementary storage device. These glasses undergo phase transitions from crystalline to amorphous and vice versa. Typical chalcogenide glasses, such as Ge-Se-Te, Ge-As-Se, As-S, As-Se, and others, are widely employed in non-volatile memory devices. These non-oxide glasses, which are made using chalcogen elements with unique phase change capabilities, are frequently more expensive than oxide glasses. [28]

1.2.6 Phase Change Materials – Literature Review

Electrospun form-stable PCFs contains paraffin as PCM:

Melt coaxial electrospinning was used to synthesize eicosane/ poly(vinylidene fluoride) (PVDF) core/shell nanofibers for thermal applications. The produced nanofibers had good thermal stability and a large energy-storage capacity, according to the results of differential scanning calorimetry and thermogravimetric analysis. The maximum concentration of eicosane in the electrospun core/shell nanofibers was 32.5 wt%, with a latent heat of 77 J/g at melting point of 39.2 °C. These shape-stabilized core/ shell composite nanofibers had good thermoregulating properties and high tensile strength for potential energy-storage applications, particularly in smart textiles. [33]

Coaxial electrospinning is used to create nanofibers with a phase-change component (octadecane) as the core and a hydrophobic shell (polyvinyl butyral). The ability of octadecane/ PVB nanofibers to regulate temperature is proved by measuring the surface and interior temperatures of model buildings covered with fibers. These octadecane/ PVB nanofibers have a melting enthalpy of 105.9 J g^{-1} and a crystallization enthalpy of 106.5 J g^{-1}, respectively. Under simulated solar irradiation, the PCM/ PVB nanofibers had good thermo-regulatory capabilities, regulating the temperature at around 28°C. [34]

Using the electrospinning technique, two biodegradable matrices, polycaprolactone (PCL) and polylactide (PLA), were used to encapsulate for the first time a phase changing material (PCM),

specifically dodecane (a paraffin with a transition temperature of 210°C), with the goal of developing coating materials with energy storage capacity for thermal insulation applications. In the encapsulated paraffin, a temperature mismatch between melting and crystallization events (the so-called supercooling effect) was discovered, which was attributed to the smaller PCM drop size inside the fibers. These ultrathin structured biomaterials are being investigated as energy storage systems for coating or wrapping temperature-sensitive products in refrigeration equipment, as well as for smart food and medical/pharmaceutical packaging. [35]

Other electrospun form-stable PCFs as Latent Heat Storage components:

Cai et al. reported the Lauric acid (LA)/ polyamide 6 (PA6) (100/ 100) ultrafine electrospun fibers in 2012 [36]. Lauric acid is included in the category of fatty acids. Fatty acids have been studied as a promising type of PCM due to their desired properties and characteristics, such as large capacitance, low vapor pressure of melts, non-toxicity, non-corrosiveness and high chemical and thermal stability [36]. In this case polyamide 6 (PA6) was used as the supporting material and uniaxial electrospinning was used as the technique for the fabrication of electrospun ultrafine Phase Change Fibers. The thermal properties of the fibers were studied by Differential Scanning Calorimetry (DSC) technique and DSC curves shown that the melting and cooling temperature values of composite fibers remain the same in comparison with the neat fibers. However, the heat enthalpies values increase with the increase of LA/ PA6 mass ratio.

Chen et al. reported the PEG (polyethylene glycol)/ CA (cellulose acetate) (43.2 wt%) and PEG/ CA (37.0 wt%) ultrafine composite fibers in 2013 [37]. PEG is a material that has been extensively studied as a promising type of PCM for its attractive advantages such as nontoxicity, non-corrosiveness, large enthalpies, and wide range of options of molecular weight [37]. In this case CA was used as the supporting material and coaxial electrospinning was used as the technique for the fabrication of electrospun ultrafine PCMs. The diameters of the fibers increase with increase in PEG content. After washing treatment, TEM analysis revealed that the core-shell structure was obtained using coaxial electrospinning. The thermal properties of the composite fibers with different PEG content were investigated by DSC technique. The DSC curves illustrate that the melting and cooling temperature values remain the same while the enthalpies values increase with the increase of PEG content.

Hu et al. used natural soy wax to fabricate biobased PCM in 2014 [38]. Soy wax has the same properties with paraffin waxes, but it is environmentally friendly, non-toxic, and cost effective.

In this study, Polyurethane (PU) was used as the supporting matrix and coaxial electrospinning was used as the technique for the fabrication of the composite fibers [38]. For the optimal outer layer solution, a concentration of 10 wt% was chosen. In addition, a variation between 10 wt% and 60 wt% was chosen for the concentration of the inner wax solution. Fibers with bead-free morphology were fabricated. TEM images shown that the soy wax was completely encapsulated in PU matrices and the core-shell structure was obtained using coaxial electrospinning.

1.3 Aim of Thesis

The primary objective of this M.Sc. Thesis is the fabrication of electrospun form stable Phase Change Fibers for potential use in thermal energy storage applications. PEO [Poly (ethylene oxide**)]** and PMMA [Poly (methyl methacrylate)] were used as the supporting materials for the PCFs in order to avoid the leakage of the PCM. PEO, a water soluble, semicrystalline polymer is preferred for the preparation of electrospun polymer nanofibers because it enhances the spinnability of polymer solutions. PMMA, an amorphous material with good processability and high environmental stability, attracts high attention as supporting material in PCMs because of its excellent mechanical properties and hydrophobicity. N-eicosane, a hydrocarbon with melting point near the human body temperature and high latent heat was chosen as the PCM.

The innovation of this thesis is that the present research project constitutes the first systematic study towards the fabrication and characterization of shape-stabilized PEO/ PMMA / n-eicosane PCFs. More specifically, PMMA (80/ 20) and PEO/ PMMA (50/ 50) PCFs were fabricated via the technique of uniaxial electrospinning in order to investigate the effect of PMMA content in the morphological and thermal properties of the materials. Also, PEO/ PMMA (50/ 50) beaded and bead-free electrospun fibers were fabricated and the behavior of the beaded and nead-free morphologies were investigated. Finally, the effect of n-eicosane content on the morphology and thermal properties of the form-stable PEO/ PMMA/ n-eicosane PCFs were scientifically investigated by using scanning electron microscopy (SEM) and differential scanning calorimetry (DSC).

Chapter 2

2 MATERIALS AND METHODS

2.1 Materials

Homopolymers: The two homopolymers poly (ethylene oxide) (PEO, $\overline{M_n}$= 600 000 g·mol^{-1}) and poly (methyl methacrylate) (PMMA, $\overline{M_n}$= 350 000 g·mol^{-1}) were purchased from Sigma-Aldrich and used as received from the manufacturer.

Poly (ethylene oxide) is a water soluble, semicrystalline polymer. It is preferred for the preparation of electrospun polymer nanofibers because it enhances the spinnability of polymer solutions. [39]. However, because of PEO's intrinsic hydrophilicity, using it as a fiber-forming homopolymer is challenging for many commercial technologies. When electrospun PEO microfibers come into contact with water, they vanish instantaneously. Post-crosslinking or the addition of a new fiber-forming homopolymer that is more hydrophobic and ideally entirely miscible with the PEO material can improve fiber integrity. An excellent candidate is poly(methyl methacrylate) (PMMA) [40]. The melting temperature of PEO is 65°C. Figure 2.1 shows the chemical structure of PEO.

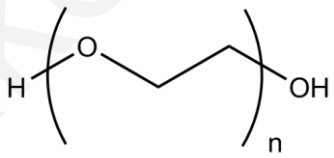

Figure 2.1: Chemical structure of PEO

Poly (methyl methacrylate) is an amorphous material with good processability, low cost, and high environmental stability compared to other synthetic hydrophobic polymers, like polystyrene and polyethylene. It can be used in a variety of fields, including lenses of glasses, windows, bullet proof security barriers, LCD screens, signs and displays [39]. PMMA as supporting material in PCMs attracts high attention because of its excellent mechanical properties and its hydrophobic nature [41] [42]. The glass temperature of PMMA is 105 °C. Figure 2.2 shows the chemical structure of PMMA.

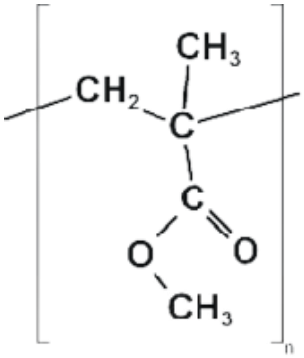

Figure 2.2: Chemical structure of PMMA

Phase Change Material: N-eicosane, 99% was purchased from Alfa Aesar and used as received from the manufacturer. N-eicosane is chemically inert and it has non-toxic and non-polluting characteristics. It has high latent heat, in comparison with other PCMs, and it has the possibility to maintain its structural integrity during repeated phase transitions without undergoing any chemical changes [43]. It has the possibility to be used in thermal regulated fibers, fabrics, foam, and thermal insulation of building materials [44]. N-eicosane has a melting point of about 34-41 °C. Figure 2.3 shows the chemical structure of n-eicosane.

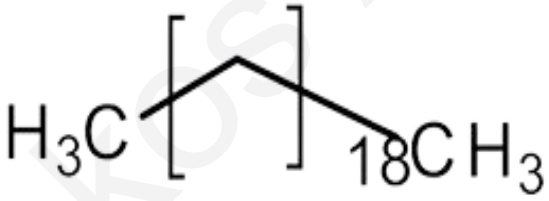

Figure 2.3: Chemical structure of n-eicosane

Solvent: Chloroform ($CHCl_3$) was used as the solvent for the preparation of all polymer solutions and it was purchased from Scharlau.

2.2 Experimental Methods

The experimental methods described below were used in the fabrication of electrospun fibers with or without the incorporation of n-eicosane as the PCM.

2.2.1 Preparation of PEO/ PMMA polymer solutions with different weight ratios

For the preparation of polymer solutions that were further used for the fabrication of electrospun PEO/ PMMA fibers, chloroform ($CHCl_3$) was used as solvent and PEO and PMMA

polymers were used as solutes. PEO/ PMMA solutions of different polymer solution concentrations (3% and 4% w/v) were prepared in chloroform. The quantities of the reactants used for the preparation of solutions are summarized in Table 2.1.

Table 2.1: The quantities of the reactants used for the preparation of PEO/ PMMA solutions with weight ratios of 100/ 0, 90/ 10, 80/ 20, 70/ 30 and 50/ 50.

Solution Code	Polymers Solution Concentration	$CHCl_3$ (ml)	PEO (g)	PMMA (g)	PEO/ PMMA weight ratio
KAv_01	3% w/v	10	0.30	0.00	100/ 0
KAv_02	3% w/v	10	0.27	0.03	90/ 10
KAv_03	3% w/v	10	0.24	0.06	80/ 20
KAv_04	3% w/v	10	0.21	0.09	70/ 30
KAv_06	3% w/v	10	0.15	0.15	50/ 50
KAv_50_50_control	4% w/v	10	0.20	0.20	50/ 50

Initially, the glass vials were placed on a high precision weighting scale and then the weighting scale was reset as shown in Fig.2.4. After that, PEO and PMMA polymers were transferred using a metallic spatula in different vials and the weights of polymers were measured using the high precision weighing scale (Fig. 2.5 and Fig. 2.6). The two polymers were transferred in the same vial with a magnetic stirring bar (Fig. 2.7) and the $CHCl_3$ solvent was added using a plastic syringe (Fig. 2.8). PEO and PMMA were dissolved in 10ml chloroform (Fig. 2.8) and a homogeneous PEO/ PMMA solution was obtain upon stirring for 1 day at room temperature (Fig.2.9).

Figure 2.4: The vials were placed on the high precision weighing scale followed by the reset of the weighing scale

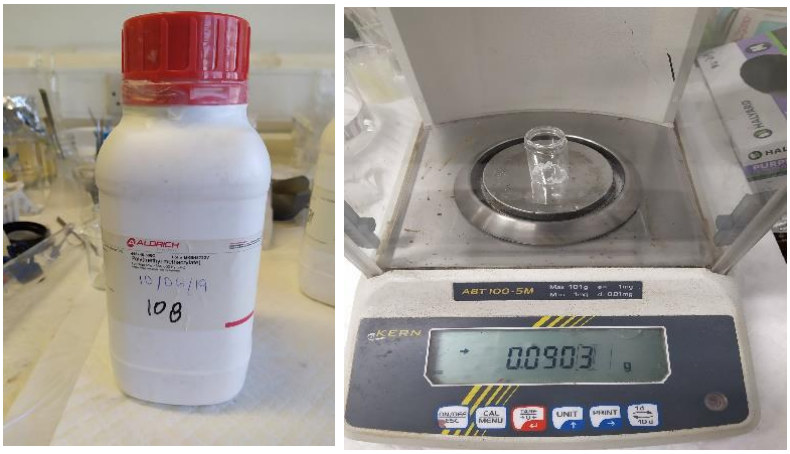

Figure 2.5: Weight measure of PMMA polymer using high precision weighing scale

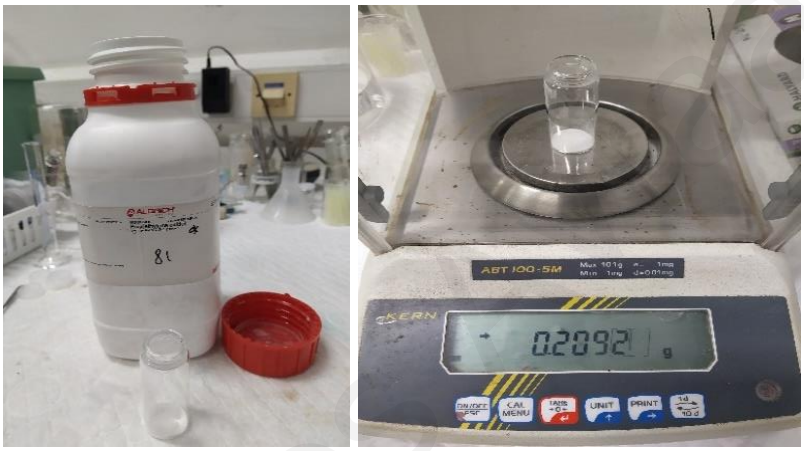

Figure 2.6: Weight measure of PEO polymer using high precision weighing scale

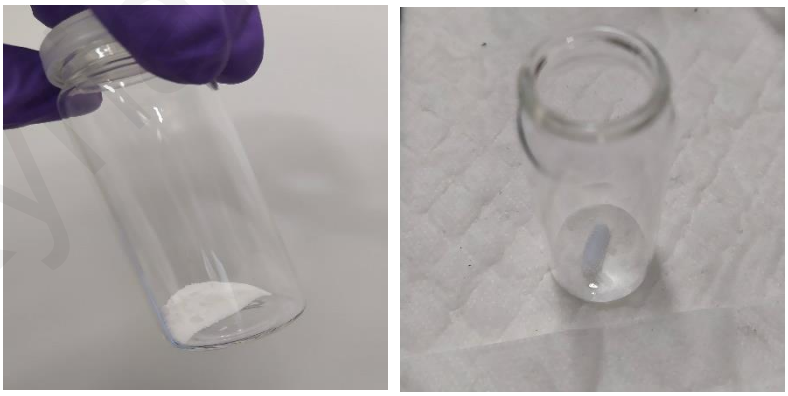

Figure 2.7: Adding the magnetic stirring bar into vial.

Figure 2.8: Measurement of chloroform using the plastic syringe.

Figure 2.9: Magnetic stirring of the prepared solution for a day at 680 rpm under ambient conditions

2.2.2 Preparation of PEO/ PMMA: 80/ 20 polymer solutions with different amounts of n-eicosane

Electrospun PEO/ PMMA fibers with 80/ 20 weight ratio were chosen for the incorporation of n-eicosane (PCM). For the preparation of polymer solutions that were used for the fabrication of electrospun PEO/ PMMA (80/20)/ n-eicosane fibers, chloroform ($CHCl_3$) was used as solvent and PEO, PMMA and n-eicosane were used as solutes. PEO/ PMMA/ n-eicosane solutions with PEO/ PMMA weight ratio of 80/20 and different n-eicosane concentrations were prepared in chloroform. The PCM content was calculated in respect to the total polymer mass (PEO/ PMMA).

The same experimental approach as described in the subsection 2.2.1 was used to prepare PEO/ PMMA (80/20)/ n-eicosane solutions, with n-eicosane (PCM) being added in different percentages in the different polymer solutions (Fig.2.10), as shown from the quantities of all reactants appearing in Table 2.2.

Table 2.2: The quantities of the reactants used for the preparation of PEO/ PMMA (80/ 20) polymer solutions with n-eicosane concentrations of 2, 5, 7.5 and 10, 15 and 20% wt.

Solution Code	Polymers Solution Concentration	$CHCl_3$ (ml)	PEO (g)	PMMA (g)	PEO/ PMMA weight ratio	N-Eicosane (g)	% N-Eicosane
KAv_07	3% w/v	10	0.24	0.06	80/20	0.006	2
KAv_08	3% w/v	10	0.24	0.06	80/20	0.015	5
KAv_09	3% w/v	10	0.24	0.06	80/20	0.0225	7.5
KAv_10	3% w/v	10	0.24	0.06	80/20	0.03	10
KAv_11	3% w/v	10	0.24	0.06	80/20	0.045	15
KAv_12	3% w/v	10	0.24	0.06	80/20	0.06	20

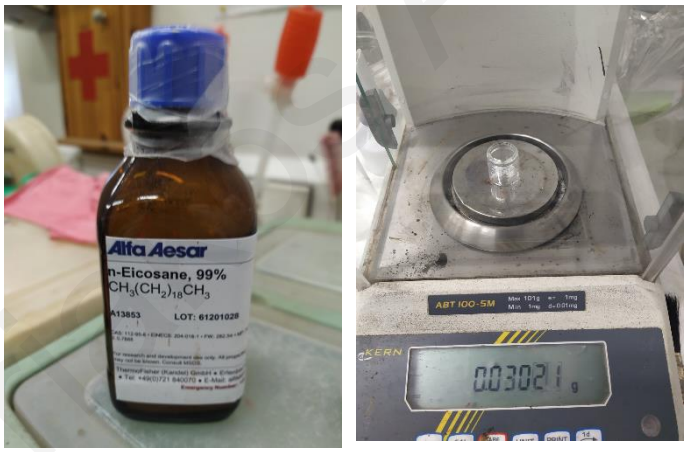

Figure 2.10: Weight measure of PEO polymer using a high precision weighting scale

2.2.3 Preparation of PEO/ PMMA: 50/ 50 polymer solutions (3% w/v polymer concentration) with different amounts of n-eicosane

Electrospun PEO/ PMMA beaded fibers with 50/ 50 weight ratio were chosen to be used as matrices for the incorporation of n-eicosane (PCM). PEO/ PMMA/ n-eicosane solutions with PEO/ PMMA weight ratio of 50/ 50 and different n-eicosane concentrations were prepared in

chloroform. The PCM content was calculated in respect to the total polymer mass (PEO/ PMMA).

To prepare PEO/ PMMA (50/50)/ n-eicosane solutions, the same experimental approach as the one described in subsection 2.2.2 was applied, but instead, a 50/ 50 polymer weight ratio was used, as shown in Table 2.3.

Table 2.3: The quantities of the reactants used for the preparation of PEO/ PMMA (50/ 50) electrospun beaded fibers with 3% w/v polymer concentration and different n-eicosane concentrations of 7.5, 10, 15 and 20% wt.

Solution Code	Polymers Concentration	$CHCl_3$ (ml)	PEO (g)	PMMA (g)	Polymers weight ratio	N-Eicosane (g)	% N-Eicosane
KAv_50_50_7.5b	3% w/v	10	0.15	0.15	50/50	0.0225	7.5
KAv_50_50_10b	3% w/v	10	0.15	0.15	50/50	0.03	10
KAv_50_50_15b	3% w/v	10	0.15	0.15	50/50	0.045	15
KAv_50_50_20b	3% w/v	10	0.15	0.15	50/50	0.06	20

2.2.4 Preparation of PEO/ PMMA: 50/ 50 polymer solutions (4% w/v polymer concentration) with different amounts of n-eicosane:

Electrospun PEO/ PMMA non-beaded fibers with a weight ratio 50/ 50 are the last material that was chosen for the incorporation of n-eicosane (PCM). The quantities of PEO, PMMA and n-eicosane used are summarized in Table 2.4. The phase change material was used in variable percentages in the different solutions, and the same experimental approach was used to fabricate PEO/ PMMA (50/ 50)/ n-eicosane solutions with a 4% w/v polymer solution concentration.

Table 3.4: The quantities of the reactants used for the preparation of PEO/ PMMA (50/ 50) electrospun non-beaded fibers with 4% w/v polymer solution concentration and different n-eicosane concentrations of 10, 15, 20 and 25% wt.

Solution Code	Polymers Solution Concentration	$CHCl_3$ (ml)	PEO (g)	PMMA (g)	Polymers weight ratio	Eicosane (g)	% Eicosane
KAv_50_50_10	4% w/v	10	0.20	0.20	50/50	0.04	10
KAv_50_50_15	4% w/v	10	0.20	0.20	50/50	0.06	15
KAv_50_50_20	4% w/v	10	0.20	0.20	50/50	0.08	20
KAv_50_50_25	4% w/v	10	0.20	0.20	50/50	0.10	25

2.2.5 Electrospinning

As mentioned previously, electrospinning is one of the most powerful techniques used in the fabrication of nano/microfibers. A typical experimental setup consists of a high voltage source, two electrodes, syringe with metallic needle, pump for the control of the flow rate and a collector where the fibers are collected. Figure 2.11 shows the custom-made experimental setup of electrospinning which is located in the Department of Mechanical and Manufacturing Engineering at the University of Cyprus.

The basic electrospinning process is that the positive electrode of the high voltage source is connected to the metallic needle while the negative electrode is connected to the grounded collector. Thus, the application of a high potential to the polymeric solution (5-40kV) leads to the generation of charged droplets of the polymeric solution at the needle's tip. A charged jet is ejected from the tip of the droplet when the electrostatic repulsive forces overcome the surface tension of the polymer solution at a critical voltage, and it is directed towards a grounded electrode. The solvent quickly evaporates during this ejection, resulting in solidification and the collecting of nano/microfibers on the collector [26].

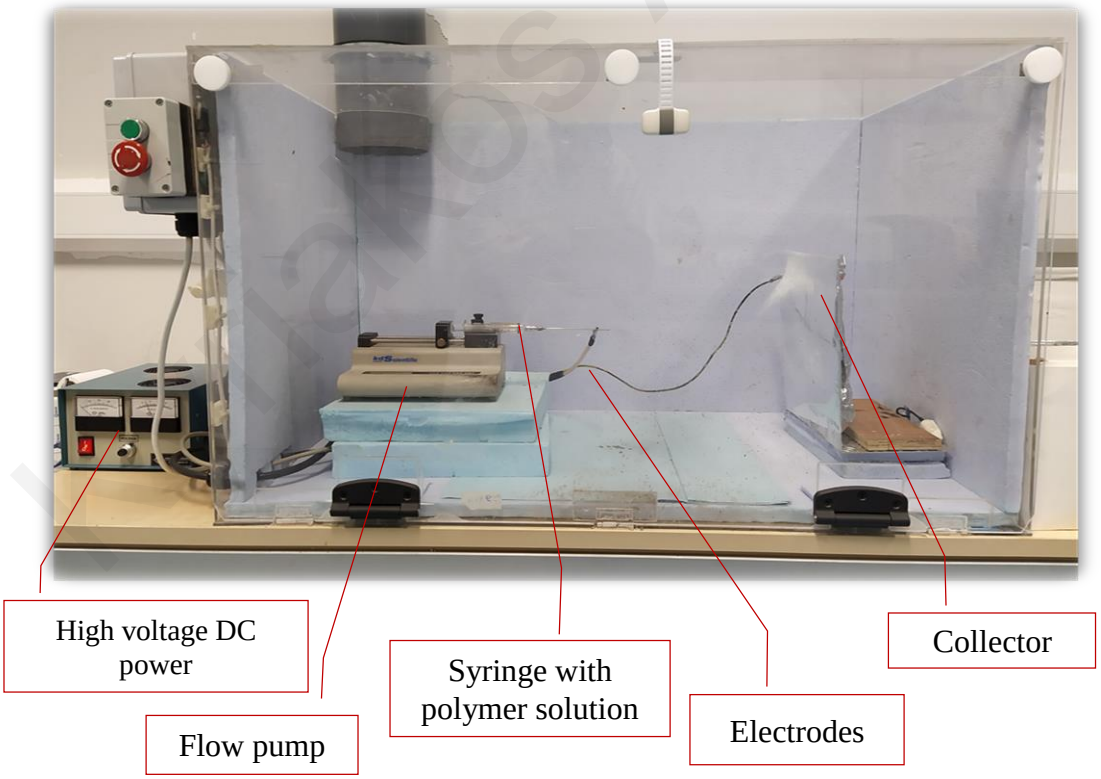

Figure 2.11: Electrospinning setup located in the Department of Mechanical and Manufacturing Engineering,University of Cyprus

In the present study, the electrospun PEO/ PMMA membranes with and without n-eicosane were fabricated by using the uniaxial electrospinning technique. Systematic parametric studies were carried out in order to determine the optimum experimental conditions for obtaining fibrous membranes. The polymer solutions were located into a 10 ml glass syringe that was connected with metallic needle with diameter of 18G. The syringe was placed on a pump with a flow rate of (4.3 ml/hr). Electric potential of 10 kV and distance of 30 cm between the tip at the edge of the syringe and the collector were applied. The polymer membranes were collected on the collector with solvent evaporation (Fig. 2.12). All equipment was placed inside an interlocked Faraday enclosure safety cabinet as shown in Figure 2.11.

Figure 2.12: Example of a polymer membrane

2.3 Characterization Methods

2.3.1 Scanning Electron Microscopy (SEM)

Scanning Electron Microscopy (SEM) is a high-resolution tool that can investigate and analyze surface phenomena of materials but does not provide any interior information. It is regarded as a potent tool for assessing the sample's crystallographic, magnetic, and electrical properties, as well as determining whether any morphological changes in a material occur as a result of modifying the sample surface with other molecules. In other words, it offers information about the sample's surface characteristics and texture, as well as the shape, size, and arrangement of the particles. The type of elements and compounds present in the sample and their relative ratios, can be reported, as well as the arrangement of atoms in single crystal particles and their degree of order. [45]

The SEM instrument is based on the principle that the primary electrons generated from the source provide energy to the atomic electrons in the specimen, which can subsequently be

released as secondary electrons (SEs). Heating or applying high energy in the range of 1-40 keV accelerates the primary electrons produced and released by the electron cannon. Scanning coils in a raster pattern scan the restricted primary electrons across the sample surface. Magnetic field lenses and metal slits within a vacuumed column focus and confine the released electrons to a monochromatic beam (with a diameter of 100 nm or less). The impinging electrons, which have been driven towards the specimens, have a lot of kinetic energy, and they lose it inside the sample by creating numerous signals from their interactions with the specimen. Electrons scatter both elastically and inelastically in the sample, and by collecting secondary electrons from each location in the specimen, an image can be produced. To achieve great resolution, SEM must operate in a vacuum to avoid electron interactions with gas molecules. [45]

Backscattered and secondary electrons are the two types of electrons that are commonly employed to create sample images. After elastic interactions occurring between the beam and the sample, backscattered electrons are reflected. Secondary electrons are produced by inelastic interactions between the electron beam and the sample, and they originate from the sample's atoms. The most relevant electrons are secondary electrons, which indicate sample morphology and topography, whereas backscattered electrons are employed to show contrasts in multiphase sample composition. [45]

Scanning electron microscopy (Vega TS5136LS- Tescan) was an important tool (Fig. 2.14) in the present study for the morphological characterization of the produced polymer-based fibrous membranes. Because the polymers are not conductive materials, prior to SEM inspection, the samples were gold sputtered using the sputtering system “K575X Turbo Sputter Coated-Emitech, Bal- tec SCD 500” (Fig. 2.13)

A small amount of material was fixed on carbon tape that was attached on the sample holder. Then, the sample holder was placed into the chamber of the sputter coating system. A gas vacuum was created by opening the argon gas valve, and the device was started by selecting the desired working settings. The running period was set to 2.5 minutes, and the supply current was set to 80 mA in all the samples. The device was turned off and the samples were removed after a thin layer of gold was applied to the surface of the samples.

Figure 3.13 Sputtering system (K575X Turbo Sputter Coated- Emitech, Bal- tec SCD 500) which is located in the Department of Mechanical and Manufacturing Engineering at the University of Cyprus.

Figure 2.14: Scanning electron microscopy (Vega TS5136LS- Tescan) which is located in the Department of Mechanical and Manufacturing Engineering at the University of Cyprus.

The microscope chamber was filled with nitrogen gas after the samples were coated with a thin layer of gold. The software determined the device's working settings, and the samples were placed in the available positions within the microscope chamber. The microscope is initially in HOME mode, with the sample at a distance of 40mm above it (Z = 40). Working Distance (WD), scan speed, probe current, acceleration voltage and magnification were among the properties of the electron beam that were adjusted. High voltage of 10kV and Emission of 72mA were used.

2.3.2 Differential Scanning Calorimetry

To ensure the storage unit's long-term performance, changes in the thermo-physical properties of potential PCMs should be detected after a series of temperature cycles. Upon applying this thermal cycling process, a PCM is considered trustworthy if it remains thermally, chemically, and physically stable. Solar applications are the most popular use for PCM-based energy storage units. Every day, at least one melt/freeze thermal cycle occurs in a solar thermal system with latent heat storage. If the melting point and latent heat of fusion of a PCM do not vary significantly after multiple operating thermal cycles, PCM is thermally stable for latent heat storage applications. As a result, it is always preferable to ensure PCM thermal stability for the latent heat storage unit's long-term performance. [27]

The differential scanning calorimetry (DSC) technique is the most frequent method used by researchers to determine the thermal characteristics of PCMs, such as the melting point and latent heat of fusion. DSC is a thermo-analytical technique in which the difference in the amount of heat required to raise the temperature of a sample and reference is measured as a function of temperature. Throughout the experiment, both the sample and the reference are kept at nearly the same temperature. The heat capacity of the reference sample should be clearly specified over the temperature range to be scanned. The essential concept of this technique is that when a sample undergoes a physical transformation, such as phase transitions, more or less heat is required than the reference to keep both at the same temperature. Whether the process is exothermic or endothermic determines whether less or more heat flow is required to the sample. Differential scanning calorimeters can quantify the amount of heat received or released during such transitions by monitoring the difference in heat flow between the sample and the reference. The plot between heat flow and temperature is then constructed to generate the DSC curve. [27]

The area under the peak is used to determine the latent heat of fusion. The commencement of the phase transition temperature is determined by line fitting the rising section of the peak. Between the onset temperature and the temperature corresponding to the curve's peak, the phase transition range is determined. In summary, the thermo-physical properties of PCMs, such as melting point and latent heat of fusion, may be determined using DSC. The observed variations in these parameters after a number of heat cycles can support the PCM's stability. [27]

DSC test on organic paraffins: Organic PCMs melt and freeze without phase separation. They crystallize without (or with a little) supercooling and are usually non-corrosive. Paraffins and non-paraffins are the two types of organic PCMs. [27]

Normal paraffins of type C_nH_{2n+2} belong to a group of saturated hydrocarbons with nearly identical characteristics. The melting temperature and latent heat of fusion increase as the "n" increases. The most popular commercial organic heat storing PCM is paraffin wax. It is mostly made up of linear chain hydrocarbons with melting temperatures ranging from 23℃ to 67℃ [27]. Due to their high heat of fusion, various phase change temperatures, little supercooling, reduced vapor pressure in a melt, and chemically inert and stable behavior, paraffins have been widely exploited for thermal energy storage. They are also available commercially at a reasonable price. These PCMs are non-toxic and environmentally friendly. Paraffins are widely accessible from a variety of suppliers. [27]

In the present study the thermal characterization of the produced fibers was performed at the Aristotle University of Thessaloniki, under the supervision of Prof. Konstantinos Chrissafis, using differential scanning calorimetry (DSC). More precisely, DSC was used to evaluate the melting and cooling temperature, latent heat of fusion, degree of supercooling and materials' thermal stability.

The Differential Scanning Calorimeter (DSC 214 Polyma, Netzsch, Thessaloniki, Greece), with precision and thermal accuracy of ± 2.00%, has been used to perform the analysis of heat flow for all the samples. To investigate the thermal stability of the as-prepared membranes, these were weighed using precision electronic balance, at an accuracy of 0.01 mg, and placed in aluminum concavus pans and lids. High purity nitrogen was supplied at a flow rate of 40 ml/min during the experiment. The samples were heated and cooled at a scanning rate of 5°C/min and the process was conducted consecutively for 30 cycles. A thermal cycle test has

been carried out in a thermostatic oven between 5 °C and 44 °C or 5 °C and 90 °C. The complete DSC setup is illustrated in Fig.2.15. DSC thermograms were generated and analyzed using Origin software.

Figure 2.15: Differential Scanning Calorimeter (DSC 214 Polyma, Netzsch) which is located in the Advanced Materials & Devices Laboratory at Aristotle University of Thessaloniki

Chapter 3

3 RESULTS AND DISCUSSION

The goal of this project, as mentioned in the Introduction part, is to fabricate electrospun Phase Change Fibbers (PCF) for potential use in thermal energy storage applications. To ensure enhanced thermal and mechanical properties of the PCMs, the diameters of these fibers were kept in the order of nano or micrometres.

These materials were characterized in respect to their chemical composition, morphology and thermal properties using a variety of materials characterisation techniques. Scanning electron microscopy (SEM) was an important tool for the morphological characterization of the polymer membranes. Differential scanning calorimetry (DSC) was used to determine the thermo-physical properties of the produced PCFs, such as melting and cooling point, latent heat of fusion and degree of supercooling. The observed variations in these parameters after a number of heat cycles can support the PCF's stability and reliability.

3.1 Characterization

3.1.1 Morphological characterization of the PEO electrospun fibrous membranes.

Fig. 3.1 shows the morphology of the PEO polymeric fibers as revealed from SEM characterization. As seen, continuous smooth fibers with bead-free morphology could be formed under the following parameters: 3% w/v was chosen as polymer solution concentration, voltage was set at 10 kV, the flowing rate was set at 3 mL/h, the diameter of the needle was 18G (1.27mm) and the needle-to-collector distance was set at 30cm. Pure PEO fibers with an average diameter of 5.085 ± 0.532 μm were obtained.

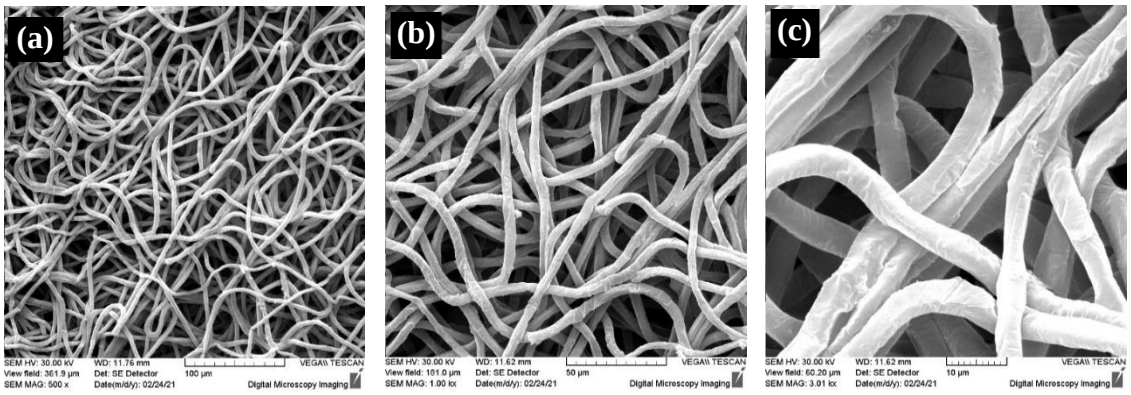

Figure 3.1: SEM images of electrospun PEO polymeric membranes. Scale bars (a): 100μm, (b): 50μm, (c): 10μm

3.1.2 Morphological characterization of PEO/PMMA electrospun fibrous membranes.

Blended fibers consisting of PEO and PMMA were fabricated by means of the electrospinning technique. The compositions of the fibers were modulated simply by varying the PEO/ PMMA weight ratio. Both PEO and PMMA are soluble in chloroform. Characteristic SEM images of blended fibers with PEO/PMMA weight ratios of 90/ 10, 80/ 20, 70/ 30 and 50/ 50 are provided in figures 3.2, 3.3, 3.4 and 3.5, respectively. The electrospinning parameters are the same as for the PEO electrospun membranes mentioned in subsection 3.1.1.

In the first three samples, the fibers were characterized by relatively smooth surfaces. However in the case where the weight ratio of PEO/ PMMA was 50/ 50, the fibers' surface roughness was enhanced and bead-on-string morphologies could be observed (Fig. 3.5). Surface roughness might be more pronounced upon increasing the PMMA content within the fibers, due to phase separation phenomena occurring between the 2 incompatible polymers (i.e. the hydrophobic PMMA and the hydrophilic PEO).

3.1.2.1 **Electrospun fibers fabricated starting from 3% w/v polymer solutions.**

PEO/ PMMA (weight ratio 90/ 10).

As seen in Fig. 3.2, continuous, bead-free PEO/ PMMA fibers with average diameter of 2.035 ± 0.547 μm were obtained starting from a 3% w/v PEO/ PMMA solution.

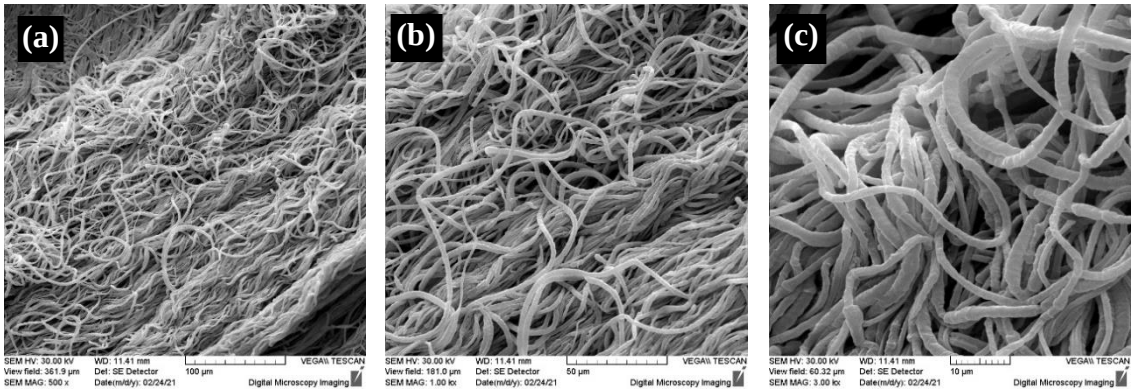

Figure 3.2: SEM images of PEO/ PMMA (weight ratio 90/ 10) electrospun polymeric membranes. Scale bars (a): 100μm, (b): 50μm, (c): 10μm

PEO/ PMMA (weight ratio 80/ 20).

Similarly, as seen in Fig. 3.3, PEO/ PMMA fibers with average diameter of 2.137 ± 0.532 μm were obtained upon electrospinning of a 3% w/v PEO/ PMMA solution.

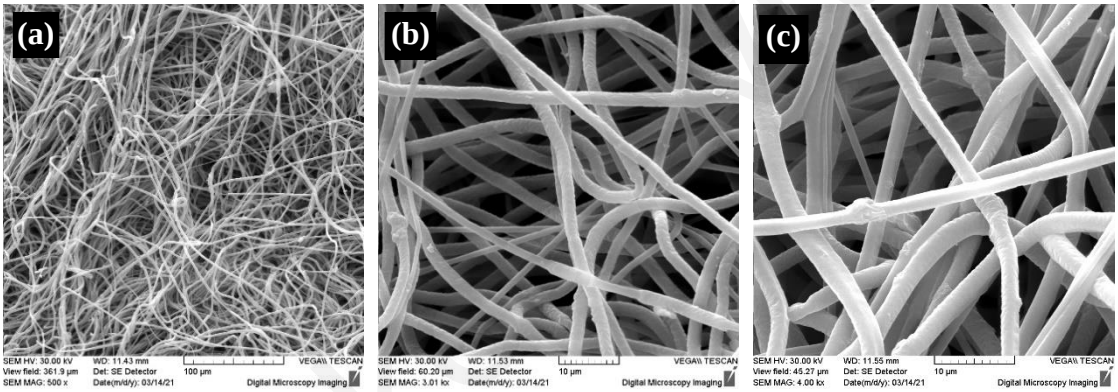

Figure 3.3: SEM images of PEO/ PMMA (weight ratio 80/ 20) polymeric membranes. Scale bars (a): 100μm, (b): 10μm, (c): 10μm

PEO/ PMMA (weight ratio 70/ 30).

From Fig. 3.4, PEO/ PMMA fibers with average diameter of 3.787 ± 0.979 μm were obtained starting from PEO/ PMMA solutions having the same polymer solution concentrations as in the previous cases (i.e. 3% wt.).

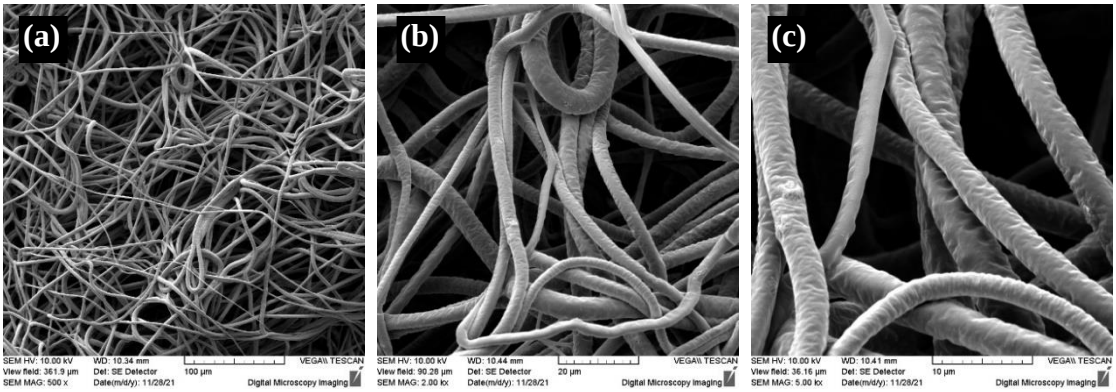

Figure 3.1.4: SEM images of PEO/ PMMA (weight ratio 70/30) electrospun polymeric membranes. Scale bars (a): 100μm, (b): 20μm, (c): 10μm

PEO/ PMMA (weight ratio 50/ 50).

As mentioned, in the case of the 50/50 PEO/PMMA systems, beaded structures were obtained from 3% w/v PEO/PMMA solution, as shown in Fig. 3.5.

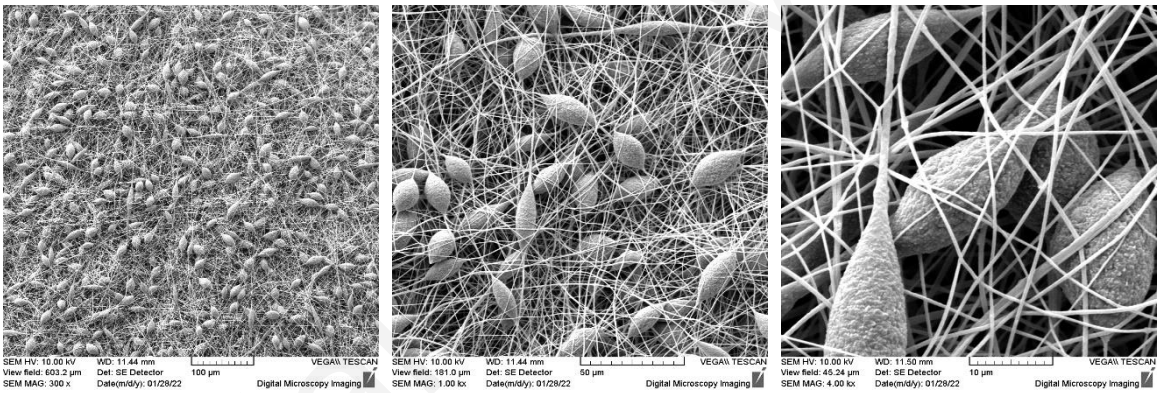

Figure 3.5: SEM images of PEO/ PMMA (weight ratio 50/ 50) electrospun polymeric membranes. Scale bars (a): 100μm, (b): 20μm, (c): 10μm

In all cases, the diameters of fibers with various weight ratios were determined using the ImageJ software. The findings of the diameters that were measured for fifty different diameter dimensions of each example are provided in Table I (APPENDIX I). Table 3.1 shows the mean diameters of blended electrospun PEO/PMMA fibers. By comparing the values corresponding to each system we may conclude that as the PMMA content of the fibers increased, the diameters of the fibers increased as well (Figure. 3.6).

Table 3.1: Mean Diameters of fibers with different PEO/ PMMA weight ratios (μm).

PEO/ PMMA 100/ 0	PEO/ PMMA 90/ 10	PEO/ PMMA 80/ 20	PEO/ PMMA 70/30
5.085 ± 0.532	2.0346 ± 0.547	2.137 ± 0.532	3.787 ± 0.979

Fig. 3.6: Increased fiber diameter upon decreasing PEO/ PMMA weight ratio

3.1.2.2 **Electrospun fibers fabricated from 4% w/v polymer solutions.**

For the fabrication of electrospun PEO/ PMMA (50/ 50) fibers without beads (bead-free morphology), the experimental parameters were changed in comparison to the previous experiment (Fig. 3.5). More precisely, the generation of a bead-free fibrous morphology is achieved by increasing the polymer concentration from 3% w/v to 4% w/v. Fig. 3.7 shows the PEO/ PMMA (50/ 50) non-beaded fibers which were obtained starting from 4% w/v PEO/PMMA solution.

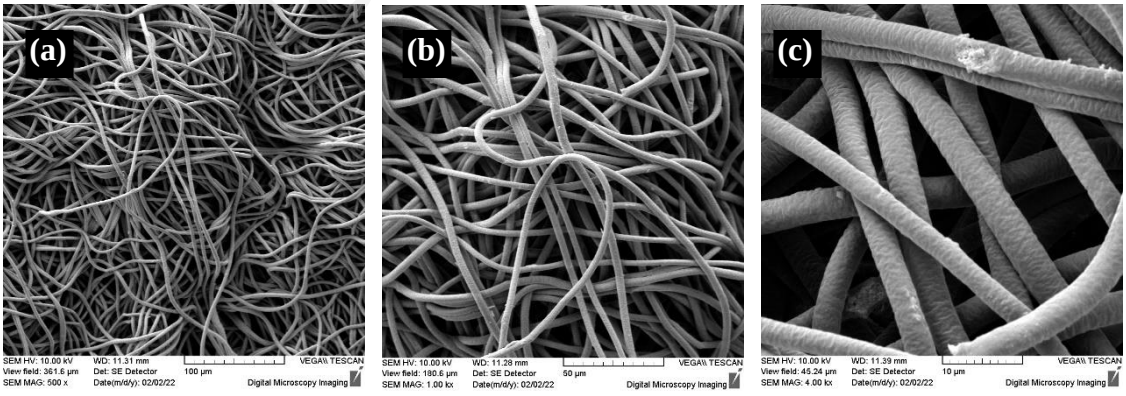

Figure 3.7: SEM images of bead-free PEO/ PMMA (mass ratio 50/50) polymeric membranes. Scale bars (a): 100μm, (b): 50μm, (c): 10μm

3.1.3 Morphological characterization of electrospun fibrous membranes PEO/ PMMA (weight ratio 80/ 20)/ n-eicosane starting from 3% w/v polymer solution concentration

The electrospun PEO/ PMMA fibers with an 80/20 weight ratio were chosen as the first material for PCM incorporation. In comparison to fibers with 70/30 weight ratio, these fibers have a higher aspect ratio and homogeneity. In addition, PEO/PMMA fibers with 80/20 weight ratio have higher PMMA content than those with 90/10 weight ratio. The presence of PMMA is considered to be significant since it promotes the development of hydrophobic interactions with the hydrophobic n-eicosane molecules to be incorporated within the fibers as the phase change component. The morphological characteristics of electrospun PEO/PMMA PCFs with variable n-eicosane content are shown in the SEM images provided in Figures 3.8 - 3.12 (2-20% wt. n-eicosane). The PCM content was calculated in respect to the total polymer mass (PEO/ PMMA) in all samples.

PEO/ PMMA (weight ratio 80/ 20)/ 2% wt. n-eicosane.

Homogeneous PEO/ PMMA/ n-eicosane fibers without beads exhibiting surface roughness were obtained starting from a polymer solution containing 2% wt. n-eicosane content in respect to the total polymer mass. (Fig 3.8). The mean diameter of PEO/ PMMA (80/ 20)/ n-eicosane 2% wt. fibers is 5.000 ± 0.532 μm.

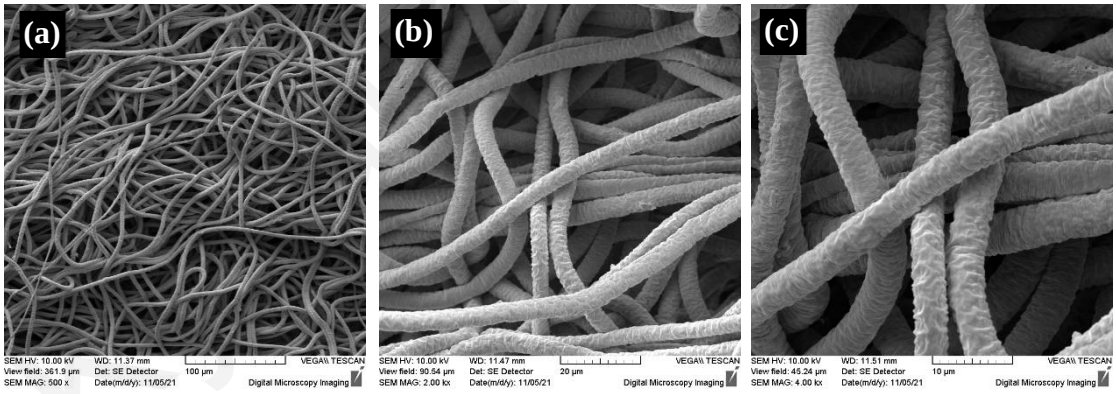

*Figure 3.8: SEM images of PEO/ PMMA/ n-eicosane **2% wt.** phase change fibrous membranes. Scale bars (a): 100μm, (b): 20μm, (c): 10μm*

PEO/ PMMA (weight ratio 80/ 20)/ 5%wt. n-eicosane.

As in the case of the PCF with 2% wt. n-eicosane content, homogeneous PEO/ PMMA/ n-eicosane fibers without beads and with surface roughness were obtained by electrospinning, starting from the polymer solution with 5% wt. n-eicosane content (Fig 3.9). The mean diameter of PEO/ PMMA (80/ 20)/ 5% wt. n-eicosane fibers is 3.719 ± 0.413 μm.

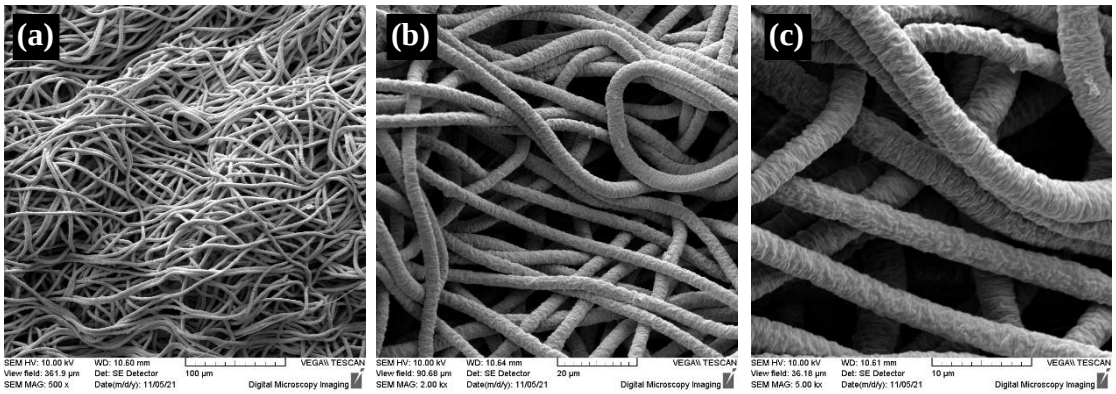

*Figure 3.9: SEM images of PEO/ PMMA/ n-eicosane **5% wt**. phase change fibrous membranes. Scale bars (a): 100μm, (b): 20μm, (c): 10μm*

PEO/ PMMA (weight ratio 80/ 20)/ 7.5% wt. n-eicosane.

PEO/ PMMA/ n-eicosane fibers without beads and with surface roughness were electrospun using a polymer solution with 7.5% wt. n-eicosane content (Fig 3.10). The mean diameter of PEO/ PMMA (80/ 20)/ 7.5% wt. n-eicosane fibers is 5.080 ± 1.717 μm.

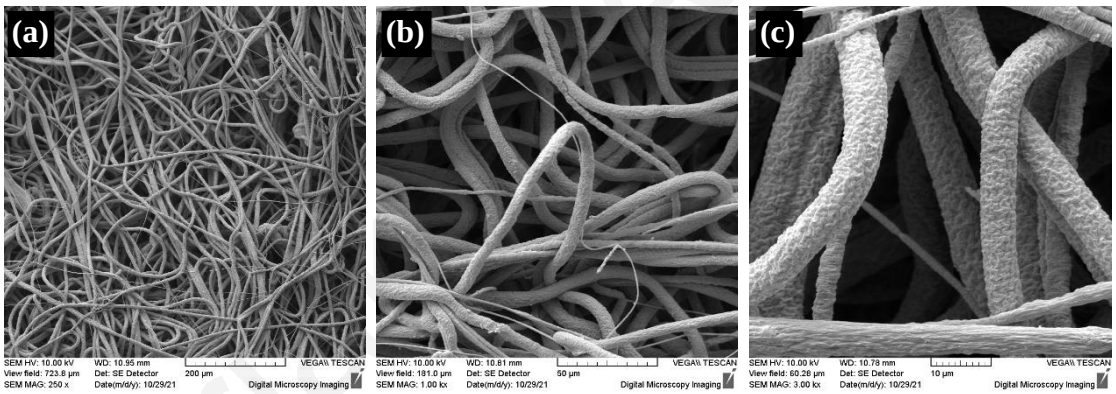

*Figure 3.10: SEM images of PEO/ PMMA/ n-eicosane **7.5% wt**. phase change fibrous membranes. Scale bars (a): 100μm, (b): 50μm, (c): 10μm*

The diameters of the fibers changed when the concentration of PCM was increased (Figure 3.13). This phenomenon might be related to changes in the characteristics of the solution, such as a considerable rise in solution viscosity as a result of the addition of n-eicosane to the polymer solution.

PEO/ PMMA (weight ratio 80/ 20)/ 10% wt. n-eicosane.

The quantity of n-eicosane that was distributed on the surface of the PEO/PMMA fibers increased as the PCM concentration increased (Figure 3.11). The mean diameter of PEO/ PMMA (mass ratio 80/ 20)/ 10% wt. n-eicosane fibers is 2.444 ± 0.444 μm.

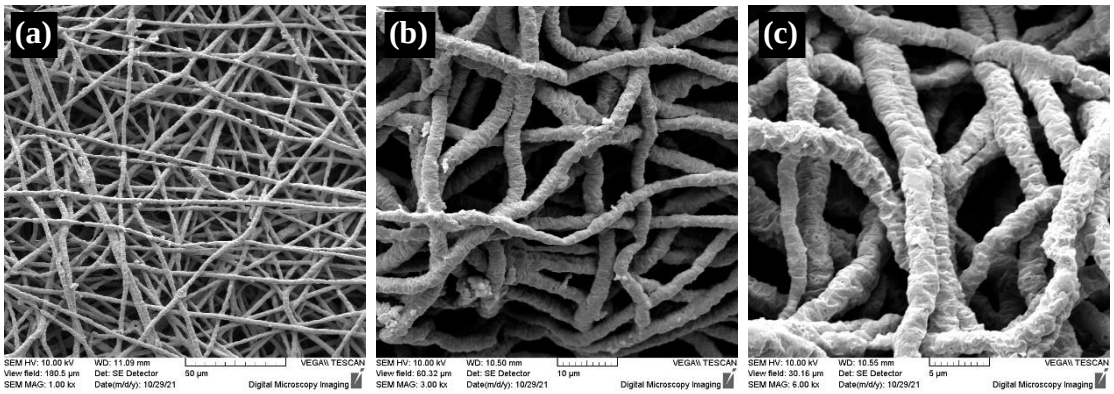

*Figure 3.11: SEM images of PEO/ PMMA/ n-eicosane **10% wt**. phase change fibrous membranes. Scale bars (a): 100μm, (b): 10μm, (c): 5μm*

PEO/ PMMA (weight ratio 80/ 20)/ 15% wt. n-eicosane.

In the case of the PEO/ PMMA/ 15% wt. n-eicosane fibers, non-uniform fiber morphologies were observed along the fiber axis due to the increase of the n-eicosane concentration (Fig. 3.12). Moreover, the fibers are characterized by high surface roughness. The mean diameter of PEO/ PMMA (mass ratio 80/ 20)/ n-eicosane 15% wt. fibers is 2.916 ± 1.046 μm.

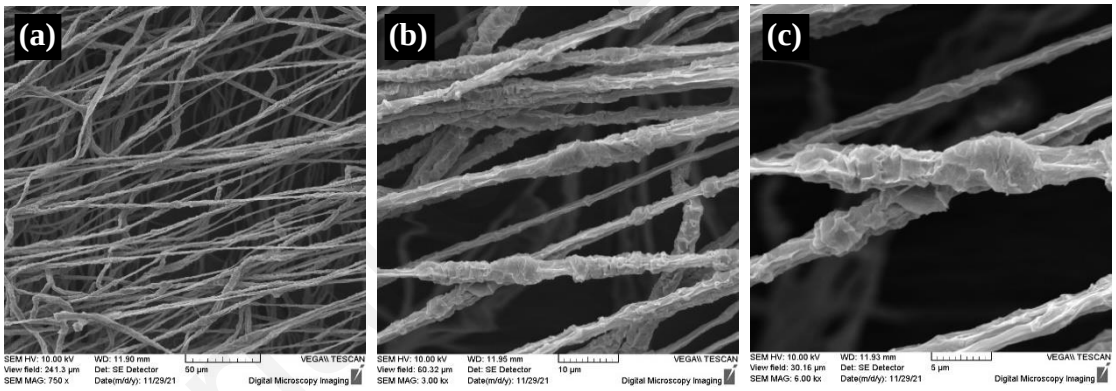

*Figure 3.12: SEM images of PEO/ PMMA/ n-eicosane **15% wt**. phase change fibrous membranes. Scale bars (a): 50μm, (b): 10μm, (c): 5μm*

Using ImageJ software, the diameters of the produced PCFs with n-eicosane content ranging from 2% wt. to 15% wt. were measured and they are listed in Table 2 (Appendix I). Table 3.2 shows the mean diameters of these fibers, and Figure 3.13 shows the mean diameters of the PCFs as a function of n-eicosane content. Lower n-eicosane contents (2, 5 &7.5% wt.) result in higher values of the mean fiber diameters while higher n-eicosane contents (10 & 15% wt.) promote the generation of fibers having smaller diameters. The diameters of the fibers may decrease due to the variations of the solutions properties occurring upon increasing the n-eicosane content. Moreover, in order to accommodate higher n-eicosane percentage, PEO/

PMMA (80/ 20) fibers tend to increase in length. Consequently, as fiber length increases, the diameter of the fibers decreases.

Table 3.2: Mean diameters for the PEO/ PMMA (80/ 20) fibers with variable n-eicosane content ranging from 2% wt. to 15% wt.

Mean Diameters of fibers with different PEO/ PMMA mass ratios (μm)				
2% wt. eic.	**5% wt. eic.**	**7.5% wt. eic.**	**10% wt. eic.**	**15% wt. eic.**
5.000 ± 0.532	3.719 ± 0.413	5.080 ± 1.717	2.444 ± 0.444	2.916 ± 1.046

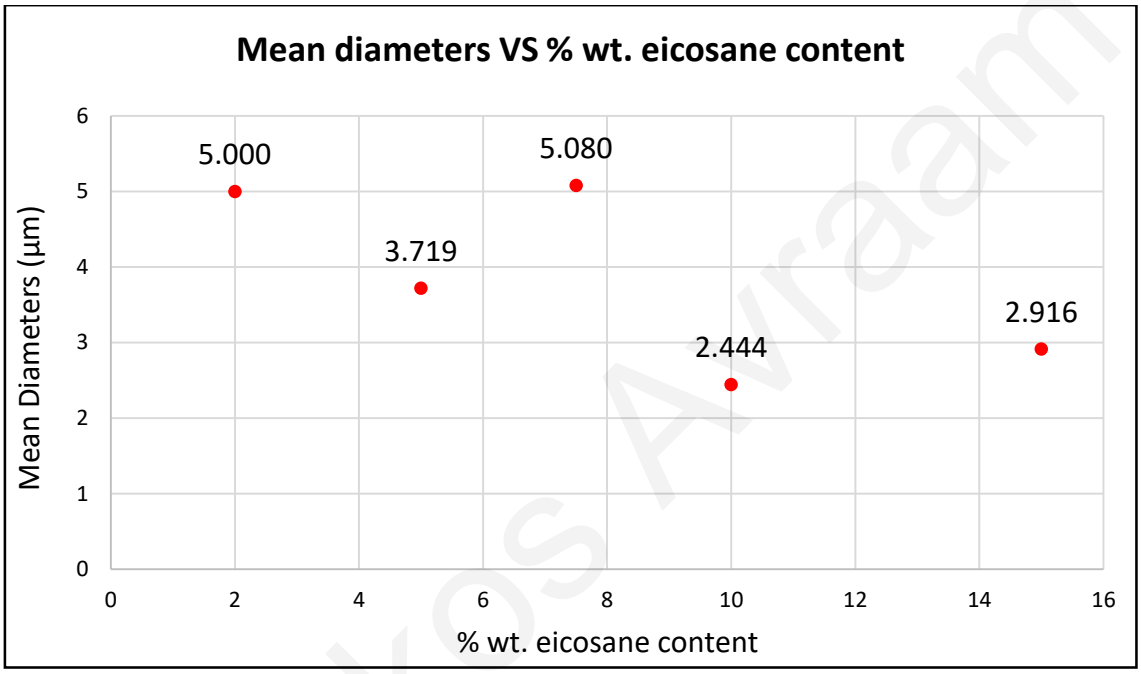

Figure 3.13: Mean diameters of the PEO/ PMMA (80/ 20) PCFs as a function of different n-eicosane content.

PEO/ PMMA (weight ratio 80/ 20)/ 20% wt. n-eicosane.

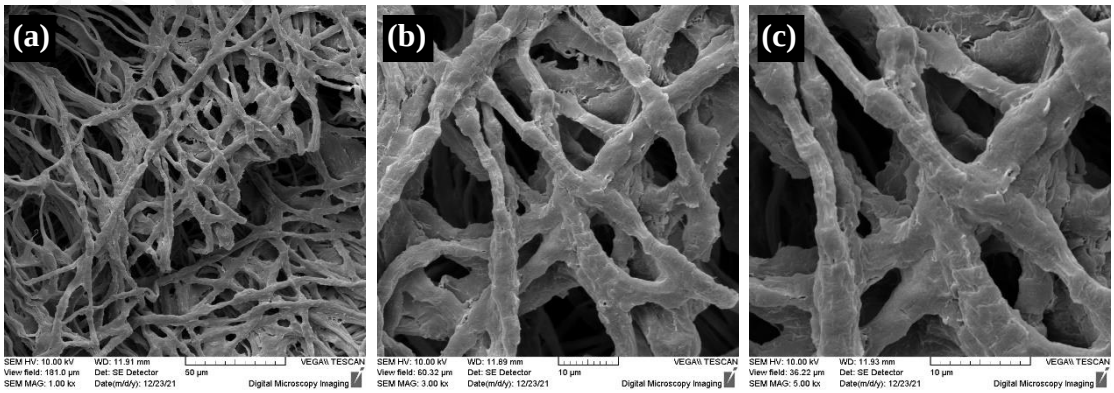

*Figure 3.14: SEM images of PEO/ PMMA/ n-eicosane **20% wt**. phase change fibrous membranes. Scale bars (a): 50μm, (b): 10μm, (c):10μm*

When n-eicosane reaches a maximum content of 20% wt., the fibrous membrane is covered by an n-eicosane thin layer and many tubercles can be observed onto the fibers' surfaces (Fig. 3.14). These are caused by aggregation phenomena occurring due to the presence of the excessive n-eicosane on the fibers' surfaces during the electrospinning process. Therefore, the incorporation of more than 20% wt. n-eicosane within PEO/PMMA blended fibers (80/20) is unfavorable for obtaining uniform, ultrafine PEO/ PMMA/ n-eicosane PCFs.

3.1.4 Morphological characterization of electrospun PEO/ PMMA (weight ratio 50/ 50)/ n-eicosane beaded fibers starting from 3% w/v polymer solution concentration.

The electrospun PEO/ PMMA beaded fibers with 50/ 50 weight ratio were also chosen for the incorporation of PCM (n-eicosane) in order to investigate the behavior of beaded fibers in terms of their thermal properties. Figures 3.15, 3.16, 3.17 and 3.18 show the beaded fibrous membranes of PEO/ PMMA (50/ 50) with variable n-eicosane concentrations (7.5% wt., 10% wt., 15% wt. and 20% wt., respectively). In all cases, beads-on-string morphologies and highly porous structures were observed.

Porous materials have been widely used in a range of applications, including adsorption, catalysis, energy conversion, and storage, and have demonstrated ready mass transfer capabilities and large storage capacities [46]. In the areas of adsorption, ultrafiltration, and ion-exchange resins, as well as carriers for catalysts and reagents, porous polymeric fibers with outstanding physical strength and increased adsorption capacities are in high demand. [47] Because of their naturally high surface area, small interfiber pores, and engineering adaptability, porous fibers have met various needs in the above domains.

The main mechanism for the production of porous fibers is phase separation based on solvent evaporation. Solvent-rich areas arise when a more volatile solvent is introduced in the electrospinning process. As soon as the solvents are evaporated, the solvent-rich regions create pores [47]. The spinning of two different polymers blended together is a second method of making porous fibers. After fiber creation, one of the polymers is removed by dissolving it in a solvent in which the other polymer is insoluble. [47]. Controlling the humidity during electrospinning is the third approach of generating porous fibers. At low humidity, for example, the chances of the electrospinning jet interacting with water molecules are minimal. Water vapor, on the other hand, easily condenses into droplets at high humidity. Because the water droplets are quite large, they are able to make appropriate contact with the jet and attach to the

fiber surfaces, resulting in the creation of circular pores/voids on the fiber surfaces. With increased humidity, the diameter of the circular pores in the fibers expands until they combine into nonuniform-shaped formations. [47]

The first possible way for the generation of porosity on PEO/ PMMA (50/ 50) beaded fibers' surfaces is the third mechanism due to the variable environmental conditions existing in the lab. The experiments of samples with PEO/ PMMA weight ratio of 80/ 20 (subsection 3.1.3) took place in July 2021 (high temperature) while the fabrication of samples with a weight ratio of 50/ 50 took place in January 2022 (low temperature). Also, porosity on PEO/ PMMA (50/ 50) fibers may be generated due to the second mechanism and the increase in PMMA content as compared to PEO/ PMMA (80/ 20) fibers (phase separation phenomena occurring between the 2 incompatible polymers). The impact of porosity on the thermal and mechanical properties of the fibers can be investigated in a future study.

PEO/ PMMA (weight ratio 50/ 50)/ 7.5% wt. n-eicosane.

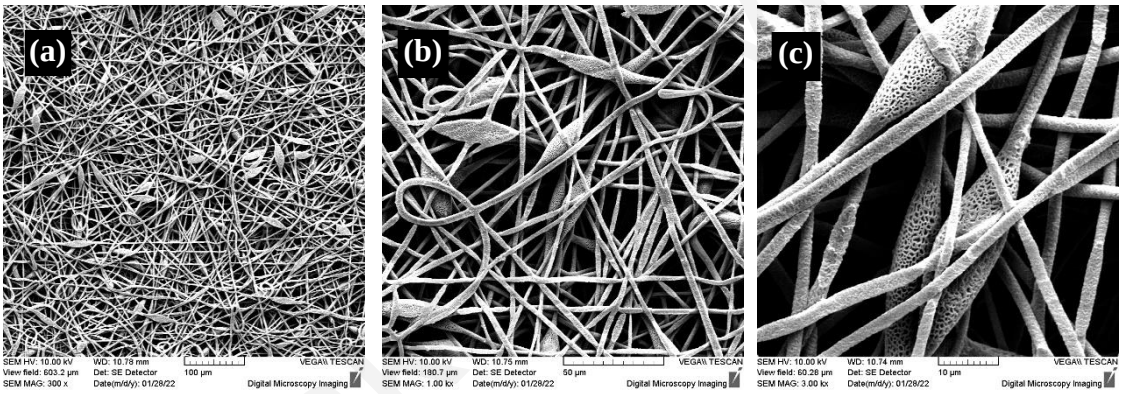

Figure 3.15: SEM images of PEO/ PMMA (mass ratio 50/50)/ 7.5% wt. n-eicosane electrospun beaded fibers. Scale bars (a): 100μm, (b): 50μm, (c): 10μm

PEO/ PMMA (weight ratio 50/ 50)/ 10% wt. n-eicosane.

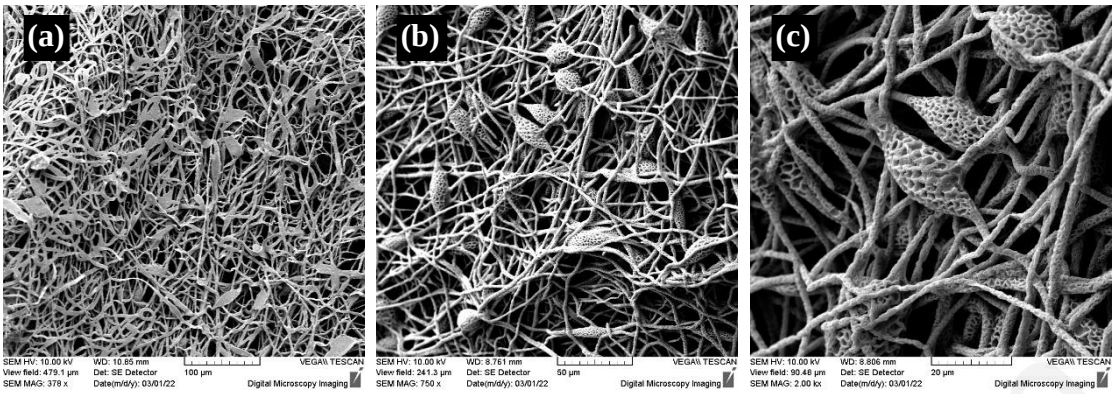

Figure 3.16: SEM images of PEO/ PMMA (mass ratio 50/50)/ 10% wt. n-eicosane electrospun beaded fibers. Scale bars (a): 100μm, (b): 50μm, (c): 20μm

PEO/ PMMA (weight ratio 50/ 50)/ 15% wt. n-eicosane.

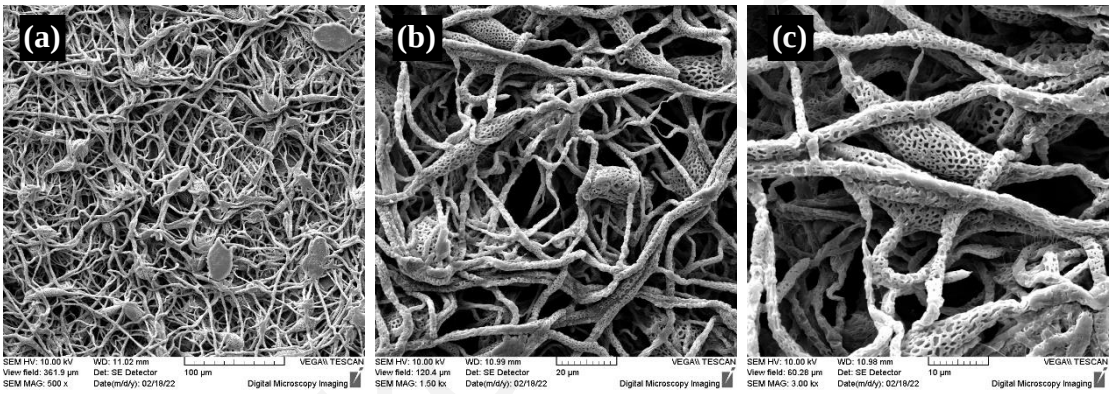

Figure 3.17: SEM images of PEO/ PMMA (mass ratio 50/50)/ 15% wt. n-eicosane electrospun beaded fibers. Scale bars (a): 100μm, (b): 20μm, (c): 10μm

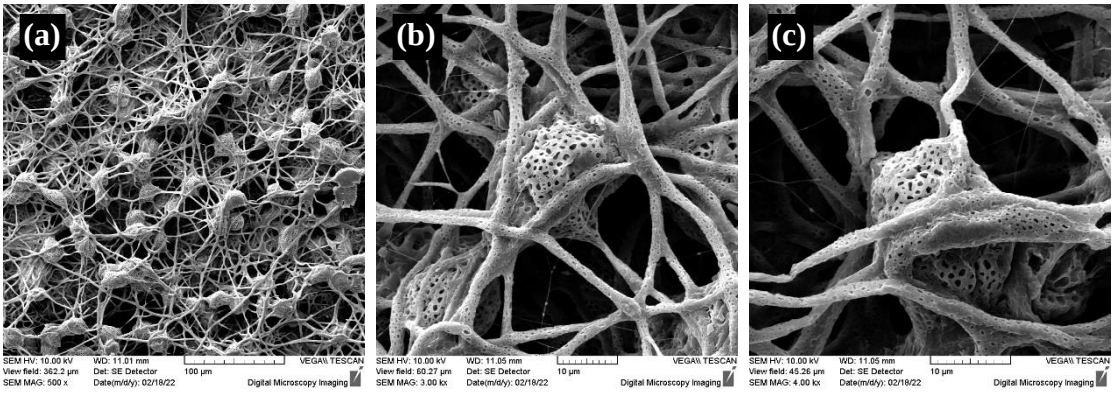

Figure 3.18: SEM images of PEO/ PMMA (mass ratio 50/50)/ 20% wt. n- eicosane electrospun beaded fibers. Scale bars (a): 100μm, (b): 10μm, (c): 10μm

3.1.5 Morphological characterization of electrospun PEO/ PMMA (weight ratio 50/ 50)/ n-eicosane non-beaded fibers starting from 4% w/v polymer solution concentration.

Bead-free, electrospun PEO/ PMMA fibers with 50/ 50 PEO/ PMMA weight ratio was the last series of materials that was chosen for the incorporation of PCM (n-eicosane) in order to compare the behavior of beaded and bead-free fibers in terms of their thermal properties. Figures 3.19, 3.20, 3.21 and 3.22 show the bead-free PEO/ PMMA (50/ 50) fibrous membranes with n-eicosane concentrations of 10% wt., 15% wt., 20% wt. and 25% wt. respectively. Bead-free fibrous morphologies were fabricated and porous fibers can be observed up to 25% wt n-eicosane content. The same behavior of porosity can be observed as in the case of PEO/ PMMA (50/ 50) beaded fibers (subsection 3.1.4). Tubercles can be seen as the amount of n-eicosane in the system increases.

PEO/ PMMA (weight ratio 50/ 50)/ 10% wt. n-eicosane.

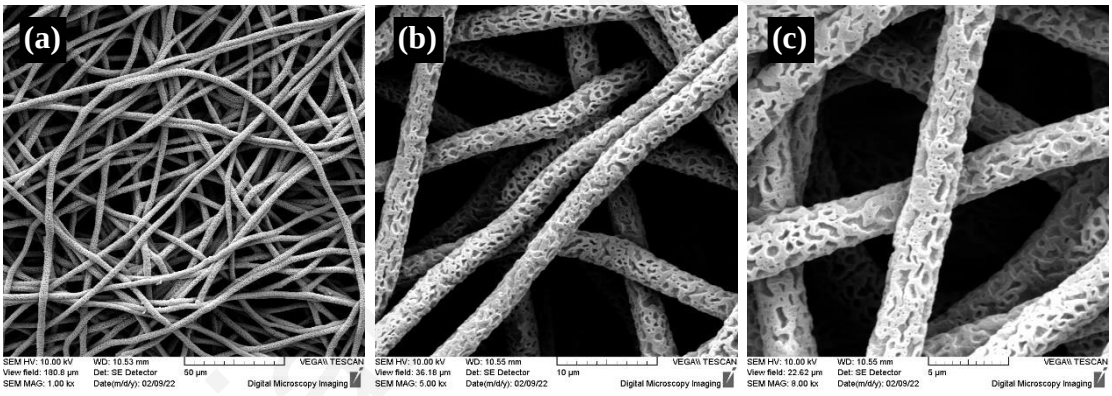

*Figure 3.19: SEM images of PEO/ PMMA/ n-eicosane **10% wt**. bead-free electrospun fibrous membranes. Scale bars (a): 50μm, (b): 10μm, (c):5μm*

PEO/ PMMA (weight ratio 50/ 50)/ 15% wt. n-eicosane.

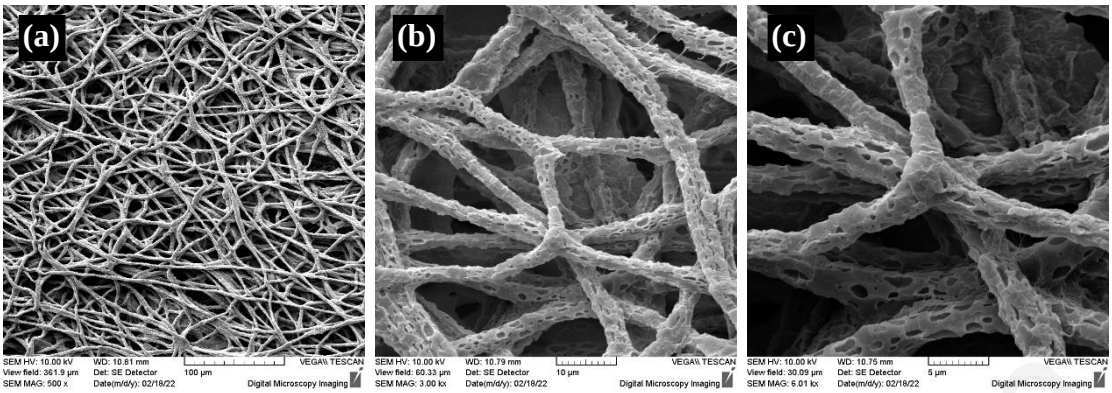

*Figure 3.20: SEM images of PEO/ PMMA/ n-eicosane **15% wt**. bead-free electrospun fibrous membranes. Scale bars (a): 100μm, (b): 10μm, (c):5μm*

PEO/ PMMA (weight ratio 50/ 50)/ 20% wt. n-eicosane.

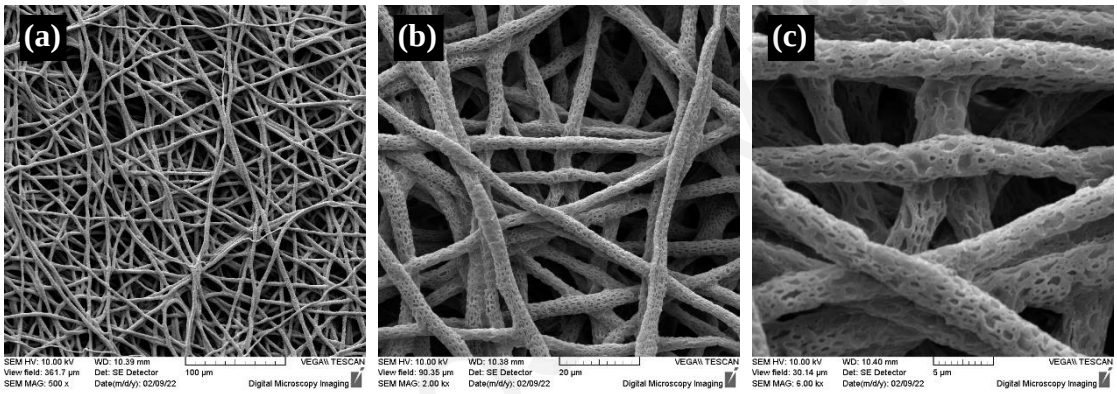

*Figure 3.21: SEM images of PEO/ PMMA/ n-eicosane **20% wt**. bead-free electrospun fibrous membranes. Scale bars (a): 100μm, (b): 20μm, (c):5μm*

PEO/ PMMA (weight ratio 50/ 50)/ 25% wt. n-eicosane.

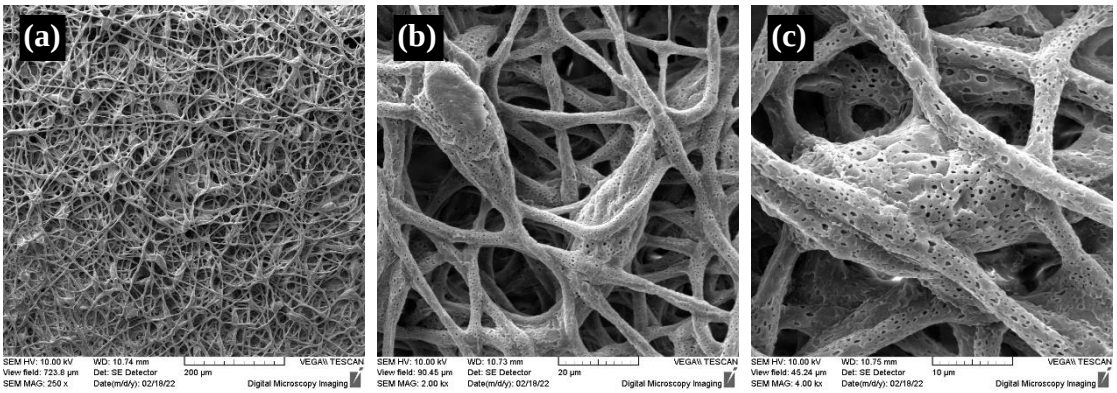

*Figure 3.22: SEM images of PEO/ PMMA/ n-eicosane **25% wt**. electrospun fibrous membranes. Scale bars (a): 200μm, (b): 20μm, (c):10μm*

The 50/50 PEO/PMMA fibrous membranes, seem to be able to accommodate a higher percentage of n-eicosane (i.e. 20% wt.) compared to the 80/20 polymer system. In the second case, when the n-eicosane content was greater than 10% wt., the fibrous membrane was coated by a thin layer of n-eicosane, and many tubercles formed on the fibers (Fig. 3.14). On the other hand, before the formation of aggregations on fibrous morphology in the PEO/ PMMA 50/ 50 polymers system, the n-eicosane content reached 25% wt. This is due to the increased PMMA content, which enables the accommodation of a higher n-eicosane percentage within the fibers, due to the development of hydrophobic interactions between the PMMA hydrophobic chains and the n-eicosane hydrophobic hydrocarbon.

Thermal characterization:

The heat transfer properties and thermal characteristics of fibrous membranes play a significant impact in the performance of a thermal energy storage substance. As mentioned in section 2, the thermal characterization of the produced fibers was performed at Aristotle University of Thessaloniki, under the supervision of Prof. Konstantinos Chrissafis, using differential scanning calorimetry (DSC). More precisely, DSC was used to evaluate the melting temperature, latent heat of fusion, degree of supercooling and materials' thermal stability.

Figures 3.23 and 3.24 show the DSC curves of n-eicosane and PEO/ PMMA composite fibers. DSC curves of both n-eicosane and PEO/ PMMA have endothermic and exothermic peaks in the range of 10 – 90°C. This result indicates that phase change processes occur for both materials (n-eicosane and PEO/ PMMA) in the above-mentioned temperature range.

3.1.6 DSC analysis of pure n-eicosane

DSC curves of pure n-eicosane are presented in Fig. 3.23. DSC results suggest that as the temperature of the sample was raised, the melting of n-eicosane was characterized by one exothermic peak, whereas the endothermic process upon cooling was accompanied by two separated peaks. These results are in line with those reported in previous studies, discussing on the melting and crystallization behavior of n-eicosane [48] [49]. More precisely, in the case of most paraffin waxes, such as n-eicosane, a **metastable rotator phase** with a transition temperature exceeding the bulk crystallization temperature has been observed. During the cooling process, the transitions from the **homogeneously nucleated liquid** to a **rotator phase** and from the **heterogeneously nucleated rotator phase** to the **crystalline phase** are commonly assigned two phase-transformation temperatures. Due to two-phase transitions, this

property causes bimodal crystallization behavior for n-eicosane. The single melting peak, on the other hand, is related to the heating process' phase transition from the stable triclinic phase to the liquid phase. [49]

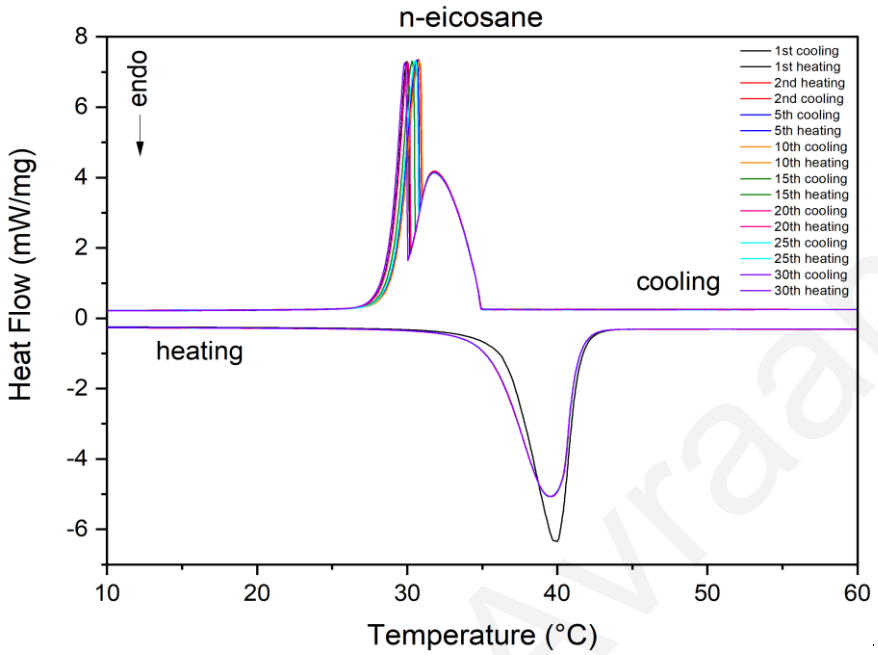

Figure 3.23: DSC curves of n-eicosane after 1, 2, 5, 10, 15, 20, 25 and 30 thermal cycles.

The n-eicosane shows two well defined separated crystallization peaks with the strongest peak maximum appearing at 30.7°C (2nd cycle) and the second peak at 31.8°C (2^{nd} cycle). The phase transition temperature of the greater crystallization peak varies after the second cycle, whereas the smaller crystallization peak remains steady. The single melting peak is found at 39.5°C (2^{nd} cycle). Crystallization and melting peaks correspond to the phase changes of solidification and fusion, respectively. The enthalpy of melting (ΔHm) and crystallization enthalpy (ΔHc) of n-eicosane were determine to be 235.7 J/g (30^{th} cycle) and 237.6 J/g (30^{th} cycle), respectively. The pure n-eicosane sample was tested for 30 thermal cycles and the enthalpy of the samples was obtained by calculating the peak area using Origin software. The experimental data is provided in Table 3.3.

Table 3.3: T_m, ΔH_m, T_{c1}, T_{c2}, $\Delta H_{c1,2}$ of n-eicosane after 1, 2, 5, 10, 15, 20, 25 and 30 thermal cycles. (Tm1: Melting temperature of peak 1, ΔHm: Latent heat of fusion, Tc1: Crystallization temperature of peak 1. Tc2: Crystallization temperature of peak 2, ΔHc1,2: Latent heat of crystallization for the peaks 1 and 2)

n-eicosane					
Cycles	**Tm (°C)**	**ΔHm (J/g)**	**Tc1 (°C)**	**Tc2 (°C)**	**ΔHc1,2 (J/g)**
1st	40	234.1	30	31.8	237.9
2nd	39.5	235.7	30.7	31.8	237.8
5th	39.5	235.8	30.6	31.8	237.6
10th	39.5	235.9	30.8	31.8	237.6
15th	39.5	235.8	30.3	31.8	237.6
20th	39.6	235.8	30	31.8	237.5
25th	39.5	235.9	30.5	31.8	237.6
30th	39.5	235.7	29.8	31.8	237.6

3.1.7 DSC analysis of pure PEO/ PMMA 80/20

Figure 3.24 shows the DSC curves of neat PEO/ PMMA fibers. The neat PEO/ PMMA membrane was tested for 30 thermal cycles.

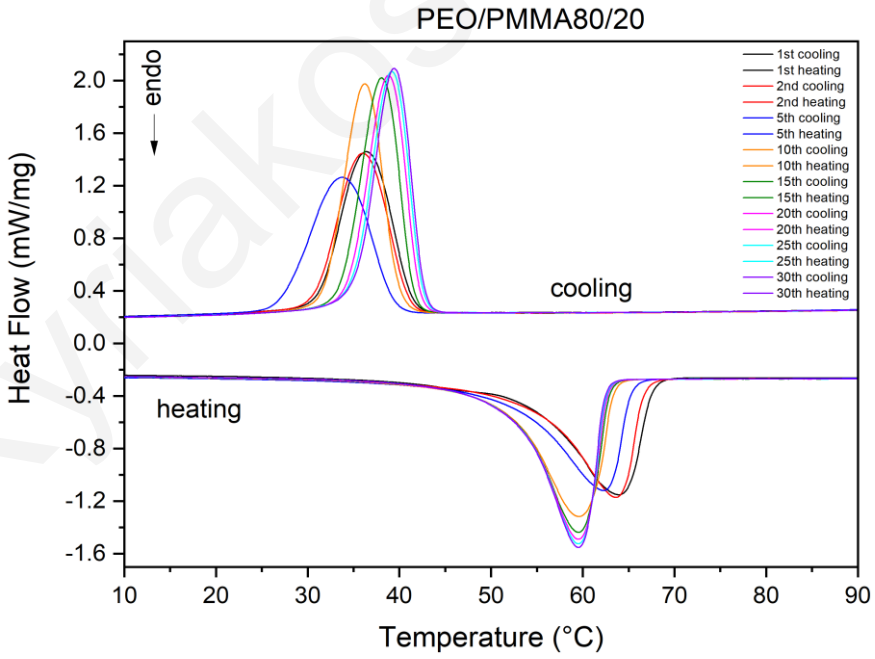

Figure 3.24: DSC curves of neat PEO/ PMMA after 1, 2, 5, 10, 15, 20, 25 and 30 thermal cycles.

The neat PEO/ PMMA fibers show a melting peak at 63.6 °C (2nd cycle) and single crystallization peak with peak maximum appearing at 36 °C (2nd cycle). The enthalpy of melting (ΔHm) and crystallization (ΔHc) of PEO/ PMMA membrane are about 115.7 J/g (30th cycle) and 113.7 J/g (30th cycle), respectively. There is a variation of phase transition temperatures and enthalpies of the electrospun neat PEO/ PMMA fibers due to the repeatedly heating and cooling of the sample which leads to the loss of the fibrous morphology of the material. Those thermal transitions correspond to PEO because the melting temperature of PEO is 65°C (as mentioned in section 2), which is close to the melting peak of the graph 63.6 °C. On the other hand PMMA, is an amorphous material with a glass transition temperature of 105 °C, as mentioned in section 2. The corresponding data are summarized in Table 3.4.

Table 3.4: T_m, ΔH_m, T_{c1}, T_{c2}, $\Delta H_{c1,2}$ of n-eicosane after 1, 2, 5, 10, 15, 20, 25 and 30 thermal cycles. (Tm1: Melting temperature of peak 1, ΔHm: Latent heat of fusion, Tc: Crystallization temperature, ΔHc: Latent heat of crystallization)

PEO/PMMA-80/20				
Cycles	**Tm (°C)**	**ΔHm (J/g)**	**Tc (°C)**	**ΔHc (J/g)**
1st	63.9	113.2	36.4	98.7
2nd	63.6	102.7	36	97.2
5th	62.2	101.3	33.8	97.6
10th	59.6	113.5	36.2	108.1
15th	59.5	115	38.1	110.5
20th	59.6	116.3	38.8	112.4
25th	59.6	116.3	39.2	112
30th	59.5	115.7	39.4	113.7

3.1.8 DSC analysis of PEO/ PMMA (weight ratio 80/ 20) / 10% wt. n-eicosane (up to 90℃)

Figure 3.25 shows the DSC curves of PEO/ PMMA fibers with 10% wt. n-eicosane. The sample was tested for 30 thermal cycles up to 90 ℃.

Fibers with 10% wt. n-eicosane content were selected because of the uniform fibrous morphology (compared to fibers with 15% wt. n-eicosane content) and the higher quantity of PCM in comparison to PCFs with 2, 5 and 7.5 % wt. n-eicosane. As shown in Figure 3.25, there is a variation of phase transition temperatures of the fibers, indicating non-repeatability and low stability of the material.

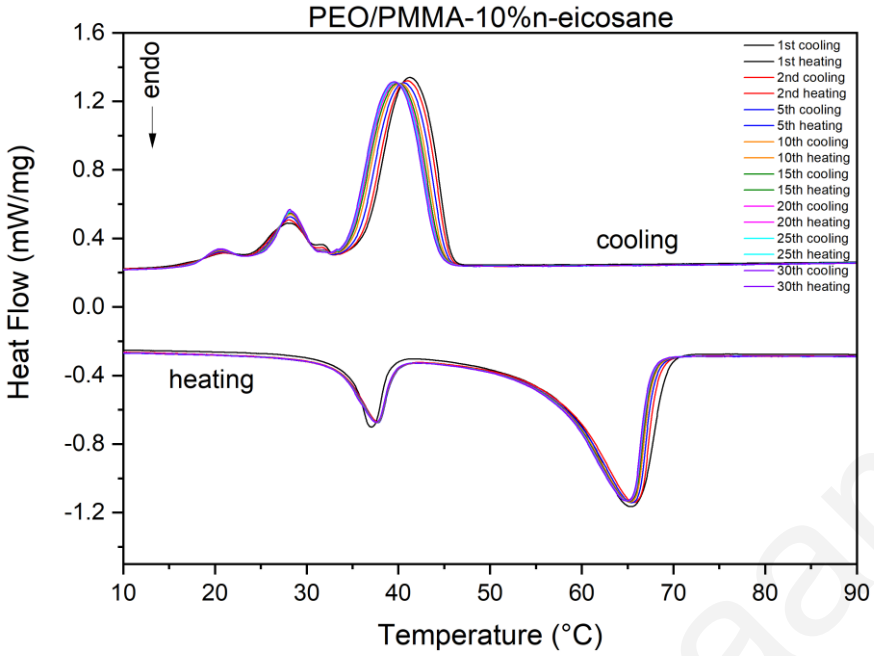

Figure 3.25: DSC curves of PEO/ PMMA/ 10% n-eicosane after 1, 2, 5, 10, 15, 20, 25 and 30 thermal cycles.

Table 3.5: T_m, ΔH_m, T_{c1}, T_{c2}, $\Delta H_{c1,2}$, T_{c3}, ΔH_{c3} of PEO/ PMMA/ 10% n-eicosane after 1, 2, 15 and 30 thermal cycles.

PEO/ PMMA/ 10% n-eicosane									
Cycles	T_{m1} (°C)	ΔH_{m1} (J/g)	T_{m2} (°C)	ΔH_{m2} (J/g)	T_{c1} (°C)	T_{c2} (°C)	$\Delta H_{c1,2}$ (J/g)	T_{c3} (°C)	ΔH_{c3} (J/g)
1st	37.1	15.5	65.4	89.9	21.2	27.9	16.2	41.2	78.9
2nd	37.7	18.1	65.7	82.4	21	28	17.6	41	78.9
5th	37.7	17.8	65.5	82.2	20.9	28.2	16.5	40.6	78.7
10th	37.7	18.1	65.2	81.9	20.6	28.3	17.2	40.2	78.3
15th	37.7	18.8	65.1	81.8	20.7	28.2	17.2	40	78.3
20th	37.6	18.1	65	81.7	20.6	28	16.7	39.9	78.2
25th	37.6	17.8	65	81.3	20.6	28.3	16.2	39.6	78.1
30th	37.6	18.5	64.9	81.4	20.6	28.2	16	39.5	78.2

Figure 3.26 shows the PEO/ PMMA/ 10% n-eicosane membrane before performing 30 thermal cycles in DSC and figure 3.27 shows the neat PEO/ PMMA membrane and the corresponding n-eicosane-loaded membranes (PEO/ PMMA/ 2% n-eicosane, PEO/ PMMA/ 5% n-eicosane, PEO/ PMMA/ 7.5% n-eicosane and PEO/ PMMA/ 10% n-eicosane) after 30 thermal cycles performed up to 90 °C. From the photographs, it becomes obvious that after the cycles, fibers became an amorphous mass and they do not remain in their initial fibrous form due to the heating of composite PCFs at temperatures above the T_m of PEO (which is 65°C). This justifies

the bad repeatability observed in consecutive thermal cycles when the DSC experiments were conducted at temperatures up to 90 ℃.

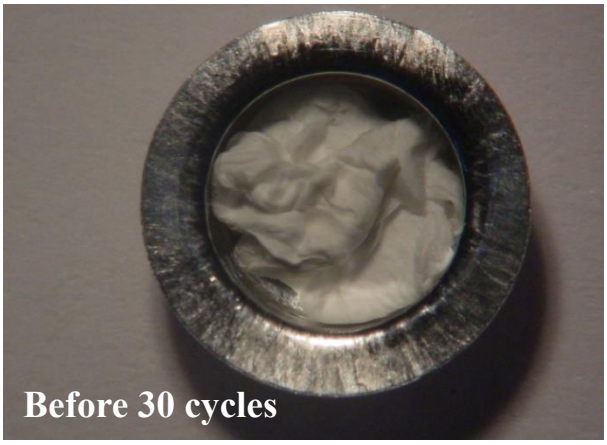

Figure 3.26: PEO/ PMMA/ 10% n-eicosane before 30 thermal cycles

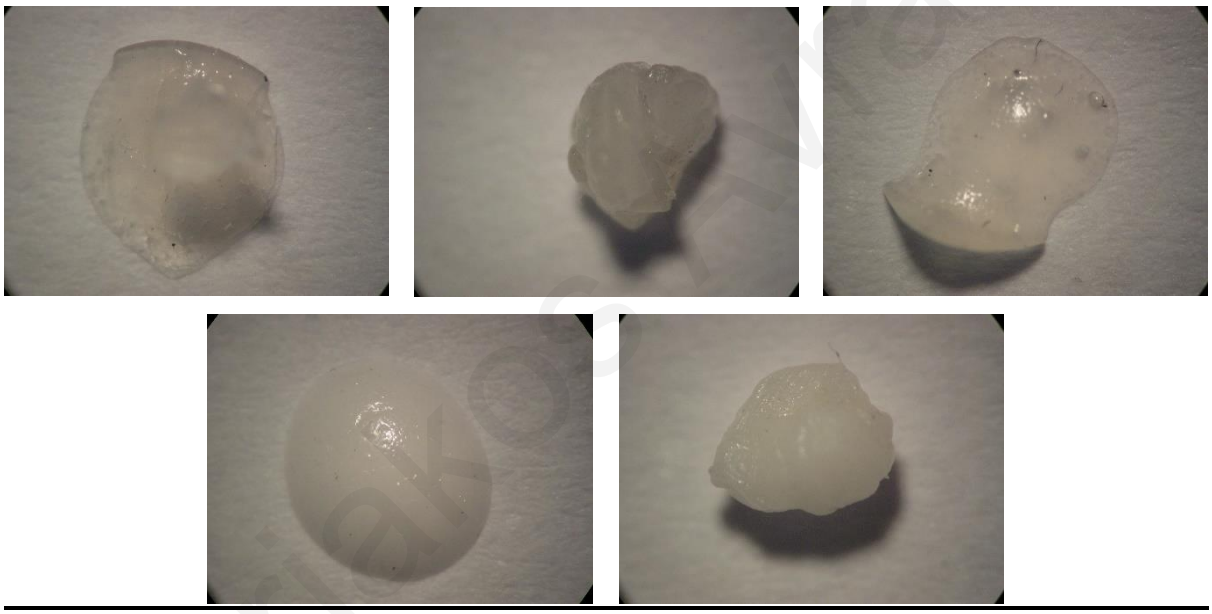

*Figure 3.27: Neat PEO/ PMMA, PEO/ PMMA/ 2% n-eicosane, PEO/ PMMA/ 5% n-eicosane, PEO/ PMMA/ 7.5% n-eicosane and PEO/ PMMA/ 10% n-eicosane after 30 thermal cycles (**until 90°C**)*

3.1.9 DSC analysis of PEO/ PMMA (weight ratio 80/20) / 10% wt. n-eicosane (up to48◦C)

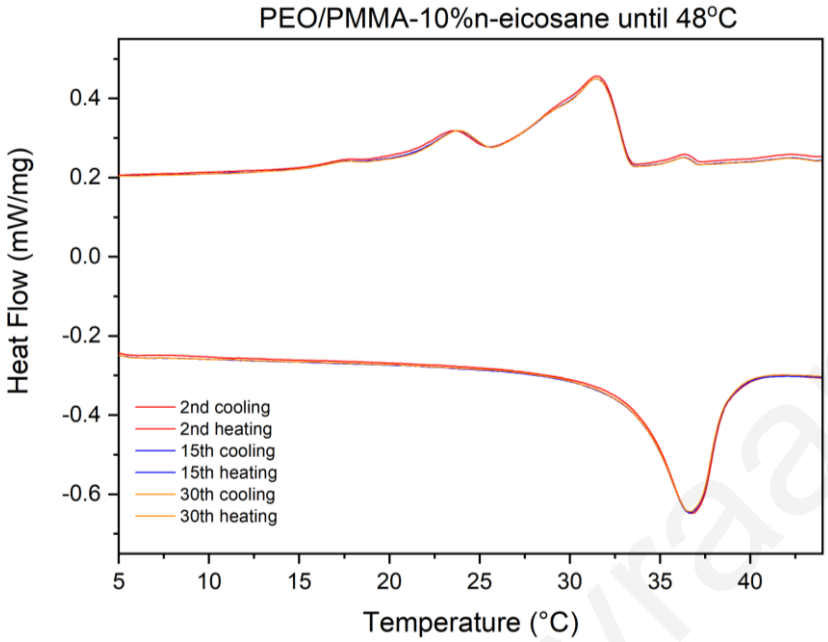

Figure 3.28: DSC curves of PEO/ PMMA/ 10% n-eicosane after 1, 2, 5, 15 and 30 thermal cycles up to 48°C.

The DSC curves of PEO/ PMMA (80/20) fibers with 10% wt. n-eicosane recorded up to 48°C shown in figure 3.28. These tests were performed to investigate the behavior of the PCF at temperature regions below the phase transition of PEO (65 °C) and study how the repeatability and stability of the obtained results are compared to those recorded for the same systems at temperatures up to 90°C (Figure 3.25).

As seen in the DSC thermogram, a small peak can be observed at 36.4°C. This peak (which does not appear in the DSC thermogram of pure n-eicosane) may be attributed to interaction phenomena taking place between the n-eicosane and the PEO or PMMA polymers. More precisely, it is likely that such interactions may have led to the generation of intermediate crystallization phases during the transition of material-eicosane from the liquid to the solid phase upon cooling.

The melting peak has peak maximum appearing at 36.7°C (2^{nd} cycle) and three crystallization peaks are found at 23.5°C (2^{nd} cycle), 31.5°C (2^{nd} cycle) and 36.4°C (2^{nd} cycle). The curves remain stable after the 2^{nd} cycle, indicating that the PEO/ PMMA /10%wt. n-eicosane phase change fibrous membrane has thermal stability and thermal reliability. The real melting (ΔH_{mr}) and cooling (ΔH_{cr}) enthalpy of PEO/ PMMA / 10% wt. n-eicosane fibers are 178.0 J/g (30^{th}

cycle) and 177.3 J/g (30th cycle). When compared to pure n-eicosane (Figure 3.23 – ΔHm=235.7 J/g and ΔHc=237.6 J/g), the addition of PEO and PMMA polymers reduces the latent heat of melting and cooling in the produced fibrous membranes. The % reduction of melting and cooling enthalpies are 24.88 % (30th cycle) and 25.38 % (30th cycle), respectively.

Table 3.6: T_m, ΔH_m, T_{c1}, T_{c2}, $\Delta H_{c1,2}$, T_{c3}, ΔH_{C3} of PEO/ PMMA/ 10% n-eicosane after 1, 2, 15 and 30 thermal cycles. (Tm1: Melting temperature of peak 1, ΔHm: Latent heat of fusion, Tc1: Crystallization temperature of peak 1. Tc2: Crystallization temperature of peak 2, ΔHc1,2: Latent heat of crystallization for the peaks 1 and 2, Tc3: Crystallization temperature of peak 3, ΔHc3: Latent heat of crystallization for the peak 3)

PEO/ PMMA (80/ 20)/ 10% n-eicosane							
Cycles	**T_{m1} (°C)**	**ΔH_m (J/g)**	**T_{c1} (°C)**	**T_{c2} (°C)**	**$\Delta H_{c1,2}$ (J/g)**	**T_{c3} (°C)**	**ΔH_{c3} (J/g)**
1st	37.4	182.0	23.5	31.5	181.0	36.4	0.4
2nd	36.7	179.0	23.5	31.5	178.0	36.4	0.4
15th	36.6	177.0	23.6	31.4	177.0	36.3	0.3
30th	36.7	178.0	23.7	31.5	177.0	36.3	0.3

The values of melting and crystallization temperatures as well as the crystallization and melting enthalpies are provided in Table 3.6. Based on these results, it is noteworthy that there is no significant temperature or enthalpy change observed after thermal cycling.

The real melting enthalpy is defined as follows:

$$\Delta Hm_r = \frac{\Delta Hm}{mass\ percentage\ of\ eicosane} * 100 \quad \text{(Equation 3.1)}$$

where ΔHm is the melting enthalpy that was measured by DSC for the mass of the whole material (PEO/ PMMA/ n-eicosane membrane). The same equation can be used for the real cooling enthalpy (ΔHc_r).

*Figure 3.29: PEO/ PMMA (80/20)/ 10% n-eicosane after 30 thermal cycles (**until 48°C)***

Figure 3.29 shows the PEO/ PMMA/ 10% n-eicosane membrane after 30 heating and cooling cycles until 45°C. The membrane seems to be very stable, and the fibers remain intact in the form of PCF without observing any n-eicosane leaching phenomena or material alteration.

3.1.10 DSC analysis of PEO/ PMMA (weight ratio 50/50) / 10% wt. n-eicosae: Beaded versus non-beaded fibers

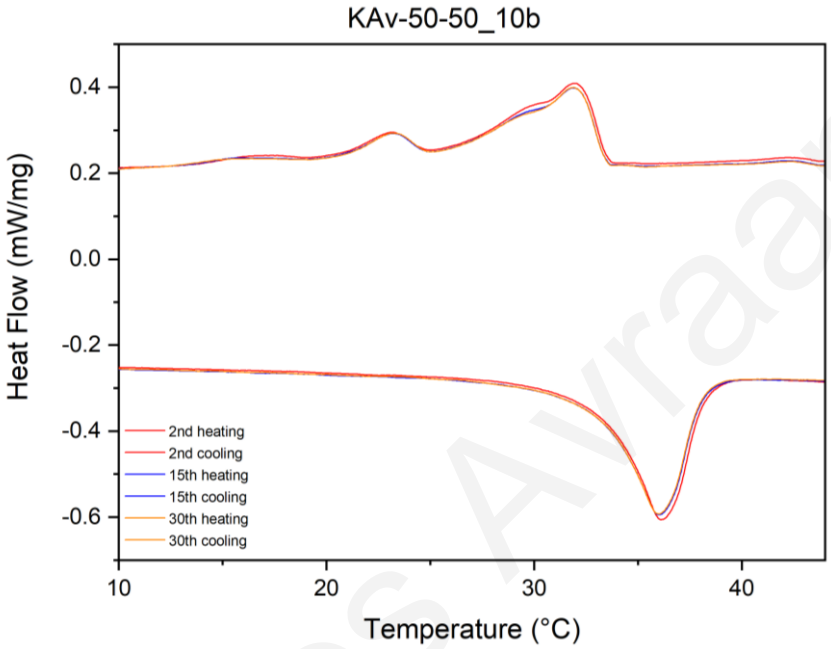

Figure 3.30: DSC curves of PEO/ PMMA/ 10% n-eicosane beaded fibers after 2, 15 and 30 thermal cycles until 44°C.

DSC curves of PEO/ PMMA (50/50) beaded fibers with 10% wt. n-eicosane until 44°C are shown in Figure 3.30. These tests were performed to investigate the behavior of the phase change beaded fibers and study how the results are changed in comparison with PEO/ PMMA (50/50) non-beaded fibers having the same n-eicosane content (i.e.10% wt. n-eicosane).

The melting peak has peak maximum appearing at 36.1°C (2nd cycle) and four crystallization peaks with the most distinct ones found at 23.2°C (2nd cycle) and 32°C (2nd cycle). The other two crystallization peaks appear as shoulders. The curves remain relatively stable after the 2nd cycle, indicating that the PEO/ PMMA /10% wt. n-eicosane beaded fibers have thermal stability and thermal reliability. The real melting enthalpy (ΔHm_r) of PEO/ PMMA / 10% wt. n-eicosane fibers is around 139.3 J/g (30th cycle) and the real cooling enthalpy (ΔHc_r) is 138.4 J/g (30th cycle). When compared to pure n-eicosane (Figure 3.23), the addition of PEO and PMMA polymers reduces the latent heat of melting and cooling in the produced fibrous

membranes. The % reduction of melting and cooling enthalpies are 40.90 % (30th cycle) and 41.75 % (30th cycle), respectively.

Table 3.7: T_m, ΔH_m, T_{c1}, T_{c2}, ΔH_c of PEO/ PMMA (50 /50)/ 10% n-eicosane beaded fibers after 2, 15 and 30 thermal cycles.

(Tm1: Melting temperature of peak 1, ΔHm: Latent heat of fusion, Tc1: Crystallization temperature of peak 1. Tc2: Crystallization temperature of peak 2, ΔHc1,2: Latent heat of crystallization for the peaks 1 and 2)

PEO/ PMMA (50/ 50)/ 10% n-eicosane beaded fibers					
Cycles	**Tm1 (°C)**	**ΔHm (J/g)**	**Tc1 (°C)**	**Tc2 (°C)**	**ΔHc12 (J/g)**
2nd	36.1	141.3	23.1	32.0	137.5
15th	36.0	139.5	23.2	32.0	130.4
30th	36.0	139.3	23.2	31.9	138.4

The values of melting and crystallization temperatures as well as the crystallization and melting enthalpies shown at Table 3.7. Based on these results, it is noteworthy that there is no significant temperature or enthalpy change observed after thermal cycling.

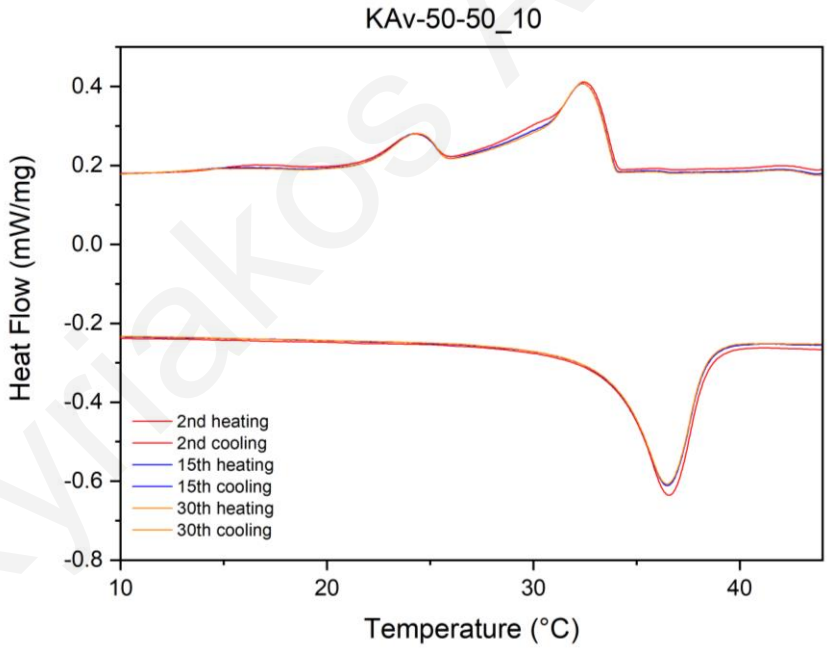

Figure 3.31: DSC curves of PEO/ PMMA/ 10% n-eicosane non-beaded fibers after 2, 15 and 30 thermal cycles until 44°C

DSC curves of PEO/ PMMA (50/ 50) non-beaded fibers with 10% wt. n-eicosane until 44 °C are shown in figure 3.31. These tests were performed to investigate the behavior of the non-beaded phase change fibers and study how the results are changed in comparison to both the

PEO/ PMMA (50/50) beaded fibers with 10% wt. n-eicosane and the PEO/ PMMA (80/20) non-beaded fibers with 10% wt. n-eicosane.

The melting peak has a peak maximum appearing at 36.5 °C (2nd cycle) and four crystallization peaks with the most distinct ones found at 24.3°C (2nd cycle) and 32.4°C (2nd cycle). The other two crystallization peaks appearing as a shoulder. The curves remain relatively stable after the 2nd cycle, indicating that the PEO/ PMMA /10% wt. n-eicosane non-beaded fibers have thermal stability and thermal reliability. The real melting enthalpy (ΔHm_r) of PEO/ PMMA / 10% wt. n-eicosane fibers is 146.7 J/g (30th cycle) and the real cooling enthalpy (ΔHc_r) is 143.4 J/g (30th cycle). When compared to pure n-eicosane (Figure 3.23), the addition of PEO and PMMA polymers reduces the latent heat of melting and cooling in the produced fibrous membranes. The % reduction of melting and cooling enthalpies are 37.76 % (30th cycle) and 39.65 % (30th cycle), respectively.

Table 3.8: T_m, ΔH_m, T_{c1}, T_{c2}, ΔH_{c12} of PEO/ PMMA (50 /50)/ 10% n-eicosane non-beaded fibers after 2, 15 and 30 thermal cycles. (Tm1: Melting temperature of peak 1, ΔHm: Latent heat of fusion, Tc1: Crystallization temperature of peak 1. Tc2: Crystallization temperature of peak 2, ΔHc1,2: Latent heat of crystallization for the peaks 1 and 2)

PEO/ PMMA (50/ 50)/ 10% n-eicosane non-beaded fibers					
Cycles	**Tm1 (°C)**	**ΔHm (J/g)**	**Tc1 (°C)**	**Tc2 (°C)**	**ΔHc12 (J/g)**
2nd	36.6	155.0	24.4	32.4	151.0
15th	36.5	147.0	24.3	32.4	149.3
30th	36.5	146.7	24.4	32.4	143.4

The values of melting and crystallization temperatures as well as the crystallization and melting enthalpies are shown in Table 3.8. Based on these results, it is noteworthy that there is no significant temperature or enthalpy change observed after thermal cycling.

Figure 3.32 shows the PEO/ PMMA/ 10% n-eicosane membrane having a non-beaded morphology, after 30 heating and cooling cycles until 44 °C. The membrane seems to be very stable, and the fibers remain as PCF without observing any n-eicosane leaching phenomena or any material alteration.

*Figure 3.32: PEO/ PMMA (50/ 50)/ 10% n-eicosane after 30 thermal cycles (**until 44°C)***

Comparison of PEO/PMMA (50/50) / 10% n-eicosane non-beaded fibers with PEO/ PMMA (80/ 20)/ 10% n-eicosane non-beaded fibers:

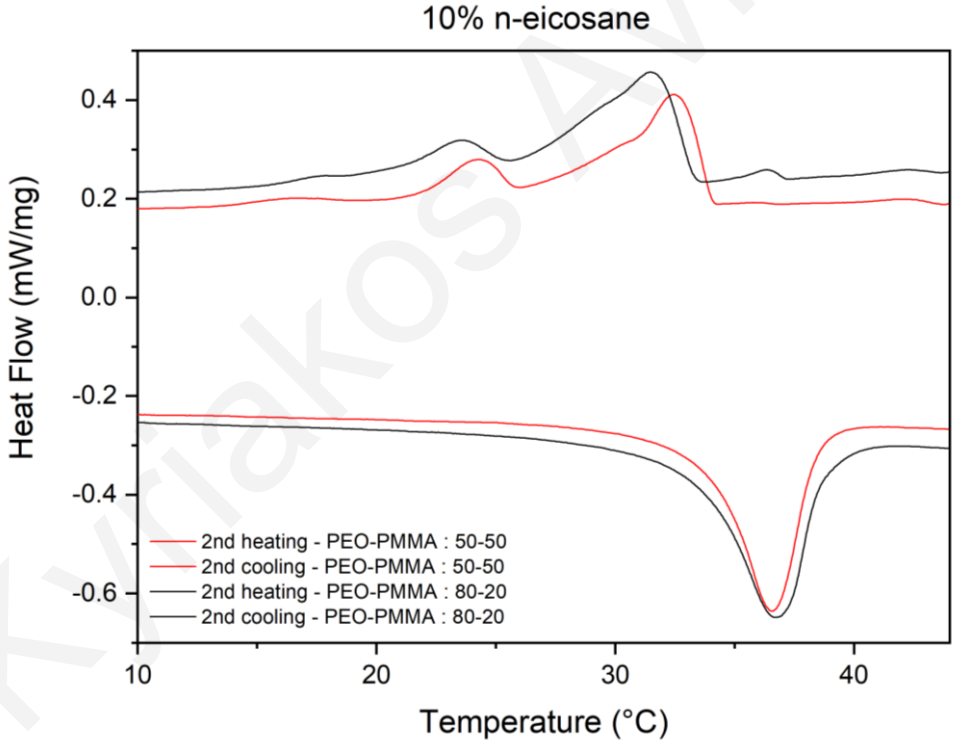

Figure 3.33: DSC curves of PEO/ PMMA fibers with weight ratios of 50/50 and 80/20 and 10%wt. n-eicosane content after 2 thermal cycles until 44°C.

The melting peak of PEO/ PMMA (50/ 50) non-beaded fibers is 36.6 °C while the melting peak of PEO/ PMMA (80/20) fibers is 36.7 °C. In the case of PEO/ PMMA (50/ 50) fibers there are two crystallization peaks at 24.3 °C and 32.4 °C but there are also two crystallization peaks

appearing as shoulders. In the case of PEO/ PMMA (80/20) an additional crystallization peak appears at 36.4°C and crystallization curves of PEO/PMMA (80/20) fibers shifting in lower temperature. In both cases, the curves remain relatively stable after the 2nd cycle, indicating that both materials have thermal stability and thermal reliability. The real melting and cooling enthalpy of PEO/ PMMA (50/ 50) non-beaded fibers are 146.7 J/g and 143.4 J/g, respectively, while the real melting and cooling enthalpy of PEO/PMMA (80/20) are 178.0 J/g and 177.3 J/g, respectively. The % reduction of melting and cooling enthalpies of PEO/ PMMA (50/ 50) non-beaded fibers (37.76% and 39.65%) is higher than PEO/PMMA (80/20) fibers (24.88 % and 25.38 %).

Comparison of PEO/ PMMA (50/ 50)/ 10% n-eicosane non-beaded fibers with PEO/ PMMA (50/ 50)/ 10% n-eicosane beaded fibers:

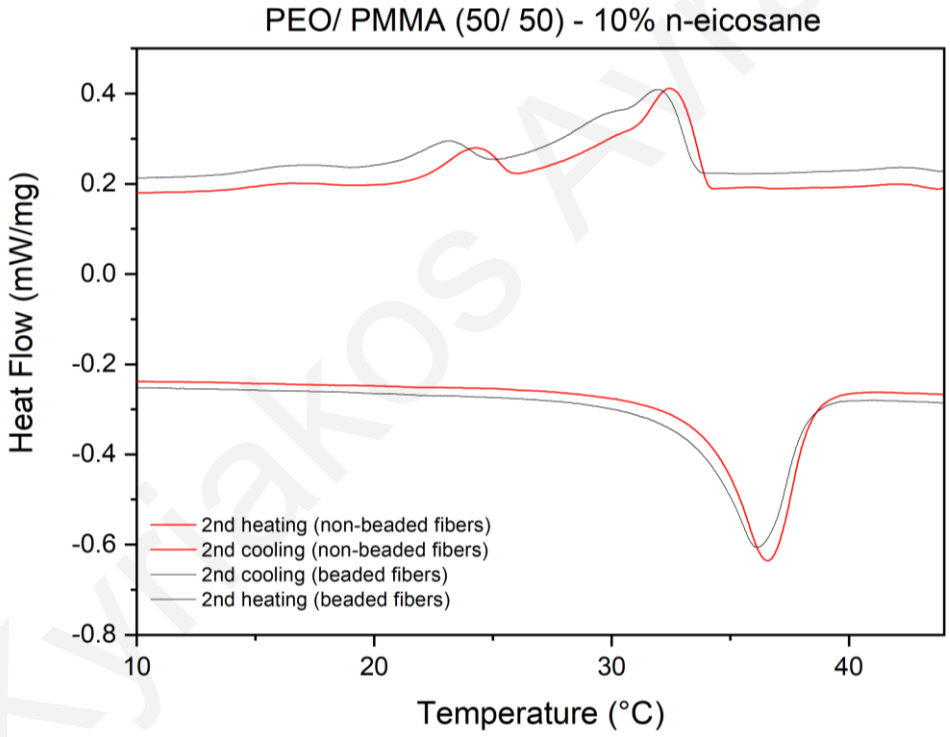

Figure 3.34: DSC curves of PEO/ PMMA (50/50) /10% n-eicosane beaded fibers and the corresponding non-beaded fibers after 2 thermal cycles until 44°C.

As seeing in Figure 3.34, the melting peak of the non-beaded fibers appears at 36.6 °C while the melting peak of beaded fibers is found at 36.1 °C. Non-beaded fibers have four crystallization peaks with the most distinct ones appearing at 24.3 °C and 32.4 °C. The other two crystallization peaks appearing as shoulders. Beaded fibers have also four crystallization

peaks with the most distinct ones appearing at 23.1°C and 32 °C and the other two peaks appearing as shoulders. The melting and crystallization curves of PEO/PMMA (50/ 50) beaded fibers shifting in lower temperatures. The curves remain relatively stable after the 2nd cycle in both cases, indicating that the two materials have thermal stability and thermal reliability. The real melting and cooling enthalpy of non-beaded fibers are 146.7 J/g and 143.4 J/g, respectively, while the real melting and cooling enthalpy of beaded are 139.3 J/g and 138.4 J/g. The % reduction of melting and cooling enthalpies of PEO/ PMMA (50/ 50) non-beaded fibers (37.76 % and 39.65 %) is higher than PEO/ PMMA (50/ 50) non-beaded fibers (40.90% and 41.75%).

3.1.11 DSC analysis of PEO / PMMA (weight ratio 50 /50) / 15% wt. n-eicosane: Beaded versus non-beaded fibers

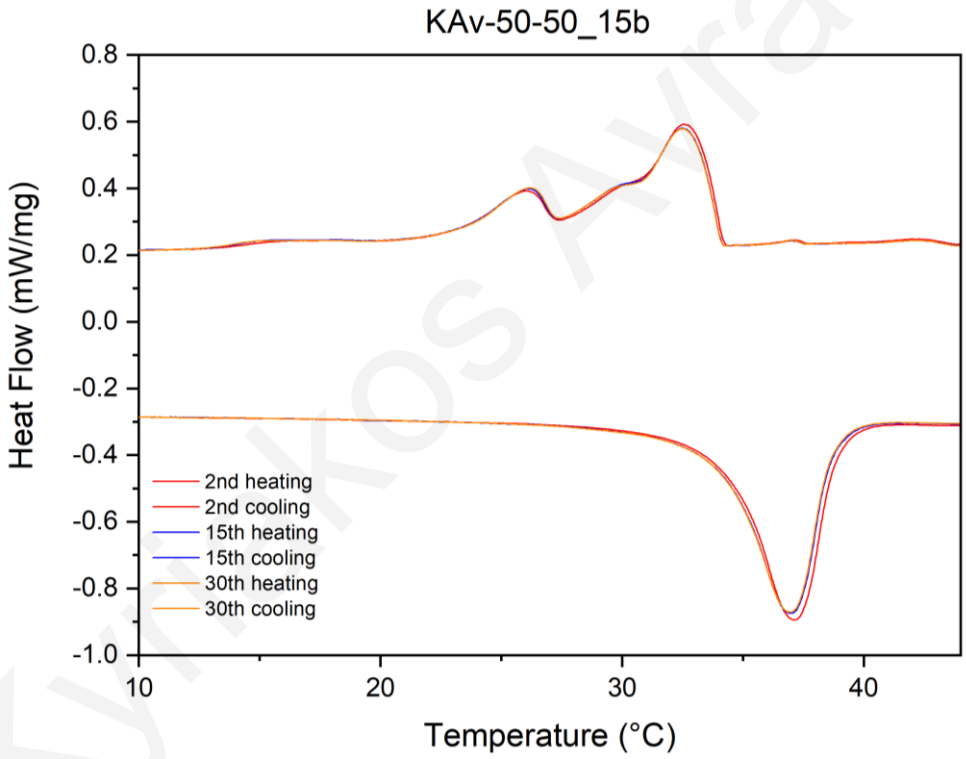

Figure 3.35: DSC curves of PEO/ PMMA (50/50) /15% n-eicosane beaded fibers after 2, 15 and 30 thermal cycles until 44°C.

DSC curves of PEO/ PMMA (50/50) beaded fibers with 15% wt. n-eicosane recorded until 44 °C are shown in figure 3.35. These tests were performed to investigate the behavior of the phase change beaded fibers and study how the results are changed in comparison with PEO/ PMMA (50/50) non-beaded fibers with 15% wt. n-eicosane content.

The melting peak has a peak maximum appearing at 37.1°C (2nd cycle) and five crystallization peaks with the most distinct ones found at 26°C (2nd cycle) and 32.5°C (2nd cycle). The other three crystallization peaks appearing as a shoulder. The curves remain relatively stable after the 2nd cycle, indicating that the PEO/ PMMA /15%wt. n-eicosane beaded fibers have thermal stability and thermal reliability. The real melting enthalpy (ΔHm_r) of PEO/ PMMA / 15% wt. n-eicosane fibers is 162.1 J/g (30th cycle) and the real cooling enthalpy (ΔHc_r) is 140.8 J/g (30th cycle). When compared to pure n-eicosane (Figure 3.23), the addition of PEO and PMMA polymers reduces the latent heat of melting and cooling in the produced fibrous membranes. The % reduction of melting and cooling enthalpies are 31.23 % (30th cycle) and 40.74 % (30th cycle), respectively.

Table 3.9: T_m, ΔH_m, T_{c1}, T_{c2}, ΔH_{c12} of PEO/ PMMA (50 /50)/ 15% n-eicosane beaded fibers after 2, 15 and 30 thermal cycles.

(Tm1: Melting temperature of peak 1, ΔHm: Latent heat of fusion, Tc1: Crystallization temperature of peak 1. Tc2: Crystallization temperature of peak 2, ΔHc1,2: Latent heat of crystallization for the peaks 1 and 2)

PEO/ PMMA (50/ 50)/ 15% n-eicosane beaded fibes					
Cycles	**Tm1 (°C)**	**ΔHm (J/g)**	**Tc1 (°C)**	**Tc2 (°C)**	**ΔHc12 (J/g)**
2nd	37.1	165.8	26.0	32.5	142.0
15th	37.0	164.2	26.1	32.5	139.1
30th	36.9	162.1	26.2	32.2	140.8

The values of melting and crystallization temperatures as well as the crystallization and melting enthalpies are shown in Table 3.9. Based on these results, it is noteworthy that there is no significant temperature or enthalpy change observed after thermal cycling.

DSC curves of PEO/ PMMA (50/ 50) non-beaded fibers with 15% wt. n-eicosane recorded up to 44◦C are shown in figure 3.36. These tests were performed to investigate the behavior of the non-beaded phase change fibers and study how the results are changed in comparison with PEO/ PMMA (50/50) beaded fibers with 15% wt. n-eicosane content.

The melting peak has peak maximum appearing at 37.8 °C (2nd cycle) and only two crystallization peaks are found at 25.8 °C (2nd cycle) and 32.0 °C (2nd cycle). The curves remain relatively stable after the 2nd cycle, indicating that the PEO/ PMMA /15 %wt. n-eicosane non-beaded fibers have thermal stability and thermal reliability. The real melting enthalpy (ΔHm_r) of PEO/ PMMA / 15% wt. n-eicosane fibers is 173.8 J/g (30th cycle) and the real cooling enthalpy (ΔHc_r) is 171.5 J/g (30th cycle). When compared to pure n-eicosane (Figure 3.23), the addition of PEO and PMMA polymers reduces the latent heat of melting and cooling in the produced fibrous membranes. The % reduction of melting and cooling enthalpies are 26.26 % (30th cycle) and 27.82 % (30th cycle), respectively.

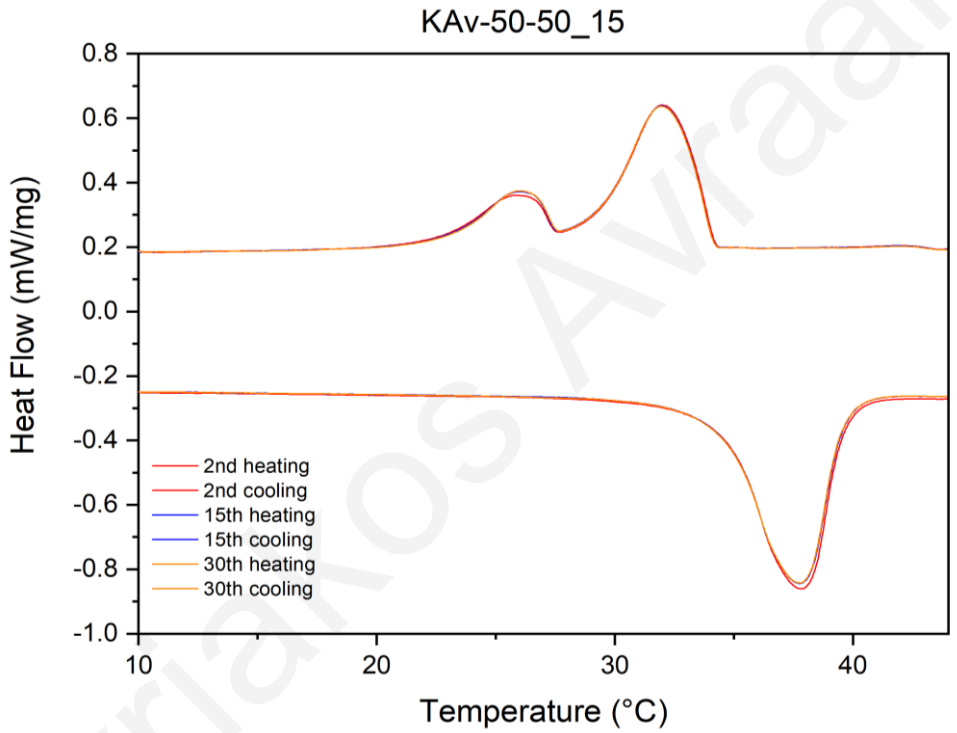

Figure 3.36: DSC curves of PEO/ PMMA (50/50) /15% n-eicosane non-beaded fibers after 2, 15 and 30 thermal cycles until 44°C.

The values of melting and crystallization temperatures as well as the crystallization and melting enthalpies are shown in Table 3.10. Based on these results, it is noteworthy that there is no significant temperature or enthalpy change observed after thermal cycling.

Table 3.10: T_m, ΔH_m, T_{c1}, T_{c2}, ΔH_{c12} of PEO/ PMMA (50 /50)/ 15% n-eicosane non-beaded fibers after 2, 15 and 30 thermal cycles. (Tm1: Melting temperature of peak 1, ΔHm: Latent heat of fusion, Tc1: Crystallization temperature of peak 1. Tc2: Crystallization temperature of peak 2, ΔHc1,2: Latent heat of crystallization for the peaks 1 and 2)

PEO/ PMMA (50/ 50)/ 15% n-eicosane non-beaded fibes					
Cycles	**Tm1 (°C)**	**ΔHm (J/g)**	**Tc1 (°C)**	**Tc2 (°C)**	**ΔHc12 (J/g)**
2nd	37.8	175.0	25.8	32.0	171.9
15th	37.7	172.5	25.9	31.9	172.7
30th	37.7	173.8	26.0	31.9	171.5

Comparison of PEO/ PMMA (50/ 50) / 15% eicosane non-beaded fibers with PEO/ PMMA (50/ 50)/ 15% eicosane beaded fibers:

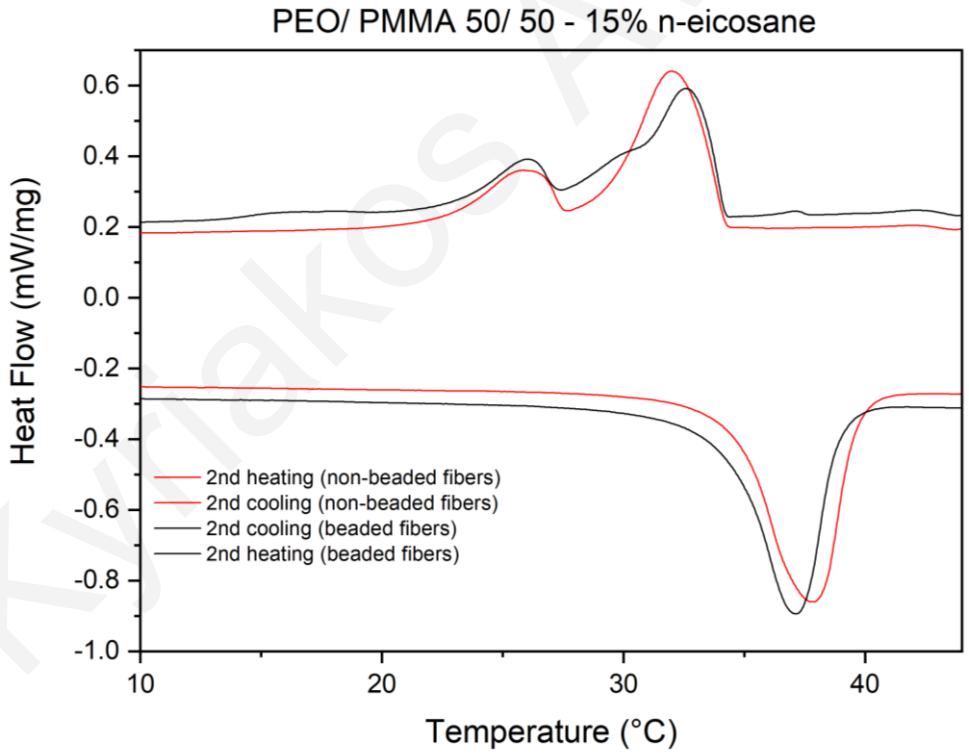

Figure 3.37: DSC curves of PEO/ PMMA (50/50) /15% n-eicosane beaded and non-beaded fibers after 2 thermal cycles until 44°C.

The melting peak of non-beaded fibers is 37.8 °C while the melting peak of beaded fibers is 37.1 °C. Non-beaded fibers have two crystallization peaks at 25.8 °C and 32.0 °C while beaded

fibers have more than 2 crystallization peaks with the more pronounced ones appearing at 26.0 °C and 32.5 °C. The melting curve of PEO/PMMA (50/ 50) bead-free fibers shifting in higher temperatures. The curves remain relatively stable after the 2nd cycle in both cases, indicating that the two materials have thermal stability and thermal reliability. The real melting and cooling enthalpy of non-beaded fibers is 173.8 J/g 171.5 J/g while the real melting and cooling enthalpy of beaded fibers are 162.1 J/g and 140.8 J/g. The % reduction of melting and cooling enthalpies of PEO/ PMMA (50/ 50) non-beaded fibers (26.26% and 27.81%) is lower than PEO/ PMMA (50/ 50) beaded fibers (31.23 % and 40.74 %).

3.1.12 DSC analysis of PEO / PMMA (weight ratio 50 /50) / 20% wt. n-eicosane: Beaded versus non-beaded fibers

DSC curves of PEO/ PMMA (50/ 50) beaded fibers with 20% wt. n-eicosane recorded up to 44℃ are shown in figure 3.38. These tests were performed to investigate the behavior of the phase change beaded fibers and study how the results are changed in comparison with PEO/ PMMA (50/50) non-beaded fibers with 20% wt. n-eicosane content.

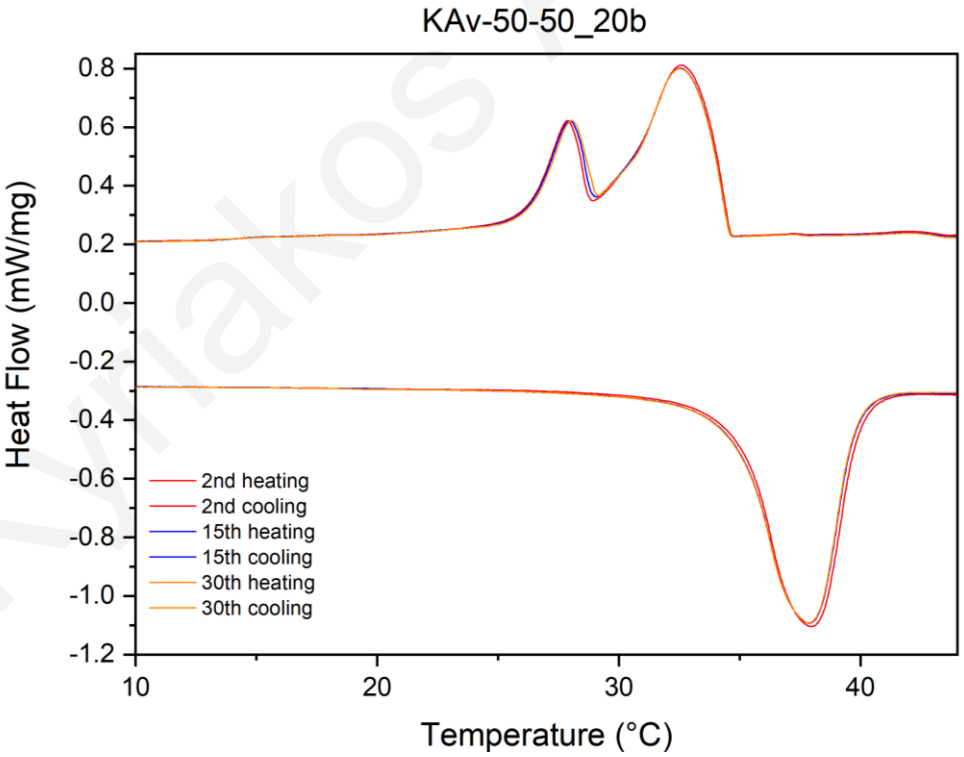

Figure 3.38: DSC curves of PEO/ PMMA (50/50) /20% n-eicosane beaded fibers after 2, 15 and 30 thermal cycles until 44°C.

The melting peak has peak maximum appearing at 38°C (2nd cycle) and two crystallization peaks are found at 27.9°C (2nd cycle) and 32.6°C (2nd cycle). The curves remain relatively stable after the 2nd cycle, indicating that the PEO/ PMMA /20%wt. n-eicosane beaded fibers have thermal stability and thermal reliability. The real melting enthalpy (ΔHm_r) of PEO/ PMMA / 20% wt. n-eicosane beaded fibers is 178.6 J/g (30th cycle) and the real cooling enthalpy (ΔHc_r) is 176 J/g (30th cycle). When compared to pure n-eicosane (Figure 3.23), the addition of PEO and PMMA polymers reduces the latent heat of melting and cooling in the produced fibrous membranes. The % reduction of melting and cooling enthalpies are 24.23 % (30th cycle) and 25.93 % (30th cycle), respectively.

Table 3.11: T_m, ΔH_m, T_{c1}, T_{c2}, ΔH_{c12} of PEO/ PMMA (50 /50)/ 20% n-eicosane beaded fibers after 2, 15 and 30 thermal cycles.

(Tm1: Melting temperature of peak 1, ΔHm: Latent heat of fusion, Tc1: Crystallization temperature of peak 1. Tc2: Crystallization temperature of peak 2, ΔHc1,2: Latent heat of crystallization for the peaks 1 and 2)

PEO/ PMMA (50/ 50)/ 20% n-eicosane beaded fibers					
Cycles	**Tm1 (°C)**	**ΔHm (J/g)**	**Tc1 (°C)**	**Tc2 (°C)**	**ΔHc12 (J/g)**
2nd	38.0	179.6	27.9	32.6	178.8
15th	37.9	175.3	28.0	32.5	177.9
30th	37.9	178.6	28.0	32.5	176.0

The values of melting and crystallization temperatures as well as the crystallization and melting enthalpies are provided in Table 3.11. Based on these results, it is noteworthy that there is no significant temperature or enthalpy change observed after thermal cycling.

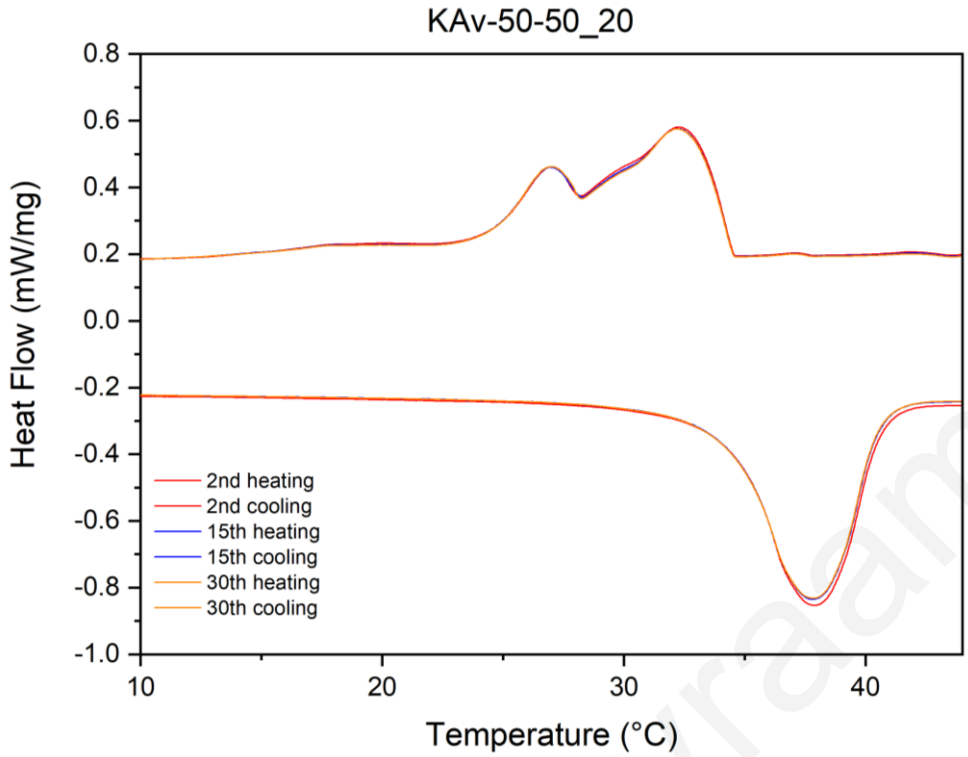

Figure 3.39: DSC curves of PEO/ PMMA (50/50) /20% n-eicosane non-beaded fibers after 2, 15 and 30 thermal cycles until 44°C.

The DSC curves corresponding to the PEO/ PMMA (50/ 50) non-beaded fibers with 20% wt. n-eicosane recorded up to 44◦C are shown in figure 3.39. These tests were performed to investigate the behavior of the phase change non-beaded fibers and study how the results are changed in comparison with PEO/ PMMA (50/50) beaded fibers with the same n-eicosane content (i.e.20% wt.).

The melting peak has a peak maximum appearing at 37.8 °C (2nd cycle) and five crystallization peaks with the most distinct ones found at 27°C (2nd cycle) and 32.2°C (2nd cycle). The other three crystallization peaks appearing as a shoulder. The curves remain relatively stable after the 2nd cycle, indicating that the PEO/ PMMA /20%wt. n-eicosane non-beaded fibers have thermal stability and thermal reliability. The real melting enthalpy (ΔHm_r) of PEO/ PMMA / 20% wt. n-eicosane fibers is 161.7 J/g (30th cycle) and the real cooling enthalpy (ΔHc_r) is 159.5 J/g (30th cycle). When compared to pure n-eicosane (Figure 3.23), the addition of PEO and PMMA polymers reduces the latent heat of melting and cooling in the produced fibrous membranes. The % reduction of melting and cooling enthalpies are 31.40 % (30th cycle) and 32.87 % (30th cycle), respectively.

Table 3.12: T_m, ΔH_m, T_{c1}, T_{c2}, ΔH_{c12} of PEO/ PMMA (50 /50)/ 20% n-eicosane non-beaded fibers after 2, 15 and 30 thermal cycles. (Tm1: Melting temperature of peak 1, ΔHm: Latent heat of fusion, Tc1: Crystallization temperature of peak 1. Tc2: Crystallization temperature of peak 2, ΔHc1,2: Latent heat of crystallization for the peaks 1 and 2)

PEO/ PMMA (50/ 50)/ 20% n-eicosane non-beaded fibes					
Cycles	**Tm1 (°C)**	**ΔHm (J/g)**	**Tc1 (°C)**	**Tc2 (°C)**	**ΔHc12 (J/g)**
2nd	37.8	163.9	27	32.2	32.13
15th	37.8	163.1	26.9	32.2	32.44
30th	37.8	161.7	27	32.2	31.9

The values of melting and crystallization temperatures as well as the crystallization and melting enthalpies are shown in Table 3.12. Based on these results, it is noteworthy that there is no significant temperature or enthalpy change observed after thermal cycling.

Comparison of PEO/ PMMA (50/ 50) / 20% eicosane non-beaded fibers with PEO/ PMMA (50/ 50)/ 20% eicosane beaded fibers:

As seeing on Figure 3.40 the melting peak of the non-beaded fibers appears at 37.8°C while the melting peak of beaded fibers can be seen at 38 °C. Non-beaded fibers have two crystallization peaks at 27°C and 32.2°C, with the 2nd one appearing as a broad bimodal shoulder, while beaded fibers have two crystallization peaks at 27.9°C and 32.6°C. The crystallization curve of PEO/ PMMA (50/50) beaded fibers shifts to higher temperatures. The curves remain relatively stable after the 2nd cycle in both cases, indicating that the two materials have thermal stability and thermal reliability. The real melting and cooling enthalpy of non-beaded fibers are 161.7 J/g and 159.5 J/g respectively, while the real melting enthalpy of beaded

fibers are 178.6 J/g and 176 J/g, respectively. The % reduction of melting and cooling enthalpies of PEO/ PMMA (50/ 50) non-beaded fibers (31.40 % and 32.87%) is higher than PEO/ PMMA (50/ 50) beaded fibers (24.22 % and 25.93 %).

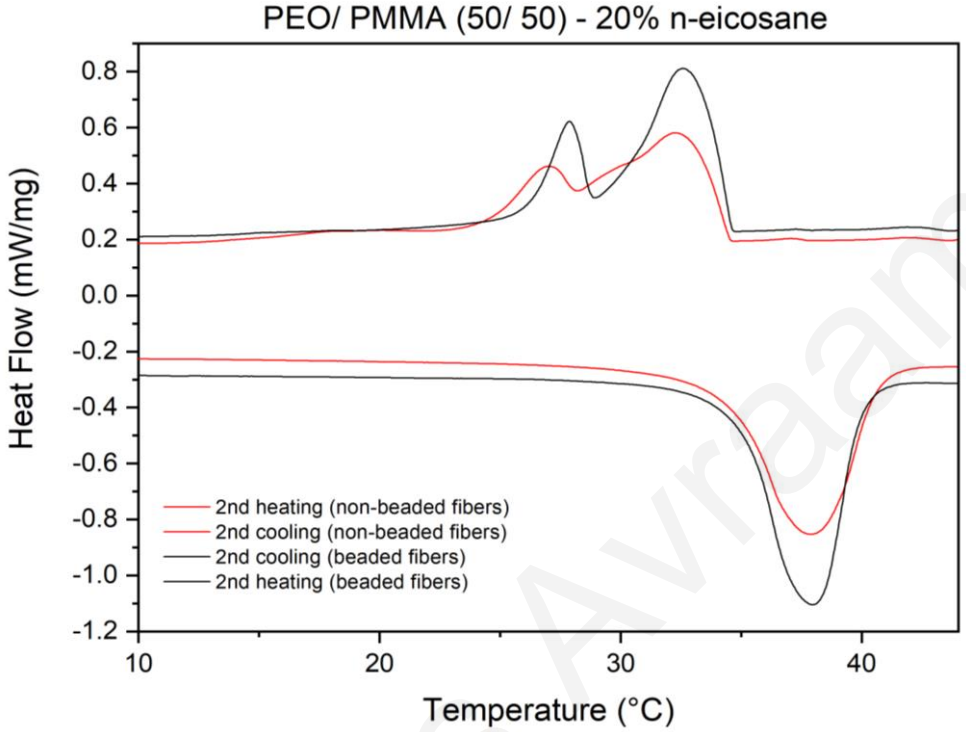

Figure 3.40: DSC curves of PEO/ PMMA (50/50) /20% n-eicosane fibers with 3% w/v (beaded fibers) and 4% w/v (non-beaded fibers) polymer concentrations after 2 thermal cycles until 44°C.

3.1.13 DSC analysis of PEO / PMMA (weight ratio 50 /50) / 25% wt. n-eicosane

The DSC curves of PEO/ PMMA (50/ 50) non-beaded fibers with 25% wt. n-eicosane recorded up to 44◦C are shown in figure 3.41. These tests were performed to investigate the behavior of the phase change non-beaded fibers containing the highest n-eicosane content.

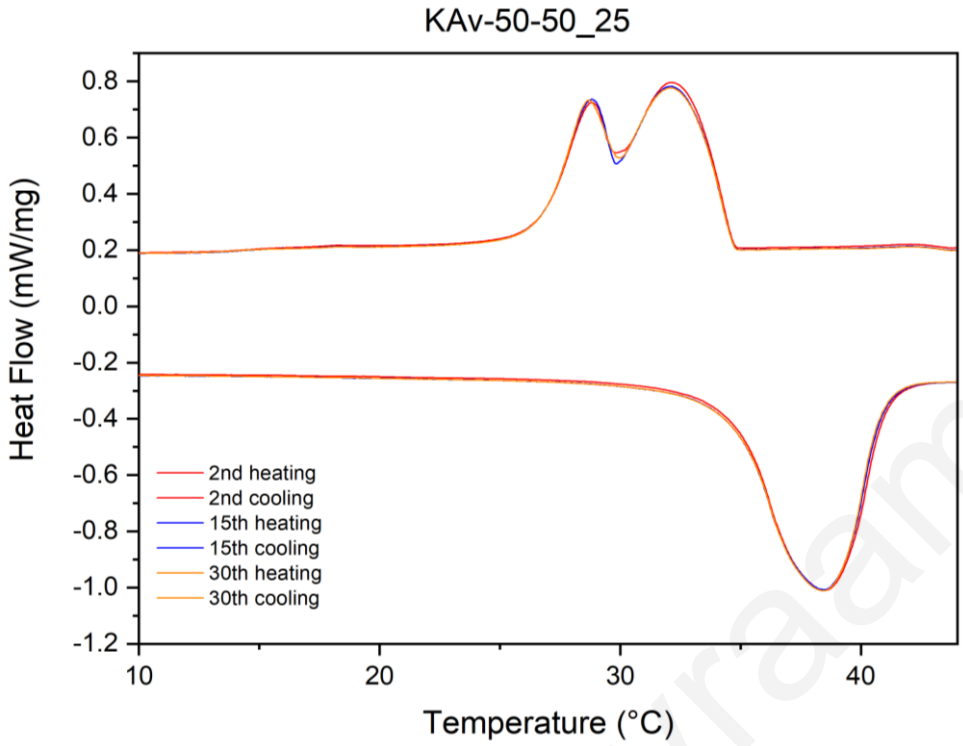

Figure 3.41: DSC curves of PEO/ PMMA (50/50) /25% n-eicosane non-beaeded fiber after 2, 15 and 30 thermal cycles until 44°C.

The melting peak has a peak maximum appearing at 38.5 °C (2nd cycle) and two distinct crystallization peaks are found at 28.8°C (2nd cycle) and 32.1°C (2nd cycle). The curves remain realtively stable after the 2nd cycle, indicating that the PEO/ PMMA /25%wt. n-eicosane non-beaded fibers have thermal stability and thermal reliability. The real melting enthalpy (ΔHmr) of PEO/ PMMA / 25% wt. n-eicosane fibers is 161.5 J/g (30th cycle) and the real cooling enthalpy (ΔHcr) is 159.0 J/g (30th cycle). When compared to pure n-eicosane (Figure 3.23), the addition of PEO and PMMA polymers reduces the latent heat of melting and cooling in the produced fibrous membranes. The % reduction of melting and cooling enthalpies are 31.48 % (30th cycle) and 33.08 % (30th cycle), respectively.

The values of melting and crystallization temperatures as well as the crystallization and melting enthalpies are shown in Table 3.13. Based on these results, it is noteworthy that there is no significant temperature or enthalpy change observed after thermal cycling.

Table 3.13: T_m, ΔH_m, T_{c1}, T_{c2}, ΔH_{c12} of PEO/ PMMA (50 /50)/ 25% n-eicosane non-beaded fibers after 2, 15 and 30 thermal cycles.

(Tm1: Melting temperature of peak 1, ΔHm: Latent heat of fusion, Tc1: Crystallization temperature of peak 1. Tc2: Crystallization temperature of peak 2, ΔHc1,2: Latent heat of crystallization for the peaks 1 and 2)

PEO/ PMMA (50/ 50)/ 25% n-eicosane non-beaded fibes					
Cycles	**Tm1 (°C)**	**ΔHm (J/g)**	**Tc1 (°C)**	**Tc2 (°C)**	**ΔHc12 (J/g)**
2nd	38.5	163.8	28.8	32.1	162.5
15th	38.5	162.8	28.8	32.1	159.6
30th	38.5	161.5	28.7	32.1	159.0

3.2 Discussion

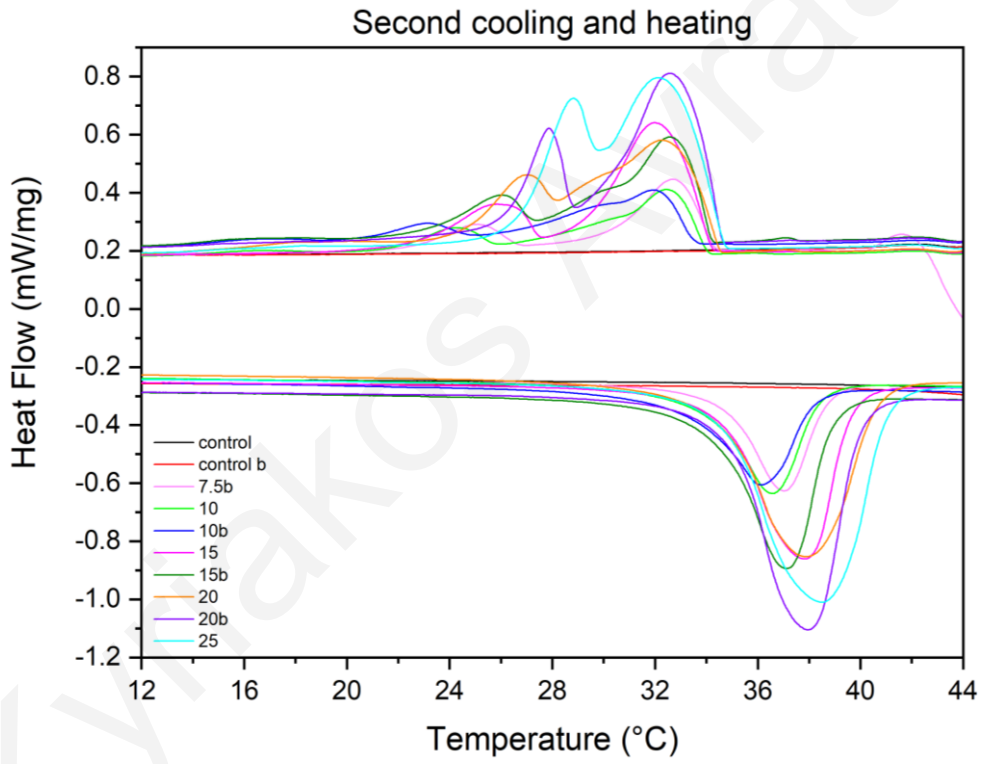

Figure 3.42: Summary of the DSC curves of PEO/ PMMA 50/ 50 (beaded and non-beaded) fibers after the 2nd thermal cycle until 44°C.

Figure 3.42 presents the DSC curves of all phase change fibrous materials prepared in this study, having various concentrations of n-eicosane. Due to the fact that the entire mass of the material (PEO/ PMMA/ n-eicosane) was used during the DSC experiment, these curves do not represent the real (normalized) DSC curves of the samples in the specific temperature range (up to 44°C). Because of this, the "real" enthalpies of the samples were calculated using Equation 3.1.

In the DSC thermograms of a few samples more crystallization peaks appear (as shoulders) (figures 3.28, 3.30, 3.31, 3.35, 3.39). The following samples, in particular, have crystallization peaks that appear like shoulders: PEO/ PMMA (80/20)/ 10% wt. n-eicosane fibers, PEO/ PMMA (50/50)/ 10% wt. n-eicosane beaded and bead-free fibers, PEO / PMMA (50 /50) / 15% wt. n-eicosane beaded fibers and PEO/ PMMA (50 /50)/ 20% n-eicosane bead-free fibers. These peaks (which do not appear in the DSC thermogram of pure n-eicosane) may be attributed to interaction phenomena taking place between the n-eicosane and the PEO or PMMA polymers. More precisely, it is likely that such interactions may have led to the generation of intermediate crystallization phases during the transition of material-eicosane from the liquid to the solid phase upon cooling.

Figure 3.43 depicts the melting enthalpies of the aforesaid fibers. The melting enthalpies of the materials range between 139.3 J/g and 178.6 J/g. Beaded fibers with a polymer weight ratio of PEO/ PMMA 50/50 and a PCM content of 20% demonstrated the highest enthalpy value of 178.6 J/g. The enthalpy value of PEO/ PMMA (80/ 20) /10% n-eicosane fibers is 178 J/g, which is very close to the highest enthalpy value. PEO/ PMMA (50/ 50)/ 10% n-eicosane non-beaded fibers have the enthalpy value of 173.8 J/g which is the highest recorded for this system. In general, the enthalpies of all three systems were high in comparison to the ones reported for other phase change materials based on n-eicosane (Table 3.14) or other paraffins (Table 1.1). Also, the enthalpies of the systems are comparable with other form stable PCFs based on paraffins as shown in table 3.15. The maximum melting enthalpy of ultrafine PCFs made by mixed-and electrospun technique is 144.8 J/g, which is lower than PEO/ PMMA (80/ 20) /10% n-eicosane fibers and PEO/ PMMA (50/ 50)/ 10% n-eicosane beaded and bead-free fibers [9].

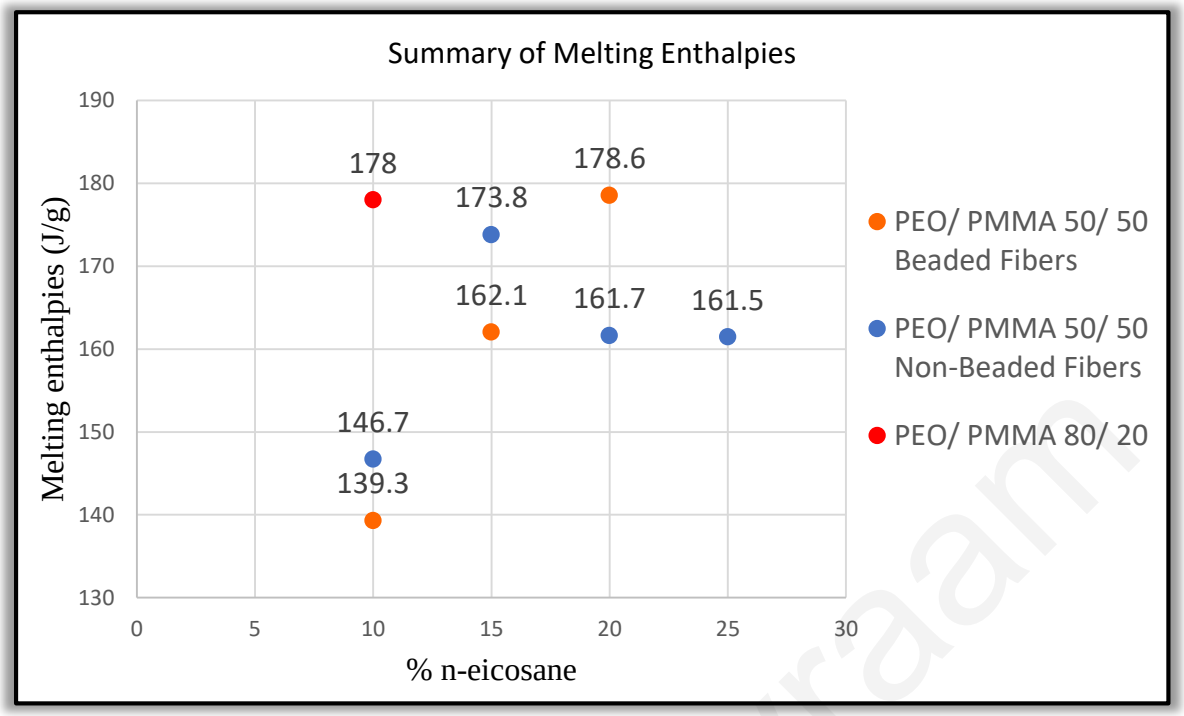

Figure 3.43: Summary of the values of melting enthalpies of PEO/ PMMA 50/ 50 (beaded and non-beaded) fibers and PEO/ PMMA 80/ 20 fibers that contain different concentrations of n-eicosane.

Figure 3.44 and figure 3.45 show the melting and cooling enthalpies of PEO/ PMMA 50/ 50 (non-beaded and beaded) fibers that contain different concentrations of n-eicosane. The storing energy (thermal enthalpy) in all composite fibers is quite close to the released energy (cooling enthalpy). The difference between the heating and cooling enthalpy is only significant in the case of PEO/ PMMA (50/ 50)/ 15% n-eicosane beaded fibers (Figure 3.45). For energy storage applications, the small difference between the two values is critical because the whole energy stored in the material is released for usage in applications.

Furthermore, Figure 3.44 show the trend line of the melting and cooling enthalpies of PEO/ PMMA 50/ 50 (non-beaded) fibers. In the case of bead-free fibers there is a maximum at approximately 17.5% wt. n-eicosane. In higher n-eicosane concentrations the melting and cooling enthalpies drop down. According to a previous report [58] as the amount of n-eicosane increases, the melting and cooling enthalpies increase, too. However, in this case the maximum enthalpy can be observed in 15% wt. n-eicosane content and in higher concentrations (20% wt. and 25% wt.) the enthalpies drop down. This may be explained by two opposite factors, the PCM loading and the interaction phenomena taking place between the polymers and the PCM during the crystallization. As the n-eicosane content increases, more PCM contributes to the

increase of enthalpy but more interactions take place between the PCM and the polymers resulting in decreased final enthalpy of the system. As shown in figure 3.46, the interaction phenomena increase exponentially and because of that the enthalpy drops in higher PCM's concentrations. So, the optimum system in PEO/ PMMA 50/ 50 bead-free fibers is the one that contains 15% wt. n-eicosane (Fig. 3.44)

Table 3.14: Phase Change materials based on n-eicosane from the literature. [50-53] [44]

No	Shell Material	Core Material	Technique	Application	Melting Temperature	ΔHm (J/g
1	Expanded graphite	n-eicosane	Vaccum impregnation	Thermal energy storage	36.41 ℃	199.4 J/g
2	PMMA	n-eicosane	Mini-Emulsion polymerization	Thermal energy storage	34.66 ℃	124.7 J/g
3	Polyurea	n-eicosane	Interfacial polymerization	Thermal energy storage	35.70 ℃	55.5 J/g
4	Urea–melamine–formaldehyde	n-eicosane	In situ polymerization	Thermal energy storage	45.3 ℃	172.0 J/g
5	Polymethylmethacrylate	n-eicosane	Emulsion polymerization	Thermal energy storage	35.2 ℃	84.2 J/g

Table 3.15: Form stable PCFs that contain paraffins from the literature. [54-57]

No	Shell Material	Core Material	PCM (%wt.)	Electrospinning approach	Scanning Rate	ΔHm (J/g)
1	PLA	Dodecane	16.7	Uniaxial	2 °C/min	20.08
2	silk	n-Octadecane	14.2	Uniaxial	5 °C/min	37.58
3	PCL	Dodecane	45	Uniaxial	2 °C/min	73.71
4	PVDF	Eicosane	32.5	Coaxial	10 °C/min	77
5	PVB	Octadecane	46.4	Coaxial	5 °C/min	105.9

On the other hand, beaded fibers show linear increase of melting enthalpy, as the n-eicosane content increases linearly (Fig. 3.45). The optimum system in PEO/ PMMA 50/ 50 beaded fibers is the system that contain 20% n-eicosane. The investigation of the latent heat of beaded fibers in higher n-eicosane concentrations would be highly intriguing.

It is worth noting that fibers with beaded morphologies are considered undesirable in numerous studies. However, the results of this investigation show that PEO/ PMMA (50/ 50)/ 20% n-eicosane beaded fibers have extremely high enthalpy values which are comparable to those of the identical systems without beads.

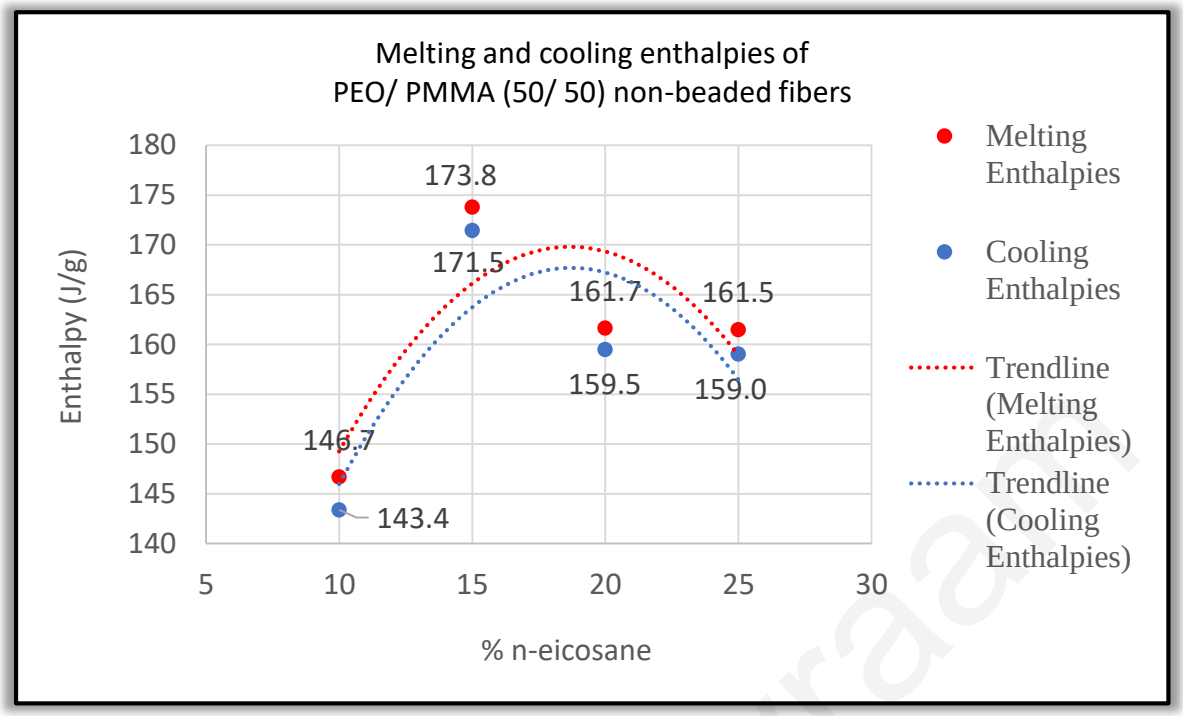

Figure 3.44: Melting and cooling enthalpies of PEO/ PMMA 50/ 50 (non-beaded) fibers that contain different concentrations of n-eicosane.

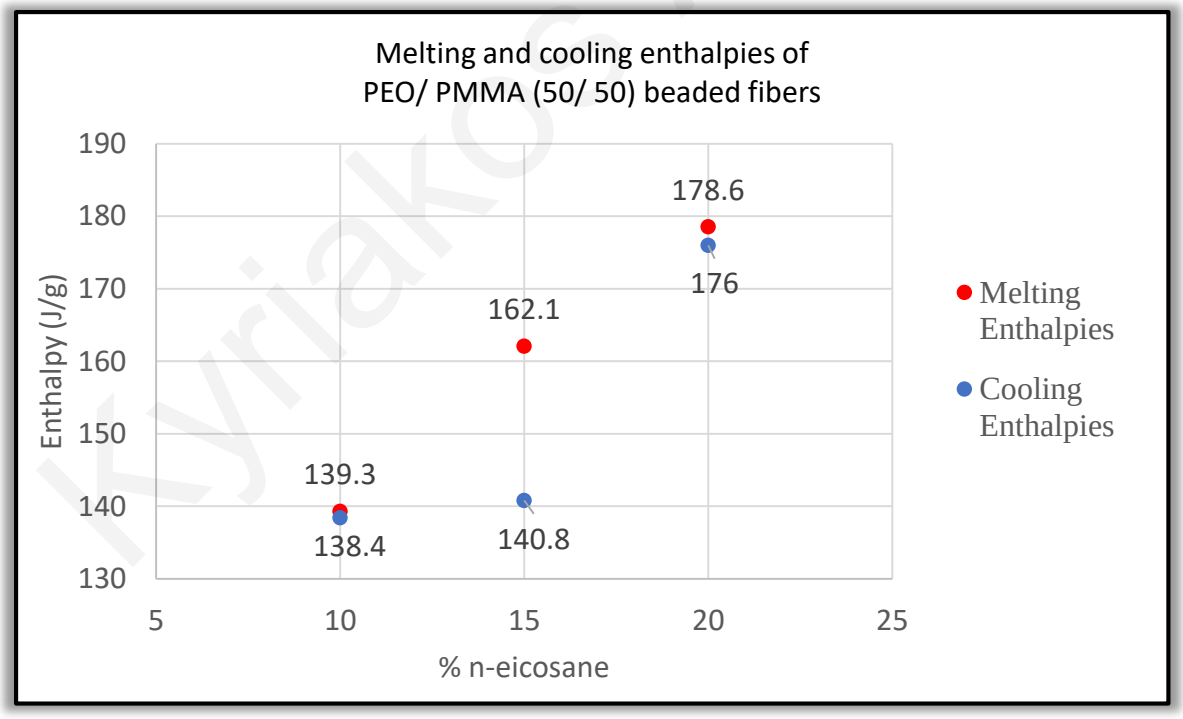

Figure 3.45: Melting and cooling enthalpies of PEO/ PMMA 50/ 50 (beaded) fibers that contain different concentrations of n-eicosane.

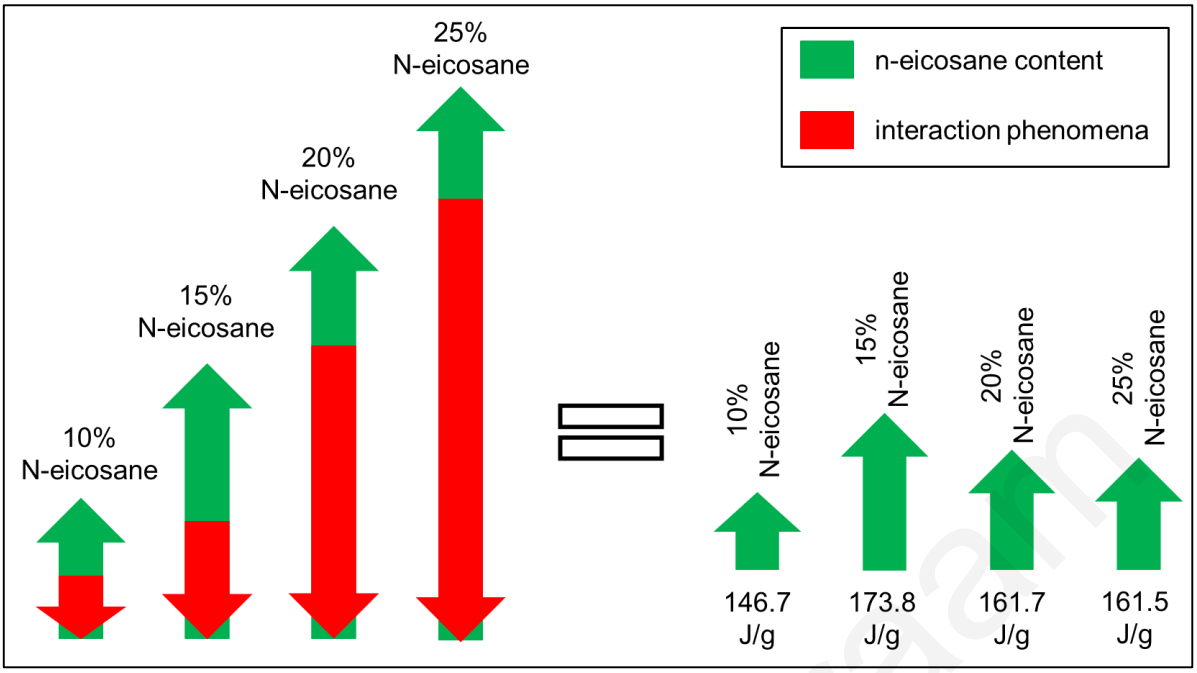

Figure 3.46: Graphic representation of the effect of the n-eicosane content (green arrows) and the interaction phenomena (red arrows) that appear between the polymers and the PCM on the melting enthalpy.

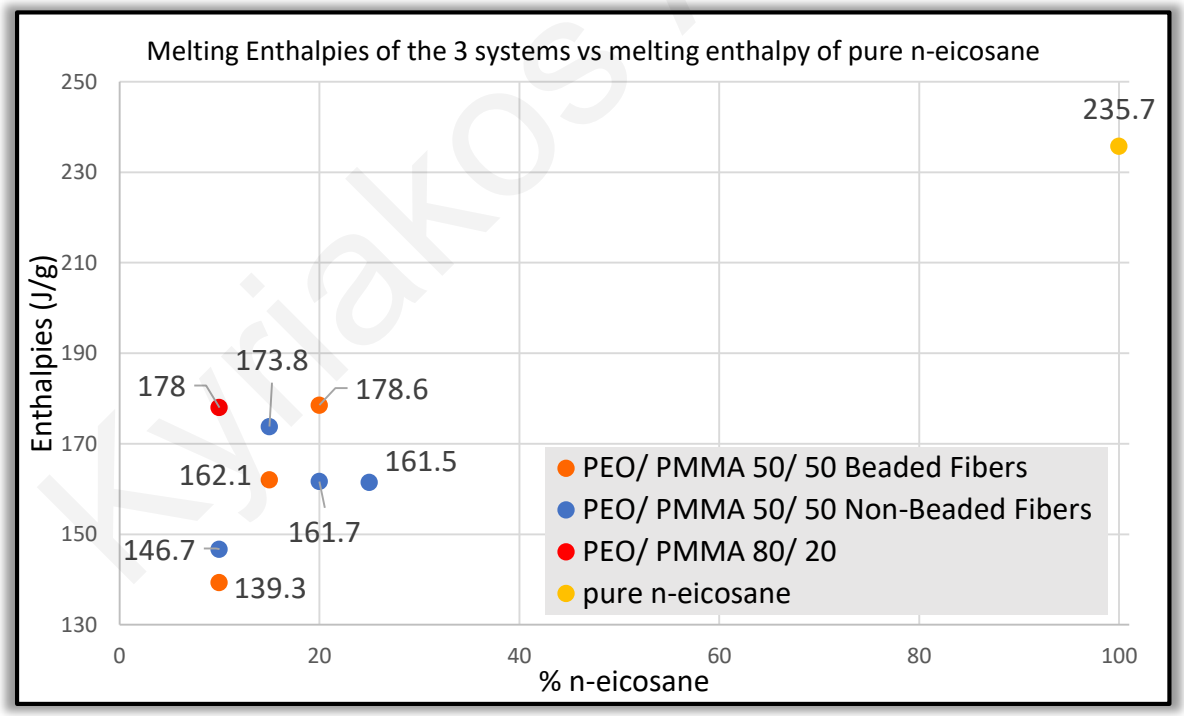

Figure 3.47: Comparison of melting enthalpies of the three systems (PEO/ PMMA (80/ 20), PEO/ PMMA (50/ 50) beaded and bead-free) fibers with the melting enthalpy of pure n-eicosane (235.7 J/g)

Table 3.16: The % reduction of melting and cooling enthalpies of the samples of the three systems (PEO/ PMMA (80/ 20), PEO/ PMMA (50/ 50) beaded and bead-free)

Sample	N-eicosane - polymers	Melting Enthalpy (J/g)	% reduction of melting enthalpy	Cooling Enthalpy (J/g)	% reduction of cooling enthalpy
Pure n-eicosane		235.7	-	237.6	-
PEO/ PMMA (80/ 20)/ 10% n-eicosane	0.03g – 0.3 g polymers	178.0	24.48 %	177.3	25.38 %
PEO/ PMMA (50/ 50)/ 10% n-eicosane beaded fibers	0.04g – 0.3 g polymers	139.3	40.90 %	138.4	41.75 %
PEO/ PMMA (50/ 50)/ 15% n-eicosane beaded fibers	0.045g – 0.3 g polymers	162.1	31.23 %	140.8	40.74 %
PEO/ PMMA (50/ 50)/ 20% n-eicosane beaded fibers	0.06 g – 0.3 g polymers	178.6	24.23 %	176	25.93 %
PEO/ PMMA (50/ 50)/ 10% n-eicosane bead-free fibers	0.04 g – 0.4 g polymers	146.7	37.76 %	143.4	39.65 %
PEO/ PMMA (50/ 50)/ 15% n-eicosane bead-free fibers	0.06 g – 0.4 g polymers	173.8	26.26 %	171.5	27.82 %
PEO/ PMMA (50/ 50)/ 20% n-eicosane bead-free fibers	0.08 g – 0.4g polymers	161.7	31.40 %	159.5	32.87 %
PEO/ PMMA (50/ 50)/ 25% n-eicosane bead-free fibers	0.10 g – 0.4 g polymers	161.5	31.48 %	159.0	33.08 %

The melting enthalpies of the fibers of the three systems (PEO/ PMMA (80/ 20), PEO/ PMMA (50/ 50) beaded and bead-free) that contain different n-eicosane content in comparison with the

pure n-eicosane are provided in Figure 3.47. The % reduction of melting and cooling enthalpies of the various samples are presented in Table 3.16 and the following observations can be made:

- The higher % reduction of melting and cooling enthalpies in comparison with pure n-eicosane present in the PEO/ PMMA (50/ 50) beaded (40.90%) and bead-free (37.76%) fibers. This is due to the combination of the following factors: (1) The low n-eicosane content (10 % wt.) in comparison with the other fibers with the same PEO/ PMMA (50/ 50) weight ratio (15% wt., 20% wt., 25% wt.). (2) The high PMMA content in comparison with PEO/ PMMA 80/ 20 fibers which promotes the development of hydrophobic interactions with the hydrophobic n-eicosane molecules resulting to lower enthalpy values.
- The lower % reduction in melting and cooling enthalpy present in PEO/ PMMA (50/ 50)/ 20% n-eicosane beaded fibers (24.23%) which is lower than PEO/ PMMA (50/ 50)/ 20% n-eicosane bead-free fibers (31.40% and 31.48%). This may be due to the beaded morphology of the fibers.
- The second lowest enthalpy reduction was observed in the case of PEO/ PMMA (80/ 20)/ 10% n-eicosane fibers. Even though there is lower n-eicosane content (10% wt.) in comparison with other systems (15% wt. 20% wt., 25% wt.), the lower PMMA content in comparison with the PEO/ PMMA (50/ 50) systems leads to the reduction of PMMA - n-eicosane interactions and as result the reduction of enthalpy is avoided.

The melting temperatures of PEO/PMMA 50/50 (beaded and non-beaded) fibers having different percentages of n-eicosane, as well as of the PEO/PMMA 80/20 fibers containing 10% n-eicosane, are shown in Figure 3.47. The materials' melting temperatures range from 36.1°C to 38°C, which is suitable for thermal energy storage applications. Liquidification occurs spontaneously during the day in the field of thermal energy storage systems for a short period of time. The PCM will not be able to store thermal energy if it remains in the solid phase during the day, thus resulting to system failure. In order to reach this goal, the PCM should be designed in such as way so as to exhibit melting temperatures that are near to the temperature conditions of a specific region during the day.

Figure 3.48 shows the melting temperatures of PEO/PMMA 50/50 (non-beaded) fibers in comparison with the melting temperature of pure n-eicosane (100 % eicosane). As shown from the trend line, the melting temperatures increase exponentially with the increase of the PCM content. The same behavior can be observed in the case of beaded fibers (Fig. 3.49).

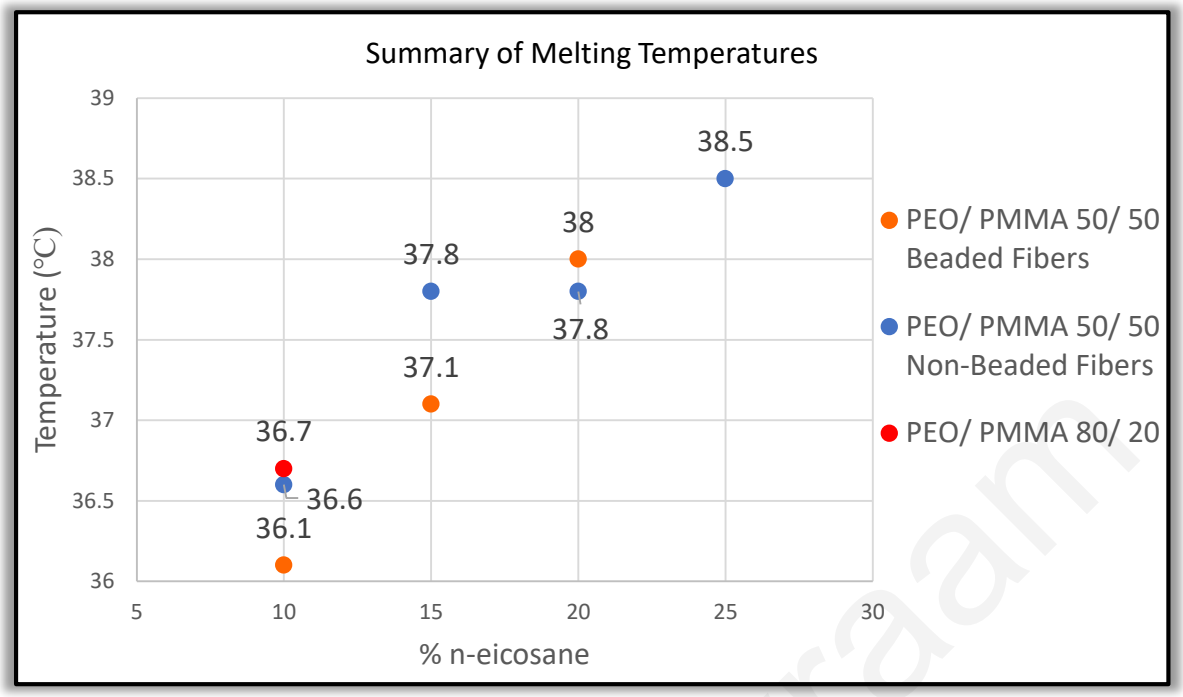

Figure 3.47: Summary of the values of melting temperatures for PEO/ PMMA 50/ 50 (beaded and non-beaded) fibers and PEO/ PMMA 80/ 20 fibers that contain different concentrations of n-eicosane.

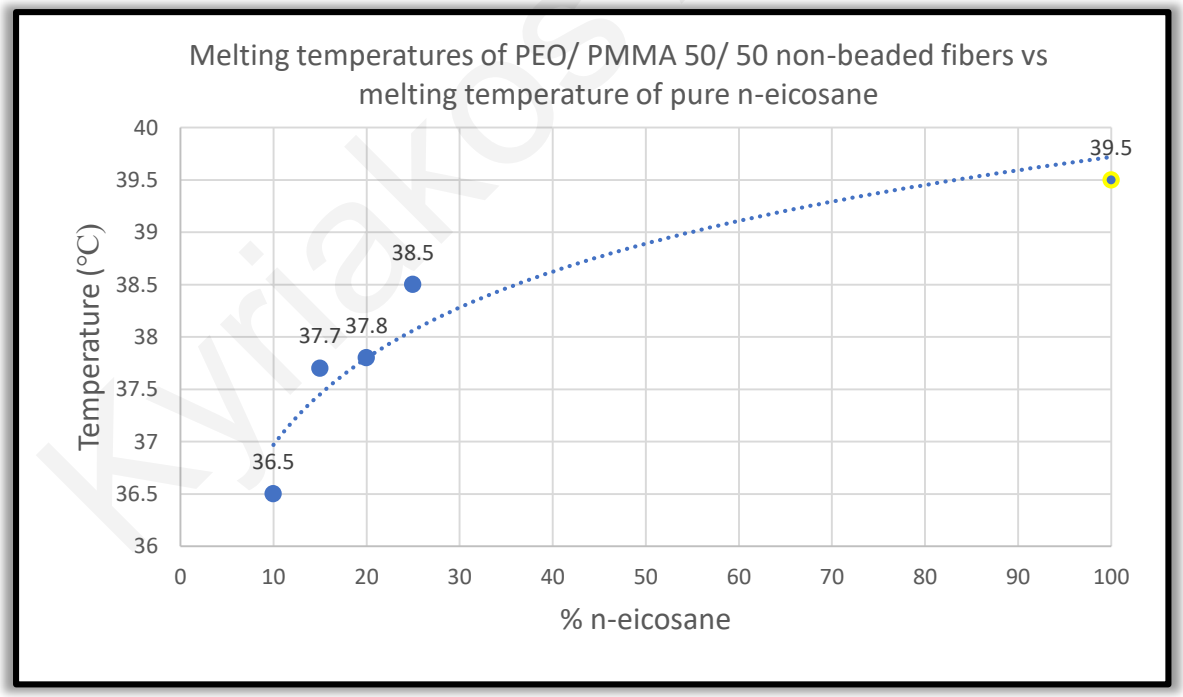

Figure 3.48: Melting temperatures for PEO/ PMMA 50/ 50 (non-beaded) fibers that contain different concentrations of n-eicosane and melting enthalpy of pure n-eicosane

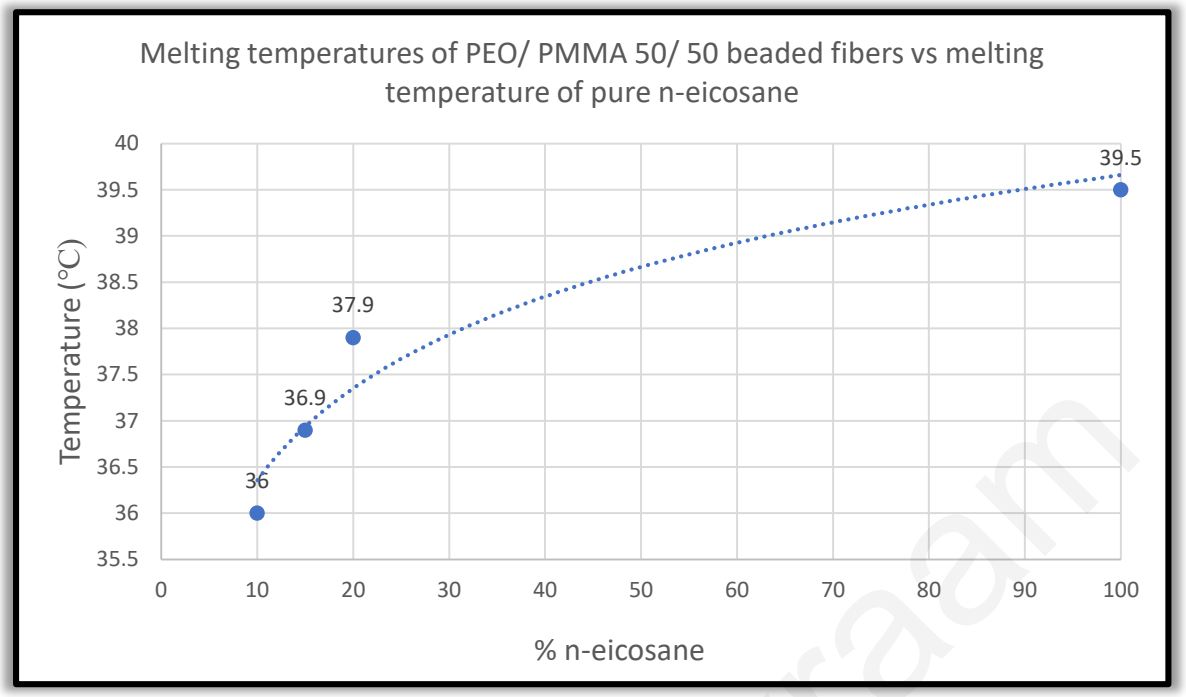

Figure 3.49: Melting temperatures for PEO/ PMMA 50/ 50 (beaded) fibers that contain different concentrations of n-eicosane and melting enthalpy of pure n-eicosane

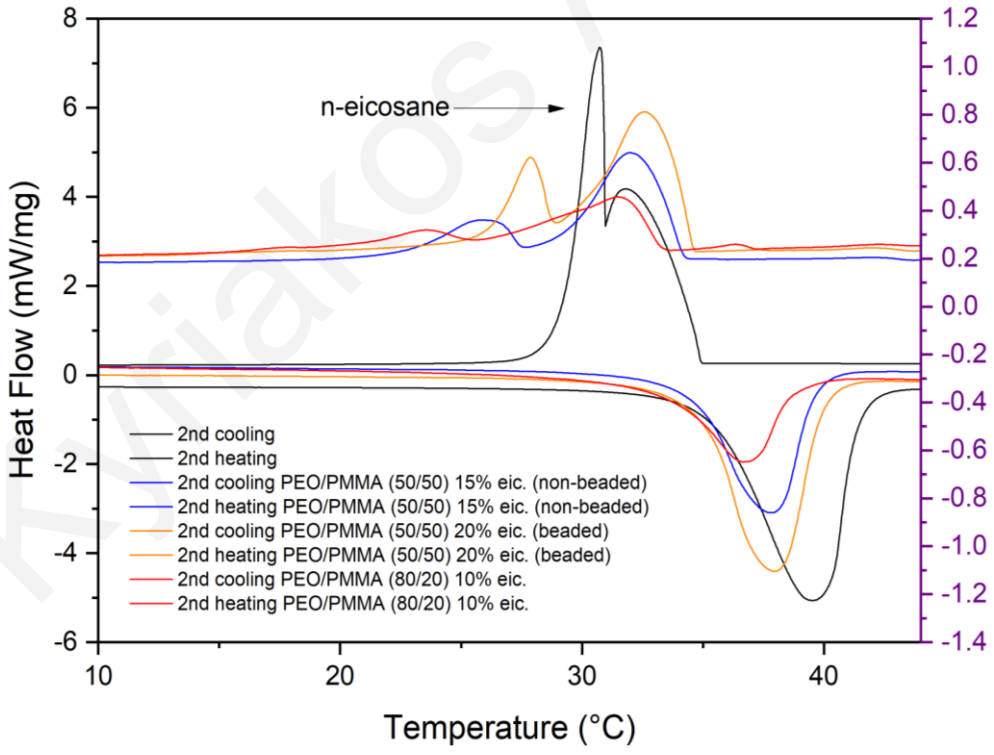

Figure 3.50: DSC curves of the systems (PEO/ PMMA (80/ 20) 10% eic., PEO/ PMMA (50/ 50) 15% n-eicosane – non-beaded fibers, PEO/ PMMA (50/ 50) 20% eic. – beaded fibers) exhibiting the highest values of melting enthalpies, as well as the DSC curves of pure n-eicosane.

In comparison to the DSC curves of pure n-eicosane, figure 3.50 displays the DSC curves of the three different systems (PEO/ PMMA (50/ 50) /15% n-eicosane (non-beaded) fibers, PEO/ PMMA (50/ 50) /20% n-eicosane (beaded) fibers, PEO/ PMMA (80/ 20)/ 10% n-eicosane fibers) with the highest melting enthalpies. The phenomenon of supercooling can be clearly seen in this graph.

The phenomenon of supercooling occurs when a material remains liquid at a temperature below its melting point. The efficiency of the PCM system may be harmed by supercooling. Entering a supercooled state is widely seen as a disadvantage in thermal energy storage devices, as it hinders the release of latent heat. The PCM does not solidify and remains liquid, preventing the system from benefiting from the latent heat. The PCM will not be able to discharge the accumulated thermal energy if it is supercooled instead of solidified. As a result, the primary aim of the PCM's presence is not met, resulting in a system failure. [59]

In comparison to pure n-eicosane, the phenomenon of supercooling is clearly suppressed in the phase change electrospun fibrous materials. This is considerd to be highly advantageous because the system will be more efficient in thermal energy storage applications. Because of the minimal temperature difference between melting and cooling, the cycles of energy storage and release from the PCM will be repeatable.

Chapter 4

4 CONCLUSIONS

In this study, electrospun PEO/ PMMA / n-eicosane microfibers with hydrophilic PEO and hydrophobic PMMA as supporting materials are successfully fabricated via uniaxial electrospinning using chloroform as solvent. N-eicosane was chosen as the PCM due to its properties such as melting point near the human body temperature and high latent heat.

Initially, continuous smooth PEO microfibers with bead-free morphology could be formed under the following electrospinning parameters: 3% w/v was chosen as polymer solution concentration, voltage was set at 10 kV, the flowing rate was set at 3 mL/h, the diameter of the needle was 18G (1.27mm) and the needle-to-collector distance was set at 30cm. Pure PEO fibers with an average diameter of 5.085 ± 0.532 μm were obtained.

After that, blended fibers consisting of PEO and PMMA were fabricated by means of the electrospinning technique. Blended fibers with PEO/ PMMA weight ratios of 90/ 10, 80/ 20, 70/ 30 and 50/ 50 using the same electrospinning parameters as for the pure PEO electrospun membranes. In the case of the 50/ 50 PEO/ PMMA fibers, beaded structures were obtained from 3% w/v PEO/ PMMA solution. By comparing the values corresponding to the other systems (90/10, 80/ 20, 70/ 30) we may conclude that as the PMMA content of the fibers increased, the diameters of the fibers increased as well. The fabrication of electrospun PEO/ PMMA (50/ 50) fibers without beads (bead-free morphology), is achieved by increasing the polymer concentration from 3% w/v to 4% w/v.

The electrospun PEO/ PMMA fibers with an 80/ 20 weight ratio were chosen as the first material for n-eicosane incorporation. Lower n-eicosane contents (2, 5 &7.5% wt.) result in higher values of the mean fiber diameters while higher n-eicosane contents (10 & 15% wt.) promote the generation of fibers having smaller diameters. When n-eicosane reaches a maximum content of 20% wt., the fibrous membrane is covered by an n-eicosane thin layer and many tubercles can be observed onto the fibers' surfaces. Therefore, the incorporation of more than 15% wt. n-eicosane within PEO/PMMA blended fibers (80/20) is unfavorable for obtaining uniform, ultrafine PEO/ PMMA/ n-eicosane PCFs.

The melting (ΔH_{mr}) enthalpy of PEO/ PMMA (80/ 20) / 10% wt. n-eicosane fibers is 178.0 J/g (30th cycle). The curves remain stable after the 2nd cycle, indicating that the PEO/ PMMA

(80/ 20) /10%wt. n-eicosane phase change fibrous membrane has thermal stability and thermal reliability. The membrane seems to be very stable, and the fibers remain intact in the form of PCF without observing any n-eicosane leaching phenomena or material alteration.

With the increase of PMMA concentration in chloroform solution, the PEO/ PMMA microfibers enables the accommodation of a higher n-eicosane percentage within the fibers, due to the development of hydrophobic interactions between the PMMA hydrophobic chains and the n-eicosane hydrophobic hydrocarbon. Because of that, electrospun PEO/ PMMA (50/ 50) beaded and bead-free fibers were also chosen for the incorporation of PCM (n-eicosane) in order to investigate the behavior of beaded and bead-free fibers in terms of their thermal properties. In comparison to PEO/ PMMA (80/ 20) fibers, PEO/ PMMA (50/ 50) seems to be able to accommodate a higher percentage of n-eicosane (e.g. 20% wt.).

PEO/ PMMA 50/ 50 /20% wt. n-eicosane beaded fibers demonstrated the highest melting enthalpy value of 178.6 J/g (30th cycle) and PEO/ PMMA (50/ 50)/ 10% n-eicosane non-beaded fibers have a melting enthalpy value of 173.8 J/g (30th cycle) which is the highest recorded for this system.

The cooling enthalpy in all composite fibers (PEO/ PMMA (80/ 20) /10%wt. n-eicosane fibers, PEO/ PMMA (50/ 50) /20% beaded fibers, PEO/ PMMA (50/ 50)/ 10% n-eicosane bead-free fibers) is quite close to the heating enthalpy. For energy storage applications, the small difference between the two values is critical because the whole energy stored in the material is released for usage in applications. The materials' melting temperatures range from 36.1°C to 38°C, which is suitable for thermal energy storage applications.

In comparison to pure n-eicosane, the phenomenon of supercooling is clearly suppressed in the phase change electrospun fibrous materials. This is considered to be highly advantageous because the system will be more efficient in thermal energy storage applications. Because of the minimal temperature difference between melting and cooling, the cycles of energy storage and release from the PCM will be repeatable.

It is worth noting that fibers with beaded morphologies are considered undesirable in numerous studies. However, the results of this investigation show that PEO/ PMMA (50/ 50)/ 20% n-eicosane beaded fibers have extremely high enthalpy values which are comparable or higher to those of the identical systems without beads.

The next step of this research is the usage of these material in real application and the further evaluation as potential thermal storage media in solar air collectors (SACs) used for space heating.

Furthermore, thermal conductivity of ultrafine PCFs plays a vital role in TES from the standpoint of thermal management since it has a significant impact on heat transfer (charging and discharging) rates. Electrospun ultrafine PCFs, like classic organic solid-liquid PCMs, have a low thermal conductivity, especially those based on a fibrous polymeric matrix [9]. Because of that, the investigation of thermal conductivity of the prepared PCFs and further enhancement using conductive nanofillers is very important. To improve the thermal conductivity of electrospun ultrafine PCFs, high thermal conductive nanoparticles Al_2O_3 have been incorporated in polymer mixed solution. Figure 4.1 show the SEM images of the PEO/ PMMA (50/ 50) particles that contain 5% wt. Al_2O_3. Aluminum Oxide has the higher thermal conductivity in comparison with other nanofillers and it has high chemical durability, and high environmental resistance [9]. However, SEM images present a particle - like flakes morphology and PCFs could not be obtained under the investigated processing conditions. So, future parametric studies can be conducted for the fabrication of electropsun PCFs that contain Al_2O_3 in order to enhance the thermal conductivity of the PCFs.

Unlike non-fibrous form-stable PCMs, electrospun ultrafine PCFs have the distinct advantage of a fibrous shape with ultrafine diameter and extremely high specific surface area, which makes them ideal for applications such as smart fabrics and clothing. The current literature, on the other hand, lacks sufficient information on mechanical properties and long-term fiber shape stability at various temperatures. Because of that, more innovative ways need to be researched further for the usage of PCFs in specific engineering applications.

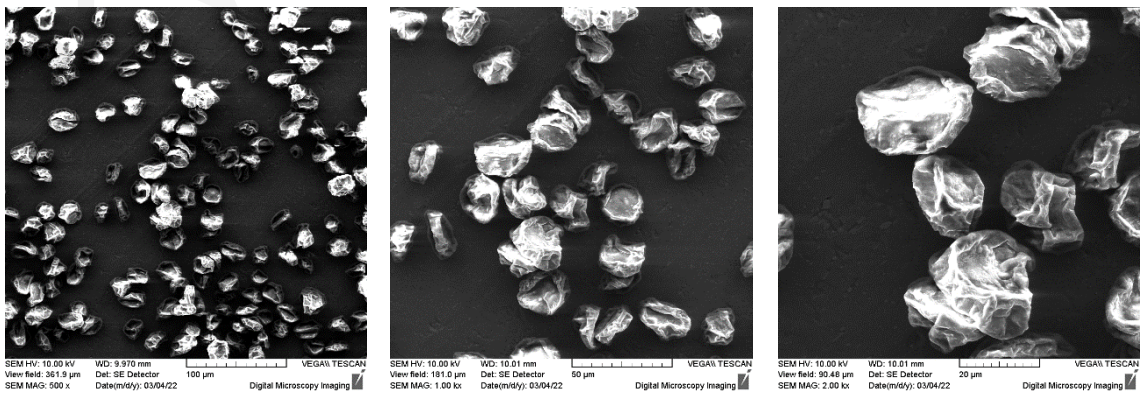

Figure 4.1: SEM images of PEO/ PMMA (mass ratio 50/50)/ 5% wt. Al_2O_3 electrospun particle – like flakes. Scale bars (a): 100μm, (b): 50μm, (c): 20μm

References

1) Qazi, Atika, et al. "Towards sustainable energy: a systematic review of renewable energy sources, technologies, and public opinions." *IEEE access* 7 (2019): 63837-63851.
2) Kalnæs, Simen Edsjø, and Bjørn Petter Jelle. "Phase change materials and products for building applications: A state-of-the-art review and future research opportunities." *Energy and Buildings* 94 (2015): 150-176.
3) Perez, Marc, and Richard Perez. "Update 2022–A fundamental look at supply side energy reserves for the planet." *Solar Energy Advances* 2 (2022): 100014.
4) *Bp Statistical Review of World Energy*. London: British Petroleum Co, 1981. Print.
5) Kenisarin, Murat M. "Thermophysical properties of some organic phase change materials for latent heat storage. A review." *Solar Energy* 107 (2014): 553-575.
6) Qazi, Atika, et al. "Towards sustainable energy: a systematic review of renewable energy sources, technologies, and public opinions." *IEEE access* 7 (2019): 63837-63851.
7) Nazir, Hassan, et al. "Recent developments in phase change materials for energy storage applications: A review." *International Journal of Heat and Mass Transfer* 129 (2019): 491-523.
8) Peng, Hao, et al. "A review on synthesis, characterization and application of nanoencapsulated phase change materials for thermal energy storage systems." *Applied Thermal Engineering* 185 (2021): 116326.
9) Wu, Yang, et al. "Review on electrospun ultrafine phase change fibers (PCFs) for thermal energy storage." *Applied Energy* 210 (2018): 167-181.
10) Tofani, Kassianne, and Saeed Tiari. "Nano-Enhanced phase change materials in latent heat thermal energy storage systems: A review." *Energies* 14.13 (2021): 3821.
11) Sharma, S. Dutt, and Kazunobu Sagara. "Latent heat storage materials and systems: a review." *International journal of green energy* 2.1 (2005): 1-56.
12) Kenisarin, Murat M. "Thermophysical properties of some organic phase change materials for latent heat storage. A review." *Solar Energy* 107 (2014): 553-575.
13) Hu, Wen, and Xun Yu. "Thermal and mechanical properties of bio-based PCMs encapsulated with nanofibrous structure." *Renewable energy* 62 (2014): 454-458.

14) Kalnæs, Simen Edsjø, and Bjørn Petter Jelle. "Phase change materials and products for building applications: A state-of-the-art review and future research opportunities." *Energy and Buildings* 94 (2015): 150-176.
15) Huang, Zhaowen, et al. "Characterization of medium-temperature phase change materials for solar thermal energy storage using temperature history method." *Solar Energy Materials and Solar Cells* 179 (2018): 152-160.
16) Pielichowska, Kinga, and Krzysztof Pielichowski. "Phase change materials for thermal energy storage." *Progress in materials science 65* (2014): 67-123.
17) Alehosseini, Elham, and Seid Mahdi Jafari. "Nanoencapsulation of phase change materials (PCMs) and their applications in various fields for energy storage and management." *Advances in Colloid and Interface Science* 283 (2020): 102226.
18) Sarı, Ahmet, Cemil Alkan, and Alper Biçer. "Thermal energy storage characteristics of micro-nanoencapsulated heneicosane and octacosane with poly (methylmethacrylate) shell." *Journal of Microencapsulation* 33.3 (2016): 221-228.
19) Sarı, Ahmet, et al. "Preparation, characterization and thermal energy storage properties of micro/nano encapsulated phase change material with acrylic-based polymer." *Polymer Science, Series B* 60.1 (2018): 58-68.
20) Rezvanpour, Mohammad, et al. "Synthesis and characterization of micro-nanoencapsulated n-eicosane with PMMA shell as novel phase change materials for thermal energy storage." *Materials Chemistry and Physics* 215 (2018): 299-304.
21) Nikpourian, Hediyeh, Ahmad Reza Bahramian, and Mahdi Abdollahi. "On the thermal performance of a novel PCM nanocapsule: The effect of core/shell." *Renewable Energy* 151 (2020): 322-331.
22) Shi, Jian, et al. "Nano-encapsulated phase change materials prepared by one-step interfacial polymerization for thermal energy storage." *Materials Chemistry and Physics* 231 (2019): 244-251.
23) Chen, Changzhong, Yiyang Zhao, and Wenmin Liu. "Electrospun polyethylene glycol/cellulose acetate phase change fibers with core–sheath structure for thermal energy storage." *Renewable energy* 60 (2013): 222-225.
24) Santangelo, Saveria. "Electrospun nanomaterials for energy applications: Recent advances." *Applied Sciences* 9.6 (2019): 1049.
25) Rezaei, Babak, et al. "Fabrication of thermal intelligent core/shell nanofibers by the solution coaxial electrospinning process." *Advances in Polymer Technology* 35.1 (2016).

26) Nikolaou, Maria, and Theodora Krasia-Christoforou. "Electrohydrodynamic methods for the development of pulmonary drug delivery systems." *European Journal of Pharmaceutical Sciences* 113 (2018): 29-40.

27) Rathod, Manish K., and Jyotirmay Banerjee. "Thermal stability of phase change materials used in latent heat energy storage systems: A review." *Renewable and sustainable energy reviews* 18 (2013): 246-258.

28) Nazir, Hassan, et al. "Recent developments in phase change materials for energy storage applications: A review." *International Journal of Heat and Mass Transfer* 129 (2019): 491-523.

29) WarrenMcLaren "The state of Phase Change Materials in Australian building design." *Architecture and Design Journal (2015)*

30) Arjun, Dakuri, and J. Hayavadana. "Thermal energy storage materials (PCMs) for textile applications." *Journal of Textile and Apparel, Technology and Management* 8.4 (2014).

31) K. Boomila "Requirements of a Space Suit and Its Components" B.Tech, Apparel *Technology, Anna University, Tamil Nadu, India (*2013).

32) Mondal, Subrata. "Phase change materials for smart textiles–An overview." *Applied thermal engineering* 28.11-12 (2008): 1536-1550.

33) Do, Cong Van, Thuy Thu Thi Nguyen, and Jun Seo Park. "Phase-change core/shell structured nanofibers based on eicosane/poly (vinylidene fluoride) for thermal storage applications." *Korean Journal of Chemical Engineering* 30.7 (2013): 1403-1409.

34) Sun, Shao-Xing, et al. "Fabrication of nanofibers with phase-change core and hydrophobic shell, via coaxial electrospinning using nontoxic solvent." *Journal of materials science* 50.17 (2015): 5729-5738.

35) Perez-Masia, Rocio, et al. "Biodegradable polyester-based heat management materials of interest in refrigeration and smart packaging coatings." *Journal of Applied Polymer Science* 130.5 (2013): 3251-3262.

36) Cai, Yibing, et al. "Electrospun ultrafine composite fibers consisting of lauric acid and polyamide 6 as form-stable phase change materials for storage and retrieval of solar thermal energy." *Solar energy materials and solar cells* 103 (2012): 53-61.

37) Chen, Changzhong, Yiyang Zhao, and Wenmin Liu. "Electrospun polyethylene glycol/cellulose acetate phase change fibers with core–sheath structure for thermal energy storage." *Renewable energy* 60 (2013): 222-225.

38) Hu, Wen, and Xun Yu. "Thermal and mechanical properties of bio-based PCMs encapsulated with nanofibrous structure." *Renewable energy* 62 (2014): 454-458.

39) Philip, Princy, et al. "Preparation and characterisation of surface roughened PMMA electrospun nanofibers from PEO-PMMA polymer blend nanofibers." *Polymer Testing* 74 (2019): 257-265.

40) Sun, Xiao-Yu, et al. "Field-driven surface segregation of biofunctional species on electrospun PMMA/PEO microfibers." *Macromolecular rapid communications* 29.17 (2008): 1455-1460.

41) Reddy, M. Ravindar, et al. "X-RD, SEM, FT-IR, DSC Studies of Polymer Blend Films of PMMA and PEO." *Materials Today: Proceedings* 3.10 (2016): 3713-3718.

42) Zhang, Xinyi, Chuqiao Zhu, and Guiyin Fang. "Preparation and thermal properties of n-eicosane/nano-SiO2/expanded graphite composite phase-change material for thermal energy storage." *Materials Chemistry and Physics* 240 (2020): 122178.

43) Shi, Jian, et al. "Synthesis and thermal properties of a novel nanoencapsulated phase change material with PMMA and SiO2 as hybrid shell materials." *Thermochimica acta 617 (2015):* 90-94.

44) Alkan, Cemil, Ahmet Sarı, and Ali Karaipekli. "Preparation, thermal properties and thermal reliability of microencapsulated n-eicosane as novel phase change material for thermal energy storage." *Energy Conversion and Management* 52.1 (2011): 687-692.

45) Sharma, Surender Kumar, et al., eds. *Handbook of materials characterization*. New York, NY, USA:: Springer International Publishing, 2018.

46) Huang, Xiubing, et al. "Shape-stabilized phase change materials based on porous supports for thermal energy storage applications." *Chemical Engineering Journal* 356 (2019): 641-661.

47) Bae, Hyun-Su, et al. "Fabrication of highly porous PMMA electrospun fibers and their application in the removal of phenol and iodine." *Journal of Polymer Research* 20.7 (2013): 1-7.

48) Al Ghossein, Rabih M., Mohammad Sharif Hossain, and J. M. Khodadadi. "Experimental determination of temperature-dependent thermal conductivity of solid eicosane-based silver nanostructure-enhanced phase change materials for thermal energy storage." *International Journal of Heat and Mass Transfer* 107 (2017): 697-711.

49) Chai, Luxiao, Xiaodong Wang, and Dezhen Wu. "Development of bifunctional microencapsulated phase change materials with crystalline titanium dioxide shell for

latent-heat storage and photocatalytic effectiveness." *Applied Energy* 138 (2015): 661-674.Li, Chuanchang, Bo Zhang, and Qingxia Liu. "N-eicosane/expanded graphite as composite phase change materials for electro-driven thermal energy storage." *Journal of Energy Storage* 29 (2020): 101339.

50) Rezvanpour, Mohammad, et al. "Synthesis and characterization of micro-nanoencapsulated n-eicosane with PMMA shell as novel phase change materials for thermal energy storage." *Materials Chemistry and Physics* 215 (2018): 299-304.
51) Lan, Xiao-Zheng, et al. "Microencapsulation of n-Eicosane as Energy Storage Material." *Chinese Journal of Chemistry* 22.5 (2004): 411-414.
52) Zhang, Xing-xiang, et al. "Crystallization and prevention of supercooling of microencapsulated n-alkanes." *Journal of colloid and interface science* 281.2 (2005): 299-306.
53) Perez-Masia, Rocio, et al. "Biodegradable polyester-based heat management materials of interest in refrigeration and smart packaging coatings." *Journal of Applied Polymer Science* 130.5 (2013): 3251-3262.
54) Zhao, Liang, et al. "Emulsion-electrospinning n-octadecane/silk composite fiber as environmental-friendly form-stable phase change materials." *Journal of Applied Polymer Science* 134.47 (2017): 45538.
55) Do, Cong Van, Thuy Thu Thi Nguyen, and Jun Seo Park. "Phase-change core/shell structured nanofibers based on eicosane/poly (vinylidene fluoride) for thermal storage applications." *Korean Journal of Chemical Engineering* 30.7 (2013): 1403-1409.
56) Sun, Shao-Xing, et al. "Fabrication of nanofibers with phase-change core and hydrophobic shell, via coaxial electrospinning using nontoxic solvent." *Journal of materials science* 50.17 (2015): 5729-5738.
57) Alkan, Cemil, Sennur Alay Aksoy, and Ruhan Altun Anayurt. "Synthesis of poly (methyl methacrylate-co-acrylic acid)/n-eicosane microcapsules for thermal comfort in textiles." *Textile Research Journal* 85.19 (2015): 2051-2058.
58) Shamseddine, I., et al. "Supercooling of phase change materials: A review." *Renewable and Sustainable Energy Reviews* 158 (2022): 112172.

APPENTICES

Appendix I – Tables of Fibers' diameters

Table I: Diameters of the fibers with different PEO/PMMA weight ratios (μm).

No	PEO/ PMMA 100/0	PEO/ PMMA 90/10	PEO/ PMMA 80/20	PEO/ PMMA 70/30
1	5.273	2.582	2.831	3.794
2	5.968	2.374	2.523	2.677
3	4.481	2.515	2.323	3.390
4	4.681	1.700	3.311	3.910
5	5.954	2.528	2.675	3.523
6	5.332	1.326	2.380	3.620
7	5.313	2.501	2.176	2.142
8	5.384	2.365	2.065	2.794
9	6.06	2.419	2.504	3.642
10	4.995	1.428	1.668	3.536
11	6.374	1.632	2.357	4.228
12	5.137	1.245	2.290	2.397
13	4.934	2.318	2.240	2.708
14	5.469	1.427	2.369	2.596
15	5.793	2.351	2.267	3.238
16	5.411	1.546	2.832	5.563
17	4.769	2.941	2.348	4.170
18	4.775	1.773	2.653	4.041
19	4.570	1.584	1.369	3.898
20	5.075	2.422	2.304	4.689
21	5.497	2.261	2.659	3.594
22	5.300	2.338	2.374	4.180
23	4.798	1.512	2.173	3.368
24	4.798	2.593	2.752	3.604
25	5.219	2.285	2.057	3.790
26	4.219	2.144	1.840	3.264
27	4.674	1.603	1.108	3.510
28	4.601	1.608	2.181	6.260
29	5.274	1.603	2.375	3.926
30	5.862	1.178	2.052	3.390
31	6.584	2.030	1.245	2.944
32	5.527	1.628	1.020	3.485
33	5.262	2.111	2.278	2.594
34	4.265	2.146	1.864	3.467
35	5.072	2.562	1.025	3.793
36	4.452	2.664	2.258	3.312
37	6.261	1.216	1.979	2.755
38	5.653	1.353	2.129	4.702
39	5.578	2.843	2.080	4.029

40	3.858	3.137	2.707	3.783
41	4.056	2.866	2.393	2.518
42	4.091	2.027	2.084	2.904
43	4.035	2.171	2.727	5.816
44	5.245	1.530	2.231	5.143
45	4.692	2.446	2.547	3.088
46	4.668	1.524	1.048	5.987
47	4.948	3.026	1.098	5.143
48	4.739	1.225	1.189	6.023
49	4.999	1.357	2.080	4.385
50	4.272	1.766	1.818	4.061

Table II: Diameters for the PEO/ PMMA (80/20) fibers with n-eicosane content ranging from 2% wt. to 15% wt. (μm).

No	PEO/ PMMA/ 2% wt. eic	PEO/ PMMA/ 5% wt. eic	PEO/ PMMA/ 7.5% wt. eic	PEO/ PMMA/ 10% wt. eic	PEO/ PMMA/ 15% wt. eic
1	4.898	3.280	4.714	2.140	1.622
2	4.697	3.546	3.192	2.194	1.939
3	5.458	3.713	4.232	2.675	3.547
4	4.475	3.490	5.958	2.184	3.773
5	5.733	4.087	7.181	2.406	2.340
6	4.971	4.394	4.212	2.435	3.074
7	4.961	3.041	6.326	1.799	4.709
8	5.037	4.213	6.659	2.675	3.215
9	4.452	3.672	1.525	2.340	2.393
10	5.348	4.332	1.500	2.230	1.974
11	4.773	3.431	3.588	1.698	3.506
12	4.860	3.463	6.180	2.607	3.461
13	2.708	3.884	4.412	2.587	1.344
14	4.703	3.806	5.281	1.736	1.521
15	4.713	3.246	4.782	2.063	1.396
16	4.487	4.036	6.075	2.556	4.489
17	4.709	3.133	3.711	2.243	4.974
18	4.568	3.538	6.718	2.643	5.465
19	5.026	3.833	4.086	1.875	2.896
20	5.398	4.463	6.018	3.079	2.284
21	5.813	3.558	6.101	1.639	2.896
22	5.650	3.476	2.593	2.109	3.201
23	5.768	3.659	5.759	1.938	3.299
24	4.759	3.759	1.690	3.063	1.945
25	4.730	3.505	5.765	2.431	1.974
26	5.052	4.133	6.297	2.918	2.728
27	5.518	4.296	5.731	2.608	4.586
28	5.468	4.188	2.118	2.805	2.982
29	5.145	3.464	6.831	2.038	4.988

30	5.256	4.163	6.931	2.694	3.705
31	4.759	3.964	1.468	2.638	2.234
32	5.713	2.960	3.811	2.637	1.408
33	4.694	2.849	6.002	2.768	1.968
34	4.396	3.624	6.664	2.033	4.065
35	4.545	3.981	4.081	2.941	4.068
36	5.421	3.047	3.450	3.048	3.144
37	5.182	3.454	6.362	2.819	2.193
38	4.923	3.636	3.572	2.847	2.192
39	4.685	4.101	7.023	2.901	2.431
40	4.756	4.099	5.595	2.399	2.621
41	5.478	3.557	6.205	1.039	3.068
42	4.821	3.669	6.786	2.617	2.520
43	5.177	3.578	4.032	3.350	3.771
44	4.405	3.825	6.836	2.548	1.374
45	4.703	3.506	7.194	2.757	2.637
46	5.641	4.271	7.240	2.390	3.110
47	5.530	3.581	3.776	2.307	3.584
48	4.832	3.319	4.069	2.443	2.630
49	5.592	3.437	7.228	3.013	3.211
50	5.600	4.668	6.460	2.311	1.339